Wake-up Receivers based on Commercial Off-The-Shelf Components: A Survey

Robert Fromm, *Student Member, IEEE,* Olfa Kanoun, *Senior Member, IEEE,* and Faouzi Derbel, *Senior Member, IEEE*

Note: This is the manuscript version of this publication. See https://doi.org/10.1109/JMW.2025.3638933 for the published version. Current version: June 22, 2026.

***Abstract*—Because radio communication is the main source of power consumption in wireless sensor nodes, duty cycling is commonly used to extend battery life. However, duty-cycled communication leads to high latency, making on-demand and event-based communication impractical. Wake-up receivers address this issue by reducing energy consumption during reception. Since most wake-up receivers operate in always-on mode, they enable low-latency and event-based communication. Given the wide variety of design approaches, a clear overview is needed. Many existing solutions are incompatible with real-world deployment, require custom fabrication, or lack repeatability. Therefore, there is a strong need to focus on prototypes based on commercial off-the-shelf components. These offer practical advantages in terms of cost, availability, and ease of integration. This article surveys the literature over the period of 2002–2024. We analyzed over 120 articles dealing with this topic. We examined, characterized, and classified 132 wake-up receiver prototypes. We identified the main building blocks of wake-up receivers and analyzed the components and circuits used. Additionally, we highlighted the strengths and limitations of current research and provided an outlook on future research directions.**

***Index Terms*—Wake-up receiver, wireless sensor network, ultra-low power, on-demand communication.**

I. Introduction

Wireless sensor networks are becoming increasingly important, enabling specialized measurement tasks and future applications. These wireless sensor networks require wireless, battery-powered sensor nodes. Maintaining a long battery life is essential for cost-effective and maintenance-free operation [1]. Since battery capacity is limited by the physical size of the sensor node, reducing power consumption is crucial. [2]

The average power consumption $\overline{P}$ required to achieve a desired battery life t for a given battery capacity Q is estimated by:

$$\overline{P} = \frac{V\,Q}{t} \tag{1}$$

Here, V represents the nominal battery voltage, typically around 3 V. Battery capacity varies significantly depending on size and technology. Small coin cell batteries provide approximately 200 mAh [3], while lithium-ion batteries in the larger form factors offer around 3000 mAh [4].

For short-term measurement tasks, a battery life of two years may be sufficient. However, in place-and-forget scenarios, battery life should be ten years. Based on (1), we estimated the minimum and maximum average power consumption for these scenarios. A small battery with a ten-year lifetime can supply only 6.8 µW, while a large battery with a two-year lifetime can provide up to 510 µW. [5]

With modern ICs and microcontrollers, power consumption can be minimized to 1 µW can be achieved by disabling unnecessary components and using sleep modes. The power demand of sensor node's measurement task varies, but short measurement intervals and efficient power management can minimize the power consumption. [6]

Generally, the highest power consumption in a sensor node occurs during transmission and reception phases of the main radio (MR). Studies analyzing different commercial RF transceivers [1], [7] show that reception power consumption is typically no less than 10 mW, while transmission power consumption is generally about twice of that. Even modern RF transceivers, such as [8], [9], exhibit similar values.

A. Power Saving Methods Without Wake-up Radio

Comparing the average power $\overline{P}$ available from the battery with the reception power consumption P_{RX} of the MR shows a difference of a factor of 100–1000. To reduce power consumption, the MR must limit its reception time. To achieve the required average power consumption $\overline{P}$, the MR's maximum duty-cycling ratio must be between 0.1–1%[1].

However, during sleep mode, wireless data communication is not possible. This creates two major risks. Firstly, so-called idle listening occurs, whenever the receiver is active but there is no data on the channel. Secondly, the missed data transmissions occur, whenever the receiver is in sleep mode, but another sensor node puts data on the channel. [6], [10]

These risks are shown in Fig. 1 (a). Different communication protocols help reduce these risks, including synchronous and pseudo-asynchronous communication protocols [1], [11], [12].

R. Fromm and F. Derbel are with Leipzig University of Applied Sciences, Faculty of Engineering, Leipzig, Germany. e-mail: robert.fromm@htwk-leipzig.de

O. Kanoun is with Chemnitz University of Technology, Professorship Measurement and Sensor Technology, Chemnitz, Germany.

[1]With significantly lower power consumption in sleep mode, we can estimate the duty cycle to be $\overline{P}$ / P_{RX}.

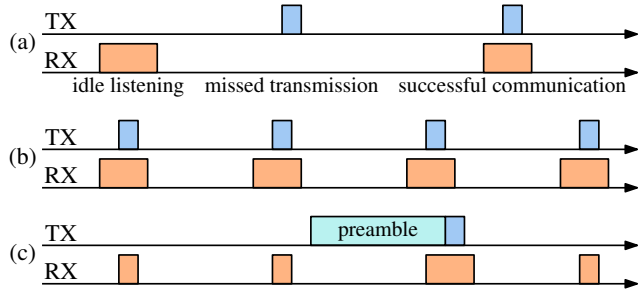

Fig. 1. Duty-cycled main radio operation. (a) Risks of duty-cycled communication: idle listening and missed transmissions. (b) Synchronized communication protocol. (c) Pseudo-asynchronous communication protocol with long preamble.

In synchronous communication, both the receiver and transmitter wake up at fixed intervals after a predefined sleep period, as shown in Fig. 1 (b). Short synchronization packets are transmitted periodically. To reduce power consumption, sleep periods should last several seconds.[2] However, long sleep periods increase communication latency. A major challenge in synchronized communication is clock drift.

High-accuracy clocks are expensive and still have limited precision. For example, clock crystals have an accuracy of 20–100 ppm, with higher costs for more accurate crystals. The absolute time drift Δt between two clocks with relative accuracy δ after an elapsed time t is estimated by:

$$\Delta t = 2\,\delta\,t \tag{2}$$

For sleep periods of one second, the clock drift is small (40–200 µs). However, if sleep periods last several minutes, the drift increases significantly to 2.4–12 ms. To compensate for this drift, the reception period must be extended, increasing receiver power consumption. [13]–[15]

In pseudo-asynchronous communication, packet transmission is event-driven. The receiver is duty-cycled and regularly checks for packets on the channel. Based on the values discussed earlier, sleep periods typically last several seconds.

To prevent packet loss, long preambles, as shown in Fig. 1 (c), or multiple retransmissions are used. Longer packet transmission increases power consumption on the transmitter side. The latency of this communication protocol depends on the receiver's sleep period and is generally high [11]–[13].

B. Wake-up Radios

Due to duty-cycled operation, battery-powered MR communication has high latency. To achieve latency in millisecond range, either power consumption increases or a different approach must be used. Wake-up receivers (WuRxs) are ultra-low-power receivers designed to solve this issue. When sensor nodes are equipped with WuRxs, they can continuously receive packets while consuming minimal power. [16]

WuRxs typically receive only special packets, called wake-up packets (WuPts). Other terms used in literature include wake-up signal (WuS) and wake-up call (WuC) [10]. The device transmitting the WuPt is called a wake-up transmitter (WuTx). In some cases, the abbreviation wake-up radio (WuR) is used, referring to the combination of WuRx and WuTx. However, when the MR and WuR operate on the same channel, no dedicated WuTx hardware is required, reducing costs. Fig. 2 illustrates the concepts of MR, WuRx, WuTx, WuR, and WuPt. [1], [17]

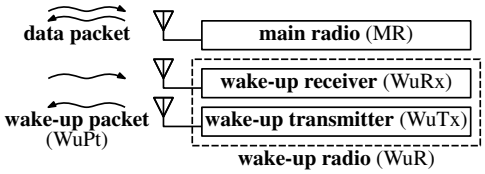

Fig. 2. The main radio can transmit and receive data packets. The wake-up radio consists of a wake-up receiver and wake-up transmitter. The wake-up transmitter sends wake-up packets.

WuRxs consume significantly less power in listening mode compared to the MR [1]. However, they have limitations in other areas, including lower data rates, reduced selectivity, and shorter communication range. Shellhammer et al. [15] and Djiroun et al. [10] claimed that WuR and MR communication should have the same communication range. However, in practice, few WuRxs achieve sensitivity levels comparable to those of MRs [18]. Degraded sensitivity leads to reduced link budget and shorter range for WuR communication[3]. Reduced link budgets can be partially compensated by increasing the transmission power.

C. Wake-up Radio Applications

Due to their low power consumption and fast response time, WuRs are ideal for applications of battery-powered sensor nodes involving sporadic events and long sleep period. They are particularly useful in industrial settings when wireless communication is required, such as for moving parts or inaccessible areas. [19]

Mobile devices, such as unmanned aerial vehicles, can read environmental sensor data. However, synchronous communication is not feasible since the arrival time of the vehicle is nearly unpredictable. Transmitting data without ensuring reception would waste energy. Instead, WuPts can be used to trigger data transmission only when a receiver is present. [20]–[23]

Most indoor localization technologies require three or more fixed anchors for triangulation. These anchors typically operate as always-on receivers, requiring mains power and expensive cabling. With WuR technology, battery-powered anchors become feasible. The target transmits a WuPt to activate the anchors, allowing long sleep periods to extend battery life. [24], [25]

Smart metering in buildings and apartments highlights the benefits of WuR communication. In older buildings, minimizing cabling efforts is essential, and battery-powered data collection units are often required. WuRs eliminate clock

[2] Typical RF packets range from 1–10 ms and depend on data rate, modulation, payload size, and overhead [8], [9]. To achieve the required duty-cycling ratio of 0.1–1%, sleep periods range from 0.1–10 s.

[3] see detailed description in Subsection II-C.

synchronization issues while reducing power consumption for both receivers and transmitters. [19]

WuRs also benefit home automation, such as lighting, shading, and heating. For these applications to feel responsive, latency must remain below one second [15]. Additionally, battery-powered devices reduce cabling efforts, particularly in retrofit installations. WuR communication improves battery life while reducing latency in smart home applications.

Various other battery-powered devices, such as holiday decorations and remote-controlled toys, consume most of their energy while idle. WuRs reduce idle power consumption, extending battery life and improving user experience [26]. By minimizing battery waste, WuRs contribute to more efficient and sustainable energy use.

D. Scope of the Article

In the literature, there are two main approaches to implementing WuR hardware. The first focuses on designing, manufacturing, and analyzing application-specific integrated circuits (ASICs) for WuRs. The second approach utilizes commercial off-the-shelf (COTS) components to design and analyze WuRs on PCBs [27]. Both methods have advantages. ASIC implementations are generally smaller and achieve better sensitivity values. However, they are costly to develop and difficult to reproduce. In contrast, COTS-based WuRs enable fast and simple prototyping, low cost, and easy repeatability [1]. Despite the advantages of ASICs, few commercial WuR chips are available [28].

Most existing integrated WuRs lack performance and are unsuitable for RF applications. For example, Rup and Bajic [29] analyzed the EFR32BG22 system-on-chip [9], which integrates a WuRx for the 2.45 GHz band. They found that the WuR communication range was limited to 15 cm, making it unsuitable for most applications.

This article surveys the literature over the period of 2002–2024 on wake-up receiver hardware design based on commercial off-the-shelf components. This article strictly focuses on research related to COTS-based WuRs. To further refine the scope, we include only articles that present and analyze WuRx prototypes at the hardware level on the physical layer. Many other articles discuss simulations or media access control (MAC) layer protocols, but they are beyond the scope of this survey. Fig. 3 shows the number of reviewed articles that present WuRx prototypes, organized by publication year. In total, we reviewed 120 articles.

E. Related Surveys and Reviews

Piyare et al. [1] published a survey on WuR hardware and MAC protocols in 2017. Since their survey had a broader scope and was published eight years ago, only 21 COTS-based WuRxs were analyzed. In contrast, our narrower focus allows for a more detailed examination of how WuRxs are constructed. By analyzing circuit designs, we identify promising approaches and suggest future research directions.

Zaraket et al. [20] provided an overview of WuR technology in 2021. Their scope was similar to that of Piyare et al. [1], yet only eight WuRx implementations in their review fit within our scope. By analyzing a larger number of articles, we provide a more comprehensive overview and conduct a statistical analysis of the research landscape.

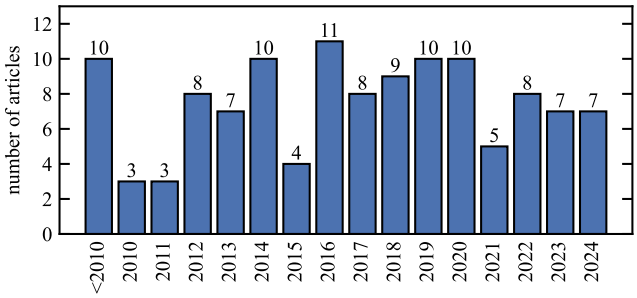

Fig. 3. Number of reviewed articles per year in this publication

Bello et al. [30] reviewed WuRs in combination with wireless energy harvesting in 2019. Our survey also covers passive WuRxs and WuRxs powered by energy harvesting. Bello et al. found only six COTS-based implementations. In contrast, we reviewed 12 articles on passive and energy-harvesting WuRxs.

Many other articles [18], [19] primarily focus on ASIC-based WuRs or MAC layer protocols. By concentrating solely on COTS components, we address a gap in the literature. Most existing studies lack detailed characterization of WuRx prototypes.

F. Structure of the Article

This article is structured as follows: In Section II, we describe the characterization of WuRxs. We first define the key building blocks based on our survey of existing research. In Subsection II-B, we classify WuRxs based on their communication channel, operating mode, and addressing capabilities. In Subsection II-C, we define the main performance parameters of WuRxs: sensitivity, latency, and power consumption. At the end of this section, we describe additional parameters, including supply voltage, robustness, reliability, cost, size, component availability, and modulation.

In Section III, we analyze the components used in WuRxs. We examine circuit implementations from the literature and explain trade-offs between different design choices. We also discuss two special operating modes: duty-cycling and power-gating. In Subsection III-H, we review the design principles of WuTxs.

In Subsection IV-A, we highlight the prototypes that achieve the best sensitivity, latency, and power consumption. In Subsection IV-B, we discuss shortcomings in current research, and in Subsection IV-C, we suggest future research directions. Finally, in Subsection IV-D, we summarize our key findings.

In Section V, we provide a table listing all parameters, characterizations, and classifications of the 132 WuRx prototypes reviewed in this publication.

II. Wake-up Receiver Characterization

When the MR and WuR operate on the same channel, the MR can be programmed to transmit WuPts. In the following discussions, we assume that the MR functions as the WuTx.

With the exception of Subsection III-H, this article focuses on WuRx implementations.

A. Building Blocks

The first building block of a WuRx is its signal input. For WuRxs operating in the RF range, antennas are used. A WuRx can either have a dedicated antenna or share an antenna with the MR. Fig. 4 illustrates these two configurations. [18], [26], [31]

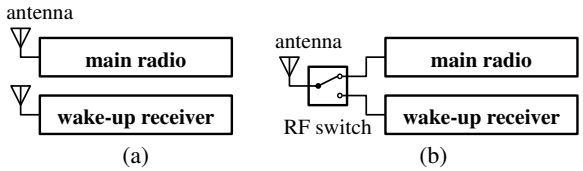

Fig. 4. (a) Dedicated antennas for the main radio and wake-up receiver. (b) Shared antenna with an antenna switch.

Both configurations have advantages and disadvantages in terms of cost and space. Small chip antennas are often more affordable than implementing an antenna switch. When using an external antenna, configuration (b) is usually cheaper and requires less space. However, antenna switches introduce a small quiescent current, increasing power consumption in sleep mode. In MAC protocol design, these two configurations must be considered. In configuration (b), receiving data packets and WuPts simultaneously is not possible. The sensor node must anticipate which communication channel is most likely to be used next. [32]

Based on our survey, we identified the key building blocks of a typical WuRx. Similar structures have been proposed in [11], [31], [33], [34]. Not every WuRx includes all building blocks, but their order and function remain consistent across most implementations. Fig. 5 illustrates the typical architecture of a COTS WuRx, highlighting the transition from RF to LF and digital signals.

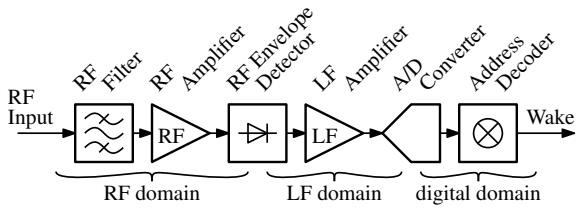

Fig. 5. Typical building blocks of a WuRx based on COTS components

Most COTS WuRxs use a passive radio-frequency envelope detectors (RFEDs) to convert the RF signal into the LF domain. In MRs, RF synthesizers and mixers are typically used for down-conversion. However, these components consume too much power for continuous operation in WuRxs [18].

An RF amplifier can boost the input signal before it reaches the RFED, improving sensitivity. However, RF amplifiers have high power consumption, making continuous operation impractical for ultra-low-power WuRxs. To mitigate this, duty-cycling or power-gating is used to reduce average power consumption. [35]

Since RFEDs often have a wide input bandwidth, RF filters are used to ensure selectivity by allowing only signals from the desired frequency band to pass. This prevents interference from affecting WuPt reception. [36]

The LF amplifier boosts the output signal of the RFED, improving sensitivity. However, adding an LF amplifier increases power consumption. [37]

The conversion from the analog to the digital domain is performed by an analog-to-digital converter (ADC). Most WuRxs use a simple 1-bit conversion via a comparator instead of a full ADC. The comparator outputs a digital symbol stream. [38]

The address decoder is an optional but important component. It prevents false wake-ups caused by interference or other packets in the channel. The decoder processes incoming symbols and checks them against a predefined address. If a match is found, the WuRx generates the wake-up signal to trigger an interrupt in the microcontroller or activate the MR. [1], [11], [17], [31], [33], [34]

B. Classification

Several articles have classified WuRxs based on different criteria. Our classification is based on Piyare et al. [1], but we made modifications to reflect recent developments. We identified three key dimensions for classifying WuRxs: channel–describing the medium and RF carrier used for WuR communication, operating mode–describing the approach of powering the WuRx components, and addressing capabilities–describing the ability to differentiate between WuPts.

1) Classification by Channel: Fig. 6 shows the number of reviewed prototypes classified by WuR channel. The RF channel is further subdivided into different frequency bands. WuRs should operate in industrial, scientific, and medical (ISM) bands or other license-free RF frequency bands [1]. They must comply with regulations regarding maximum transmission power, duty cycle, and bandwidth.

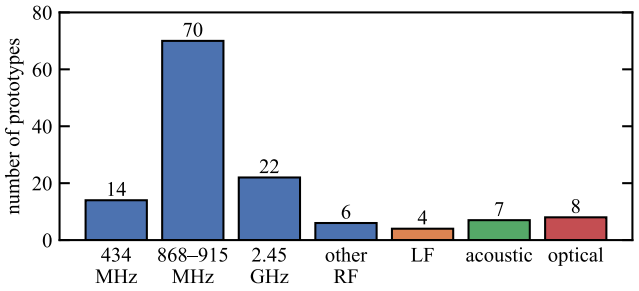

Fig. 6. Number of analyzed prototypes classified by communication channel. All RF-based channels are colored in blue. Basagni et al. [39] presented two prototypes operating at 868 MHz and 434 MHz. Bdiri et al. [40] and Zhang et al. [28] did not specify their channels. In total, 113 prototypes operate in the RF range.

Most reviewed articles focus on RF-based WuRxs. The majority operate in the sub-Gigahertz bands at 868 MHz and 915 MHz, which are preferred due to different regional regulations. This frequency range appears optimal for wireless sensor nodes with WuRxs.

The 2.45 GHz band is used by 22 articles. It allows for smaller antennas and wider bandwidth but suffers from a higher free-space path loss (FSPL), which is approximately 9 dB higher than at 868 MHz.[4] [41]. Additionally, WuRx sensitivity tends to degrade at higher frequencies due to reduced RFED efficiency [42].

Only 15 WuRx prototypes operate at 434 MHz. This band has a 6 dB lower FSPL than 868 MHz, providing better range. However, the license-free bandwidth is limited to 1.85 MHz, restricting data rates. Additionally, WuPts must be carefully designed to remain within regulatory limits.

We found six implementations using non-standard carrier frequencies: Malinowski et al. [43] proposed a passive WuRx at 300 MHz but did not justify the frequency choice. Petäjäjärvi et al. [44] developed a super-regenerative receiver for human-body communication at 28 MHz. The low carrier frequency improved sensitivity to −97 dBm. Del Prete et al. [42], [45] optimized RFED matching circuits for simultaneous operation at 868 MHz and 2.45 GHz. Woias et al. [46] proposed a WuRx at 315 MHz, a license-free band in some countries, though this was the only reviewed article using this frequency. Polonelli et al. [47] developed an ultra-wideband WuRx centered at 3.9936 GHz. The ultra-wideband approach allows license-free operation at low transmission power. However, due to the low WuRx sensitivity, the FSPL was only 17 dB. Theoretically, the range is only 42 mm [41].

Only 19 reviewed implementations used non-RF wake-up channels. LF wake-up communication is commonly used in automotive keyless entry systems. The car transmits a fixed-message LF WuPt at 120–135 kHz using a coil transmitter. The key continuously monitors the LF channel with specialized low-power ICs. Upon detecting a valid pattern, the key transmits an RF response to unlock the car. [48]

Researchers have adapted this approach for wireless sensor networks: Benoit et al. [49] used LF wake-up communication for battery-powered light curtains in automatic doors. Chen et al. [23] triggered sensors from an unmanned aerial vehicle using LF signals. Mohaghegh et al. [50] estimated distances by measuring received signal strength indicator (RSSI) of the LF signal. Wolling et al. [51] proposed human-body communication via LF signals, where contact with an LF-emitting electrode enables MR communication.

Acoustic WuRxs enable communication in environments where RF signals do not propagate well, such as underwater: Sanchez et al. [52], [53] and Schulthess et al. [54] developed underwater acoustic WuRxs using different LF sound frequencies and microphones. Schaechtle et al. [55] proposed an ultrasonic WuRx that communicates through metal plates using a 1.2 MHz carrier.

Acoustic WuRxs can also be triggered by smartphones, unlike RF WuRxs, which require dedicated transmitters: Höflinger et al. [56] and Bannoura et al. [57] used smartphone loudspeakers to trigger WuRxs at 18 kHz and 20 kHz, just above the human hearing range.

[4]FSPL = 31.2 dB at 1 m and 868 MHz, FSPL = 40.2 dB at 1 m and 2.45 GHz. The 868 MHz band achieves 2.8 times the range for the same FSPL.

Optical WuRxs rely on light-based signals: Ma and Paradiso [58] proposed an optical WuRx in 2002, using a flashlight to transmit an 8-bit WuPt. The receiver consumed only 1.5 µW in standby mode. Carrascal et al. [59], Ramos et al. [60], and Dudko and Overmeyer [61] integrated solar panels with optical WuRxs, using harvested energy for wake-up detection. Saez et al. [62] proposed using two complementary optical signals (red and blue LEDs) to create a differential wake-up signal. They also extended this concept to RF using two different frequencies (838 MHz and 868 MHz).

Non-RF WuRs serve specific applications but have significant drawbacks for wireless sensor networks: RF signals suffer less attenuation over distance compared to optical, acoustic, or LF WuPts. Optical WuR communication requires line-of-sight. Non-RF WuRs typically require more power, reducing battery life when the WuTx is also battery-powered. For example, Carrascal et al. [59] used a 10 W light source. For typical wireless sensor network applications, RF WuR communication remains the solution with the highest number of applications.

2) Classification by Operating Mode: Fig. 7 shows the number of reviewed prototypes classified by their operating mode. We identified five different operating modes. Always-on WuRxs are the most common type, with 102 prototypes identified. These receivers operate continuously and can receive WuPts at any time. Their power consumption remains constant in idle mode.

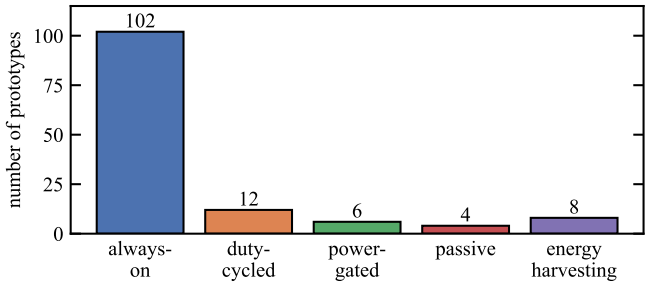

Fig. 7. Reviewed prototypes classified by operating mode

Some always-on WuRxs apply a slight duty cycle. For example, certain WuRx ICs support duty cycles of 11, 20, 33, and 50% [63]. However, articles often lack detailed information about which settings were used [64], [65]. In [66], we implemented a 50% duty cycle in our WuRx.

Duty-cycled WuRxs operate with higher power consumption in reception mode, typically in the milliwatt range. They achieve excellent sensitivity by using high-power RF components, as shown in Fig. 5. Several studies [34]–[36], [67], [68] used RF amplifiers to enhance sensitivity. Ma et al. [69], [70] replaced passive RFEDs with power detectors to improve performance. da Silva et al. [71] implemented a WuRx using the CC1200 MR.

By applying a high duty-cycling ratio, these WuRxs reduce average power consumption to the microwatt range. However, they require longer WuPts to ensure the receiver is active during transmission. Alternatively, Shellhammer et al. [15] proposed synchronizing the WuTx and WuRx to avoid long

WuPts, though clock drift must be managed through periodic resynchronization.

Power-gated WuRxs activate additional high-power components after detecting a WuPt preamble. Bdiri et al. [37], [65], [72] used an RF power detection circuit to activate a high-power LF amplifier. Benbuk et al. [21], [73], [74] activated pulse-width detectors and address correlators only after detecting a WuPt preamble. The supply voltage for these additional components is controlled by a power switch, significantly reducing power consumption in idle mode.

Passive WuRxs require no power from the sensor node's battery and rely entirely on the received RF signal. Studies [5], [75]–[77] proposed passive WuRxs that rectify and amplify the RF WuPt using only passive components. These designs achieve very limited communication range and lack addressing capabilities, as address matching requires active components.

Energy-harvesting WuRxs use active components but generate their power from external sources. Most implementations [16], [77]–[83] use simultaneous wireless information and power transfer (SWIPT), where the WuPt carries both energy and addressing information. Fabbri et al. [80], [81] designed energy-harvesting WuRxs supporting microcontroller-based addressing. Saab et al. [84] harvested ambient RF signals to power their prototype. Optical WuRxs [59]–[61] used solar cells for both power and signal transmission.

3) Classification by Addressing Capabilities: Fig. 8 shows the number of reviewed prototypes classified by addressing capabilities. Many studies do not explicitly describe the addressing features of their WuRxs. In 13 articles, no information on addressing capabilities was available at all. Conversely, 16 articles explicitly showed that no addressing capabilities were utilized.

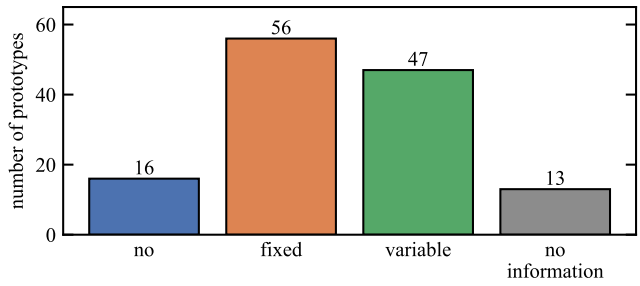

Fig. 8. Reviewed prototypes classified by addressing capabilities

Addressing capabilities play an important role in WuRx design. They help reduce overhearing by ensuring that a WuRx wakes up only when its assigned address is transmitted. Without addressing, multiple WuRxs in range may wake up unnecessarily, leading to increased activity of the MR and higher power consumption. However, implementing addressing capabilities introduces trade-offs. Sensitivity may degrade[5], WuPts become longer, and additional power is required for address matching components [85]. In scenarios with few WuRxs in range, a WuRx without addressing capabilities may be sufficient [12].

[5]Sensitivity may degrade, as higher signal-to-noise ratio is required to detect the address information.

WuRxs can have fixed or variable addressing. Fixed addressing allows the receiver to wake up only when a specific address is received. Shift-register-based circuits typically support only a single predefined address in the comparison circuit. Many MAC protocols require cluster broadcasts, where multiple nodes wake up simultaneously using a single WuPt [27], [86]–[89]. In such cases, a second address, called a cluster address [90], or a bit mask [91] is needed to allow multiple WuRxs to respond.

We characterized nearly all WuRxs that use a microcontroller for address matching as having variable addressing. A microcontroller can be programmed to recognize multiple addresses and trigger an interrupt accordingly. However, there are exceptions where microcontrollers are used without variable addressing. Doorn et al. [92] used the microcontroller's ADC to measure LF amplitude without performing address matching. In [93], we proposed a WuRx where the RS-232 interface of the microcontroller was used to match the LF signal. Since the LF signal is a square wave, only signals matching the baud rate of the RS-232 interface were accepted, meaning this WuRx did not have addressing capabilities.

C. Sensitivity, Latency, and Power Consumption

In wireless communication, the range of a link depends on several factors, including link budget, carrier frequency, antenna gain, antenna efficiency, the position of the transmitter and receiver, and the surrounding environment [41]. Many of these factors cannot be adjusted in wireless sensor networks and are fixed for a given application. Even antenna gain is often limited to values close to one, as omnidirectional antennas are preferred. These antennas are crucial for typical place-and-forget applications, where sensors must be deployed without requiring specialized knowledge or equipment [29], [89]. Directional antennas require precise alignment, which increases installation complexity and cost.

The link budget is the most critical factor influencing the range of WuR communication. It is defined as the ratio between transmission power and receiver sensitivity. Transmission power is limited by regulatory restrictions for license-free frequency bands. However, in practice, the transmission power of commercial WuTx ICs is often lower than the regulatory maximum. As a result, the sensitivity of the WuRx plays a dominant role in determining the communication range. [89]

Sensitivity, latency, and power consumption are the most important parameters for evaluating WuRxs. These parameters are interdependent and must be balanced for optimal performance [18], [19], [38]. For example, WuRxs with high sensitivity often use RF amplifiers or power detectors, which increase power consumption. On the other hand, duty cycling can reduce power consumption but increases latency, as the WuRx cannot receive WuPts while in sleep mode. In such cases, the WuTx must transmit multiple WuPts to ensure successful wake-up [20]. The following subsections provide detailed discussions on sensitivity, latency, and power consumption, along with definitions and measurement methods.

1) Sensitivity: There is no universally accepted definition of receiver sensitivity. In our previous work [66], [94], we

discussed the need for a clear definition. Different studies define sensitivity in various ways, leading to inconsistencies in reported values. Many articles describe sensitivity as the lowest reception power at which the WuRx can receive a WuPt [30], [95]. Magno and Benini [38] defined it as the lowest power level where the WuRx can receive a WuPt reliably. Bdiri et al. [65] described a packet error rate (PER)-based measurement with PER = 1% as the sensitivity limit.

The transition of PER from 0% to 100% near the sensitivity threshold is not sharp. In [66], we observed that the transition occurred over more than 2 dB. Other WuRxs may exhibit even wider transitions. Some studies define sensitivity at a lower PER threshold, while others use a higher threshold, leading to an uncertainty of at least 2 dB [30], [38], [65], [95]. In [66], we used a 30% PER threshold, justifying this choice based on the typical collision rate in busy wireless sensor networks.

Another ambiguity in sensitivity measurements concerns the definition of RF power. In amplitude modulation or on-off keying (OOK), the peak-envelope power and average signal power are not equal. For a square-wave LF signal with a 50% duty cycle, the difference is 3 dB. In some WuPts with additional LF OOK modulation, the difference is approximately 6 dB, as discussed in Subsection III-E. Studies indicate that average signal power is generally used in RF communications. Del Prete et al. [45] explicitly based their experiments on average power. Many articles measure WuPt power using spectrum analyzers, which also report average power [65], [95]. Even the ETSI EN 300 220-1 effective-radiated power measurement is based on spectrum analyzers [96]. However, some studies use peak-envelope power instead. Sutton [97] employed pulse modulation of an RF generator for sensitivity measurements. Khodr et al. [98] reported both the on and off RF levels of the WuPts.

In [66], we defined sensitivity based on average signal power. Converting sensitivity values between different definitions requires precise knowledge of WuPt timing and coding, which is often not provided in the reviewed articles. Performing these sensitivity conversion for the reviewed articles is therefore nearly impossible.

In cases where sensitivity was not explicitly measured or specified, we estimated it using Friis' equation [41], based on reported values for range, frequency band, and transmission power. In Section V, we marked such estimations with footnote 11.

2) Latency: Generally, latency is defined as the total time required for an event detected by a transmitting node to propagate to the receiving node. This includes WuPt transmission, address matching, and the activation of the interrupt signal. Fig. 9 illustrates the timing components that contribute to latency.

When a sensor node transmits a WuPt, a setup time t_{setup} is required to initialize the WuTx. If the MR is used as the WuTx, it must start up and be configured before transmission [13]. Most WuPts consist of a preamble (t_{pream}) followed by address symbols. The duration of the address transmission, t_{addr}, depends on the number of symbols n_{sym} and the symbol rate f_{sym}:

$$t_{\text{addr}} = n_{\text{sym}} / f_{\text{sym}} \tag{3}$$

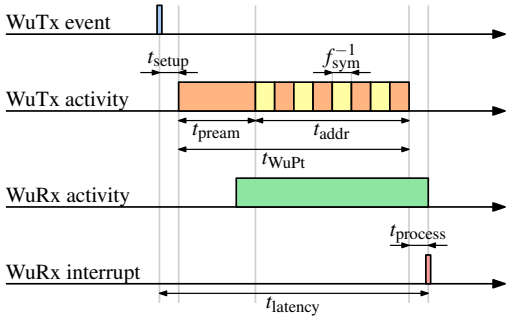

Fig. 9. Timing diagram illustrating WuR communication latency

The WuRx requires the preamble to initialize its reception mode and ensure reliable address decoding. Since only a few symbols are needed for addressing, high symbol rates are not essential [1]. After receiving all address symbols, the WuRx may need additional time t_{process} to process the address before raising the interrupt signal [99].

The total latency of WuR communication t_{latency} is given by:

$$t_{\text{latency}} = t_{\text{setup}} + t_{\text{WuPt}} + t_{\text{process}} \tag{4}$$

$$t_{\text{WuPt}} = t_{\text{pream}} + t_{\text{addr}} = t_{\text{pream}} + n_{\text{sym}} / f_{\text{sym}} \tag{5}$$

However, setup time and processing time are often not specified in the reviewed articles. To provide a standardized metric, we use WuPt duration t_{WuPt} as a measure of the communication latency in this article. This is also the value, we displayed in Section V.

With asynchronous duty-cycled WuRxs, the WuPt duration must be longer than the cycle period of the WuRx ($t_{\text{WuPt}} > t_{\text{cycle}}$). Longer WuPts not only increase communication latency but also impact WuTx power consumption. The longer the WuPt, the longer the WuTx remains active. [1] Since MR transmission power is typically in the milliwatt range, this significantly affects battery life in battery-powered WuTx nodes. In some applications, where the WuTx is mains-powered, its power consumption is less critical.

3) Power Consumption: According to our definition, the power consumption of a WuRx refers to the total power used by all its components without any WuPts on the channel. However, it is often unclear which components should be included in this measurement. For example, if a microcontroller is used for address matching, its power consumption might be included in the WuRx's total power. In [93], we argued that the microcontroller remains available for other tasks and should not be considered part of the WuRx power consumption. The clock oscillator of the microcontroller must remain active to ensure immediate response to a WuPt. However, since most wireless sensor nodes require a running clock for other tasks, its power consumption should not be attributed to the WuRx. Some studies, such as [17], include the microcontroller's power consumption in their measurements.

The power consumption of a WuRx can be estimated based on the circuit schematic and the components used. However, it should always be verified through direct measurement. The quiescent current of the ICs used in the WuRx is often the

primary contributor to power consumption. Low-power ICs should be chosen during design, but other factors can also increase power consumption and are often overlooked.

All resistors in a WuRx circuit can result in unwanted power loss. High-value resistors should be used to minimize the power loss. For example, a 1 MΩ resistor consumes 9 µW at 3 V, while a 10 MΩ resistor reduces this to 900 nW. However, high resistance can slow down circuit response due to parasitic capacitances. A 10 MΩ resistor with 1 pF capacitance forms a low-pass filter with a 16 kHz cutoff frequency, which may limit performance[6]. Additionally, large resistors in series with decoupling capacitors can significantly increase the turn-on time of the WuRx. Charging a 1 µF capacitor through a 10 MΩ resistor takes 30 s to reach 95% of the supply voltage[7].

Resistors connected to IC outputs can also increase power consumption when the outputs are activated. For example, the preamble detection circuit proposed by Magno et al. [38] uses a 1 kΩ and 100 kΩ resistor in series on a comparator output, as shown in Fig. 10. When the comparator output is turned on, approximately 28 µW are consumed, assuming a 1.8 V supply voltage and a 200 mV diode drop from the 1N5817 datasheet. To prevent unnecessary power loss, the circuit should ensure that the comparator output is active only for short durations or automatically turns off.

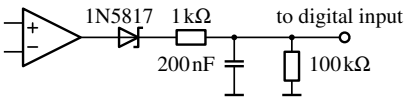

Fig. 10. Schematic of the preamble detector proposed by Magno et al. [38]

Pull-up and pull-down resistors are commonly used in digital circuits to set a known signal state. Pull-up resistors are required whenever an open-collector or an open-drain circuit is connected to a digital input. However, when an open-drain output is in the low state, current flows through the pull-up resistor, increasing power consumption. The resistor value is limited by speed requirements and the parasitic capacitance of traces and inputs.

Different address correlator designs illustrate the impact of resistor choice on power consumption. Ammar et al. [100] used a multi-input AND gate to check for a full address match, as shown in Fig. 11 (a). This method requires specialized ICs or multiple cascaded logic gates. Khodr et al. [98] proposed using open-drain XNOR gates instead, as seen in Fig. 11 (b). The outputs are connected together with a pull-up resistor to ensure a high state when all address symbols match. However, when at least one XNOR gate outputs a low level, current flows through the pull-up resistor, increasing power consumption. The prototype photograph in [98] shows a 390 kΩ resistor. A 390 kΩ pull-up resistor at 3 V results in 23 µW of additional power loss. Only if all address symbol are matched, no XNOR gate is low and the output is pulled high by the pull-up resistor.

Capacitors in the circuit can also increase power consumption if they are frequently charged and discharged. The power

[6] $f_c = 1/2\pi RC$
[7] $t_{95\%} = 3RC$

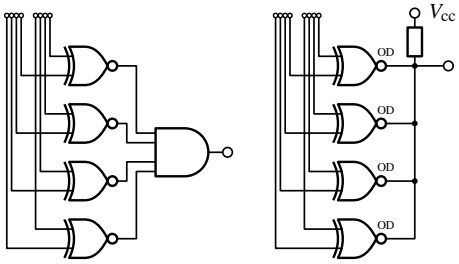

Fig. 11. Schematics of 4-bit address correlators. (a) Design by Ammar et al. [100], using XNOR gates and a multi-input AND gate. (b) Design by Khodr et al. [98], using open-drain XNOR gates.

dissipation caused by a capacitor C is

$$P = (V_{\max}^2 - V_{\min}^2)\, f C, \tag{6}$$

where $V_{\min}$ and $V_{\max}$ are the lower and upper voltage limits of a square-wave signal with frequency f applied to the capacitor. [101, p. 754]

Decoupling capacitors are essential for circuit stability, but in duty-cycled or power-gated WuRxs, they are repeatedly charged and discharged as the ICs power on and off. A 100 nF capacitor at 3 V with a 30 Hz duty-cycling frequency dissipates 27 µW.

Ammar et al. [100] proposed a local oscillator using a resistor, a capacitor, and inverters. The design uses a 12.5 nF capacitor at 200 kHz, where the capacitor charges and discharges between the hysteresis limits of a logic gate, estimated at 30% and 70% of the 0.9 V supply voltage. Based on (6), this results in 810 µW of additional power dissipation.

Most WuRx implementations consume more power during WuPt reception than in idle mode. Some studies include this behavior by estimating power consumption based on expected network traffic [35], [65], [72]. However, actual power consumption varies depending on the communication environment. Instead of estimating an average power value, we prefer using a separate measurement false wake-up energy waste (FWuEW), which quantifies the additional energy consumed during an unintended wake-up. False wake-ups can occur due to WuRx malfunctions, noise, interference, or unintended packets on the channel. [20], [30]

For always-on WuRxs, FWuEW is generally low. However, for duty-cycled and power-gated WuRxs, it is higher due to increased power consumption during reception. Both types of WuRxs extend their reception window when they detect a WuPt preamble, further increasing energy consumption.

FWuEW is an important parameter that should be measured and reported for all WuRx implementations. It allows researchers to accurately calculate or simulate the real power consumption of a WuRx in specific applications and protocols. However, only few articles provide detailed FWuEW measurements. Calculating this value for all reviewed implementations is beyond the scope of this article, as it requires detailed schematics and firmware behavior, which are often not fully disclosed in publications.

D. Secondary Wake-up Receiver Parameters

Sensitivity, latency, and power consumption are the three main parameters defining WuRx performance. These were discussed in the previous subsection. This subsection focuses on additional parameters such as supply voltage, robustness, reliability, cost, size, component availability, and modulation.

1) Supply Voltage: Fig. 12 shows the supply voltages used in the reviewed prototypes. For 31 prototypes, supply voltage information was not available. Most prototypes operate between 3.0–3.3 V, which aligns with the voltage of common batteries such as coin cells or two alkaline cells. Operating within this range eliminates the need for voltage converters.

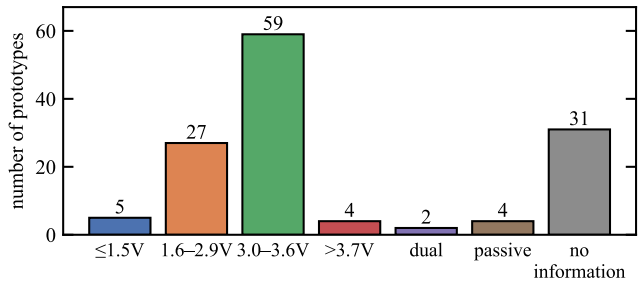

Fig. 12. Reviewed prototypes classified by supply voltage. Passive WuRxs [5], [75]–[77] do not require a supply voltage.

Some prototypes operate at lower voltages between 1.6–2.9 V, requiring voltage conversion when powered by standard batteries [19]. Linear regulators offer low quiescent power but have limited efficiency, while switching regulators provide high efficiency but require additional components and generate switching noise [101, pp. 594f]. Lowering the supply voltage reduces power consumption, as many circuits draw less current at lower voltages. In [66], reducing the voltage by 20% from 3.0 V to 2.4 V decreased power consumption by 29% from 9.9 µW to 7.1 µW. Lithium-ion batteries require voltage converters since their maximum voltage (4.2 V) exceeds the limits of many common ICs [4].

Five prototypes in our survey operate at extremely low voltages of 1.5 V or less [27], [44], [100], [102], [103]. While this reduces power consumption, it also limits the choice of compatible ICs.

Undervolting ICs is another method to extend battery life [104]. However, this approach requires extensive testing to ensure stability across temperature variations. Additionally, different temperature ranges must be tested to exclude any temperature-depended effects. Some articles [14], [105] appear to undervolt LF receiver ICs, but they do not discuss reliability.

Four articles [21], [67], [106], [107] use voltages above 3.6 V. Additionally, Saez et al. [62] employ a dual supply of $\pm 3,$ V. Higher voltages require additional batteries or boost converters, which can be implemented using charge pumps or switching regulators. Charge pumps are simple and low-cost but have lower efficiency and limited current capacity [101, pp. 638f].

2) Robustness and Reliability: False wake-ups occur when a WuRx activates due to noise, interference, or unintended packets. This leads to unnecessary power consumption and can increase collisions if the protocol allows immediate MR transmission after wake-up [1], [53], [108], [109]. If the addressing algorithm is not univocal, unintended wake-ups can happen when non-matching WuPts appear on the channel [90]. This issue is further discussed in Subsubsection III-F5.

Since most WuRxs use wideband RFEDs, they are susceptible to interference from nearby frequency bands. In [36], we measured the signal-to-interference ratio of our WuRx prototypes and found that adding narrow RF band-pass filters improved robustness. Indoor range tests confirmed better immunity against environmental interference.

Missed wake-ups occur when a valid WuPt is on the channel, the WuRx is within range, but the signal is not detected. PER measurements can reveal whether the WuRx suffers from random packet loss. WuRx prototypes should minimize packet loss to ensure reliable operation. [20]

Addressing reliability is also crucial. Some coding schemes experience packet loss when long sequences of consecutive symbols occur–high run length limit (RLL). Special coding techniques can mitigate this issue, which we will discuss in Subsubsection III-F4. [90]

3) Cost, Size, and Component Availability: Piyare et al. [1] suggested that a WuR should cost only 5–10% of the total sensor node cost. However, we argue that WuRs enable applications that were previously impossible due to battery life limitations. In some cases, WuRs may justify higher costs if they extend network lifetime or reduce cabling efforts.

COTS WuRxs are useful for prototyping and small-scale production. However, for large-scale manufacturing, WuR designs should transition to ASICs to reduce cost and size. While cost considerations are important, some research prototypes include multiple RF front-ends, increasing complexity and price. For example, some designs use multiple RF front-ends to detect frequency-shift keying (FSK) WuPts [27], [62], [107], [110]. The trade-off between cost and performance should be carefully evaluated.

Certain designs also require bulky components. For instance, Hutu et al. [107] proposed a WuRx using cavity filters for an orthogonal frequency-division multiplexing (OFDM)-based wake-up scheme. These filters were large (15×5 cm), making them impractical for small sensor nodes.

In [36], we discussed alternative RF filter technologies. Filters based on microstrip lines require resonator sections. More sections are needed for sharper filter response. However, the size grows linear. Each section requires a minimum path length of a quarter wavelength. For 868 MHz, $\lambda/4 = 86$ mm. Even with specialized folding techniques, such filters are larger than the typical sensor node's battery. Filters like these are not suitable to be used in the sub-Gigahertz bands.

Prototypes should use commercially available components to ensure reproducibility. However, many studies rely on obsolete components. For example, 40 prototypes in our survey used the HSMS-285x diode, which was discontinued in 2017 [111]. Some articles published after 2020 still use this component [112]–[116]. Similarly, the ATA5283 LF receiver used in [46], [117] was discontinued in 2008 [118]. One the other hand, the articles were published in 2018 and 2019.

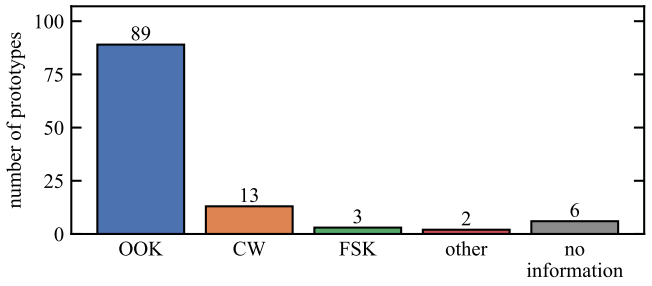

Fig. 13. Reviewed RF prototypes classified by modulation scheme

4) Modulation: Fig. 13 presents the number of RF prototypes reviewed in this study, categorized by the modulation technique used. A significant majority, 89 out of 113 RF prototypes, utilize on-off keying (OOK). Passive RFEDs can directly decode OOK signals, where the presence of an RF signal represents a high state (H), and the absence represents a low state (L). Many WuRxs also apply secondary modulation in the LF domain, which is discussed in Subsection III-E and Subsubsection III-F2.

The sharp transitions in OOK signals lead to a high occupied bandwidth for the WuPt. Regulatory constraints limit the bandwidth available for license-free RF transmission. For OOK modulation, the bandwidth of the WuPt is significantly larger than the highest frequency of its envelope. Del Prete et al. [45] simulated a WuPt bandwidth of 37 kHz for a maximum envelope frequency of 1 kHz. In our previous experiments [66], we measured a WuPt bandwidth of approximately 1 MHz for an envelope frequency of 18.7 kHz.

Pulse shaping can reduce the bandwidth of OOK-modulated signals by smoothing transitions. Magno et al. [38] claimed that Gaussian OOK is commonly used. Marinkovic et al. [102] also mentioned Gaussian OOK. However, there are no other studies providing measurements or discussions on pulse shaping.

This article differentiates between OOK and continuous wave (CW). CW is considered a simplified form of OOK, where the WuRx detects only the presence or absence of an RF carrier. CW-based WuRxs typically lack addressing capabilities.

Three reviewed WuRx prototypes can receive frequency-shift keying (FSK) WuPts by employing multiple RF channels transmitting OOK signals. This is achieved by using two complementary OOK signals to generate a switched FSK signal. These designs require duplicate RF front-ends.

Petrioli et al. [27] implemented a 4FSK WuRx by using four RF front-ends in parallel. A power splitter connects a single antenna to four channels, each consisting of an RF band-pass filter and a MAX2015 power detector for RF-to-LF conversion. The selected frequency channels were 2.410, 2.435, 2.455, and 2.480 GHz, with frequency deviations ranging from 20 MHz to 25 MHz.

Saez et al. [62] proposed a two-channel FSK-based WuRx. It operates on the 838 and 868 MHz channels, with a frequency deviation of 30 MHz. An MIC863 operational amplifier subtracts the signals from both channels, and the AS3933 differential amplifier processes the output. Compliance with legal requirements for transmission on 838 MHz is necessary.

Gavrikov et al. [110] used a similar approach, employing channels at 2.404 and 2.474 GHz, with a frequency deviation of 70 MHz. A MAX409 operational amplifier generates the difference signal.

FSK-based WuRxs offer potential improvements in sensitivity by using complementary channels. However, they have significant disadvantages. These systems require multiple RF front-ends, increasing costs and the number of required components. Using a single antenna necessitates power splitters, which introduce an insertion loss of 3 dB for a two-way splitter. Large frequency deviations require multiple WuTxs for transmission, further increasing cost and antenna requirements. If the frequency deviation is small, RF band-pass filters must be highly selective to prevent crosstalk between differential channels. Since commercially available filters have limited selectivity, FSK-based WuRxs require larger frequency deviations than those typically used for FSK communication in conventional MRs [36].

Two reviewed articles used different approaches for modulating the RF carrier. Del Prete et al. [45] investigated power-optimized waveforms for WuPts. By using OOK with a duty cycle below 50%, they increased the peak-envelope power while maintaining a constant average power. Higher peak-envelope power resulted in a greater output voltage from the RFED, improving sensitivity. A 9 dB improvement was measured when the duty cycle was reduced to 12.5%. However, reducing the duty cycle leads to shorter WuPt pulses, which increases the occupied bandwidth. Simulations showed that a 12.5% duty cycle with a symbol width of 1 ms resulted in a bandwidth of 140 kHz.

Hutu et al. [107] implemented a frequency-signature-based WuPt using an OFDM transmitter. This method encodes a specific pattern of sub-carriers to represent a WuRx address. Four distinct frequency components were used in the 915 MHz band. The WuRx processed direct and complementary paths, where the complementary path contained filters with an inverse frequency response. By subtracting the signals from both paths, the WuRx could distinguish valid WuPts from background noise. This design enabled the detection of six different addresses.

III. Wake-up Receiver Components

A. RF Front-end

As shown in Fig. 5, the RF domain consists of the RF input, RF filter, and RF amplifier. The RFED is discussed separately in Subsection III-B.

1) RF Input: As discussed in Subsection II-A, the MR and WuRx can either share an antenna via an antenna switch or use a dedicated antenna. If the antenna is shared, its design depends on the requirements of both the sensor node and the MR. However, when a separate WuRx antenna is used, it can be optimized for wake-up communication.

Directional antennas can improve the WuR range by increasing antenna gain. However, they have limitations when sensor nodes communicate with multiple nodes in different directions.

The need for proper alignment complicates the deployment of place-and-forget sensor networks, as trained personnel would be required for installation. Directional antennas must be correctly aligned, otherwise the antenna's directivity reduces the WuR range.

Some studies integrate the antenna and RFED into a rectenna, which is common in RF energy harvesting applications. This design improves sensitivity but is typically optimized for higher received power levels, making most rectennas unsuitable for long-range WuR communication [89], [119]. Only a few studies [78], [120], [121] implement this approach.

Most reviewed prototypes use a 50 Ω input impedance. Most matching circuit are designed for a 50 Ω input.

2) RF Filter: Out of the 113 RF prototypes reviewed in this study, only 24 utilized RF filters. Among these, 17 incorporated surface acoustic wave (SAW) filters. We previously discussed the advantages and limitations of different filter technologies in [36]. Filters based on lumped components often lack precision due to manufacturing tolerances in COTS components. Microstrip-based filters, while more precise, require significant physical space, as discussed in Subsubsection II-D3. SAW filters are well suited for WuRx applications because they offer high accuracy, narrow bandwidth, low insertion loss, and compact size.

Hutu et al. [107] used cavity filters in their WuRx prototype. As described in Subsubsection II-D4, these filters enabled the reception of OFDM-like signals. Although cavity filters provide excellent selectivity, they are large in size. However, they allow for customized filter responses that enable the frequency signature detection.

Parks [122] implemented a notch filter using lumped components, including a tunable capacitor for fine adjustments. The filter exhibited a sharp reflection coefficient sweep S_{11}, demonstrating high selectivity [122, p. 56]. However, the insertion loss of the filter was not measured.

Petrioli et al. [27] developed an active filter using varactors for a 4FSK-compatible WuRx, as discussed in Subsubsection II-D4. This filter achieved a bandwidth of less than 10 MHz, but its insertion loss was not specified. Additionally, the filter consumed 168 µW of power.

A significant drawback of SAW filters is their insertion loss, which typically reduces the input signal by approximately 3 dB. This loss directly affects WuRx sensitivity because it reduces the power reaching the following building block. [5], [36], [93] In controlled lab experiments, a WuRx without a SAW filter demonstrates an approximately 3 dB improved sensitivity than one equipped with such a filter [36].

Despite this drawback, RF filters provide clear benefits. Experiments show that they reduce bandwidth, improve selectivity, and offer better interference rejection. In indoor measurements, WuRxs with sensitivities around −80 dBm benefited significantly from having SAW filters [36]. However, results from Oller et al. [123] were mixed, suggesting that the impact of RF filtering may depend on environmental factors.

RFEDs generally exhibit much wider bandwidths than SAW filters. Reducing bandwidth helps minimize Johnson–Nyquist noise and reject interference from adjacent frequency bands. The 868 MHz and 915 MHz bands are particularly susceptible to interference from high-power RFID and GSM signals [123]. Our research [36] confirmed that SAW filters effectively suppress these interfering signals. Further studies are needed to determine whether all WuRx designs benefit from RF filtering.

3) RF Amplifier: The RF amplifier in a WuRx is commonly referred to as a low-noise amplifier (LNA), although LNAs also exist in the LF domain. Among the 113 RF prototypes reviewed, only 11 incorporated RF amplifiers. The high power consumption of RF amplifiers often necessitates duty-cycling techniques to reduce energy usage. Only Bdiri et al. [35] and our own prototypes presented in [34], [36] achieved an average power consumption below 100 µW through effective duty-cycling. Other WuRxs equipped with RF amplifiers were designed for continuous operation [27], [106], [116], [124], [125] or had insufficient duty-cycling to significantly reduce power consumption [67], [68].

Some studies [34], [36], [68], [124] used COTS RF amplifiers. These devices provide limited gain and consume significant power. In [34], two cascaded amplifier ICs achieved a gain of 27.6 dB, but their total power consumption was 20 mW.

In contrast, custom-designed RF amplifiers optimized for WuRxs achieve higher gain with lower power consumption. Since WuRxs typically use OOK modulation, high linearity is not necessary, allowing for simplified amplifier designs. When designing RF amplifiers for duty-cycled WuRxs, fast turn-on times are crucial. Faster response times allow the WuRx to detect WuPts quickly, minimizing active periods and improving energy efficiency. [35]

Several studies [35], [67], [106] developed WuRx amplifiers using bipolar junction transistors (BJTs). Bdiri et al. [35] designed a two-stage common-collector amplifier that achieved 35.5 dB gain while consuming only 1 mW.

Frøytlog et al. [106] implemented a cascoded BJT amplifier with a buffer stage for impedance matching between the RF amplifier and RFED. This design achieved 30.9 dB gain with 6 mW power consumption. However, it required a 6 V supply, necessitating additional batteries or a boost converter. In a later design [67], the power consumption was reduced to 3 mW, but the gain decreased to 23 dB.

Wu et al. [116] developed a WuRx with a sensitivity in the range of −98 to −90 dBm. Their design employed a reflection amplifier based on a tunnel diode, a device characterized by negative differential resistance. Using microstrip matching, they achieved 38 dB gain at 915 MHz, while consuming only 226 µW. However, the tunnel diode used (AI301A) is no longer commercially available, making replication difficult. In general, no tunnel diodes are off-the-shelf available today, and they can only be obtained as stock remainder. Therefore, it is difficult for other researchers to reproduce this design.

B. RF Envelope Detector

Fig. 14 presents the classification of the reviewed RF prototypes based on the RFED technology. A significant majority, 99 out of 113 prototypes, use diode-based RFEDs. The following subsections focus on different diode-based RFED

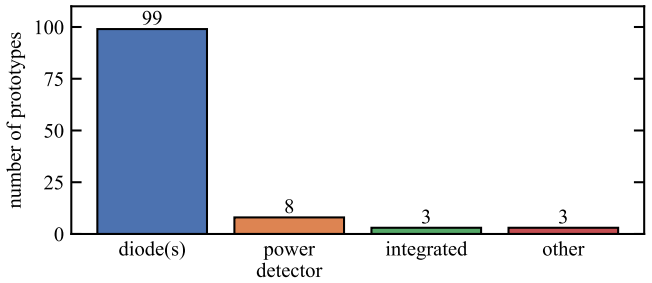

Fig. 14. Reviewed RF prototypes classified by RFED technology

configurations. Other detection technologies are discussed at the end of this subsection in Subsubsection III-B6.

1) Diode-based Envelope Detector Theory: A diode acts as a nonlinear element that rectifies the RF signal. After low-pass filtering, only the low-frequency envelope remains. As discussed in Subsubsection II-D4, passive RFEDs detect OOK signals. With proper RF band-pass filtering, they can also receive FSK signals [62], [110].

The open-circuit output voltage V_{ED} of the diode-based RFED depends on the incident RF power P_{RF}. This function has two distinct regions. In the square-law region at low power levels, V_{ED} is proportional to P_{RF}. In the linear region at higher power levels, V_{ED} is proportional to the square root of P_{RF}. [126, p. 585] Most WuRxs operate in the square-law region, while energy-harvesting rectifiers are often optimized for the linear region [45]. The boundary between these regions is given by:

$$V_{\mathrm{ED}} < n V_{\mathrm{T}} \approx 26\,\mathrm{mV}, \text{ with } n \approx 1, T = 300\,\mathrm{K} \tag{7}$$

V_{T} is the thermal voltage, calculated by Boltzmann's constant, absolute temperature, and electron charge. For typical WuRx RFEDs, this boundary corresponds to an RF power of approximately $-30\,\mathrm{dBm}$ [42], [93]. In the square-law region, the output voltage of the RFED follows:

$$V_{\mathrm{ED}} = \gamma P_{\mathrm{RF}} \tag{8}$$

where γ represents the voltage sensitivity of the RFED, which is a key performance indicator. [126, p. 568]

The video resistance R_{v} of the RFED can be modeled as a Thévenin equivalent resistance. It contributes to the Johnson–Nyquist noise voltage, given by:

$$V_{\mathrm{n}} = \sqrt{4 k_{\mathrm{B}} T f_{\mathrm{BW}} R_{\mathrm{v}}} \tag{9}$$

where k_{B} represents Boltzmann constant, T absolute temperature, and f_{BW} signal bandwidth.

Despite its importance, no study has systematically measured RFED noise levels. The actual noise likely depends on the diode configuration, environmental factors, and filtering. The video resistance can be estimated by measuring the voltage drop under different loading conditions, as demonstrated in [93].

2) Diode Configuration: Three main diode configurations are commonly used in WuRxs and are presented in Fig. 15. The single diode (SD) configuration performs half-wave rectification. The voltage doubler (VD) configuration uses two diodes to achieve full-wave rectification, theoretically doubling the output voltage. The VD presented in Fig. 15 is known as the Greinacher voltage doubler. The input of the circuit must be AC-coupled to allow for RF and LF signal to share the same ground reference. The voltage multiplier (VM) configuration extends the voltage doubler concept to multiple stages, increasing the output voltage further. The VM presented is known as the Dickson voltage multiplier. The VM can be extended freely to utilize six, eight, ten, or more diodes. [127]

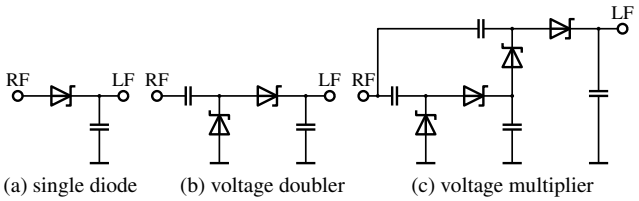

Fig. 15. Schematics of typical diode configurations used in the reviewed prototypes

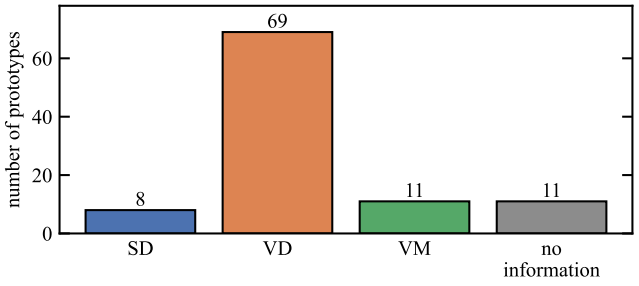

Fig. 16. Reviewed prototypes with diode-based RFEDs classified by diode configuration

Fig. 16 shows the distribution of prototypes based on diode configurations. A majority, 68 out of 99, use the VD configuration. Fewer studies use the SD configuration, with only eight prototypes.

Pursula et al. [128] analyzed the performance of biased and unbiased SD configurations. Their results showed improved voltage sensitivity with biasing. However, the sensitivity values remained lower than those reported in other studies. The voltage sensitivity of different RFEDs is further discussed in Subsubsection III-B5.

McCaffrey et al. [129] used a different single-diode configuration. Their design included an AC-coupled input capacitor, as shown in Fig. 15 (b). The circuit used a single-wave rectifier with a diode connected to ground. This design is well known in RF energy harvesting applications, where it provides good efficiency at high RF input power levels [127]. In their prototype, the diode was biased using a $2\,\mathrm{V}$ source and a $3.3\,\mathrm{M\Omega}$ resistor.

Siniscalchi et al. [103] also implemented a biased SD configuration. Their study focused on the impedance matching network of the RFED. However, their sensitivity measurements relied on an external RF amplifier, an analog-to-digital converter, and numerical data analysis on a computer. A practical WuRx should integrate LF amplification and address decoding using low-power circuitry.

Trinh et al. [75] proposed a WuRx with a SD-based RF front-end, but they amplified the LF signal with a VM. The OOK signal was modulated at 20 kHz, and the LF VM provided passive amplification. The VM increased the output signal by a factor of four. Since this WuRx operated in the linear region of the diode RFED and had degraded sensitivity, the VM provided an effective 10 dB improvement.

The VM configuration was used with varying numbers of stages. Studies such as [78], [102], [130] implemented a four-diode VM. Kaushik et al. [77] used the highest number of stages among the reviewed prototypes, incorporating 14 diodes in their RFED.

Some studies examined the trade-offs between low and high stage counts in voltage multipliers. Increasing the number of stages theoretically increases the output voltage. However, parasitic effects and losses reduce actual performance [76]. Additionally, higher stage counts increase the video resistance R_v of the RFED. This increased resistance leads to additional noise and can significantly affect the circuit when loaded by an amplifier stage or address decoder.

In [93], we measured an video resistance of approximately 5 kΩ per diode. A 12-diode VM would therefore reach an estimated 60 kΩ, which could become problematic due to loading effects in the subsequent circuit stages. Furthermore, increasing the number of diodes raises the cost and complexity of the RF front-end due to additional components [123].

3) Diode Components: Schottky diodes are the preferred choice for RFEDs due to their low forward voltage and suitability for high-frequency applications. Among the 99 reviewed prototypes, only four different diode components were identified. Fig. 17 shows the distribution of these components across the reviewed articles.

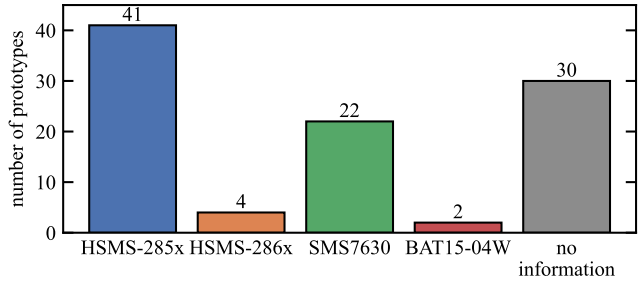

Fig. 17. Reviewed prototypes with diode-based RFED classified by the utilized diode component

The HSMS-285x family is the most widely used in the reviewed prototypes. However, this component was discontinued by the manufacturer in December 2017 [111]. The HSMS-286x series has slightly different properties compared to the HSMS-285x. The HSMS-286x was used in only four studies [103], [128], [129], [131].

The SMS7630 is a well-known alternative and remains in production. Del Prete et al. [42] used this component in 2015. It is also the standard choice in prototypes developed by our research group. Other researchers have used the SMS7630 in studies such as [68], [78], [98], [105]. In [93], we compared the HSMS-285x and SMS7630, finding that the HSMS-285x exhibited 28% higher voltage sensitivity. However, its video resistance was also 68% higher.

Polonelli et al. [47], [132] proposed using the BAT15-04W diode in their RFED. However, the articles did not provide a clear justification for this choice, nor did it include measurements of voltage sensitivity or video resistance.

4) Impedance Matching: Impedance matching is crucial for ensuring that most of the RF power is transferred to the RFED. Without proper matching, RF reflections can significantly reduce voltage sensitivity. Typically, 50 Ω impedance matching is used when WuRxs include RF filters, antenna switches, or unified antennas. However, when a dedicated antenna is used, matching to the antenna impedance is possible. Fig. 18 shows the number of reviewed prototypes classified by their impedance matching technology. [133]

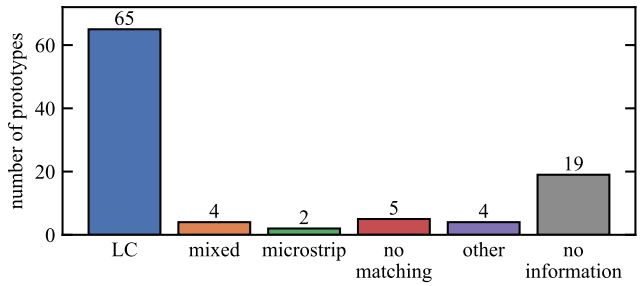

Fig. 18. Reviewed prototypes with diode-based RFED classified by the utilized matching technology

A majority of 64 out of 99 passive RFED prototypes use lumped components (LC) for impedance matching. Different circuit designs are employed to optimize the RFED input. Inductors in the nanohenry range and capacitors in the picofarad range form resonance circuits that minimize losses. Matching circuits with high-quality factors improve gain and reduce reflections. However, these circuits are highly sensitive to frequency shifts by diode parasitics.

Del Prete et al. [45] used microstrip lines for impedance matching. Their design included a shorted and an open stub to create a dual-band matching circuit for the 868 MHz and 2.45 GHz bands. Saab et al. [84] designed a rectifier circuit for harvesting ambient wireless signals in the 2.45 GHz band. Their design included dedicated transmission lines for the feed, load, and low-pass filter. Some studies used a combination of lumped components and microstrip lines for impedance matching [42], [75], [79], [98].

Three studies incorporated impedance matching directly into their rectenna designs [78], [120], [121]. In these designs, the RFED is matched to the antenna impedance rather than the standard 50 Ω. This approach is beneficial because antennas can be designed with higher impedances that better match passive RFEDs [134].

Frøytlog et al. [106] used a buffer circuit with BJTs to match between their RF amplifier and RFED. Their design used a push-pull stage with npn and pnp transistors. However, the study did not provide details on the reflection coefficients or matching performance. The buffer circuit consumed 600 µW, making it unsuitable for always-on operation.

Some studies did not specify whether they included impedance matching circuits. However, in [47], [92], [123], [130], [131], it was clearly shown that no matching circuits were used. The absence of impedance matching leads to reduced voltage sensitivity and degraded WuRx sensitivity. In these studies, reported sensitivity values ranged between -48 to -31 dBm.

5) Voltage Sensitivity: Voltage sensitivity is a key parameter for evaluating the performance of an RFED and its impedance matching circuit. It quantifies how effectively the RFED converts RF power into an output voltage. Voltage sensitivity can be measured by applying a CW signal to the RFED and recording the resulting output voltage. According to (7), the output voltage per diode stage should not exceed 26 mV, as this is the upper limit of the square-law region [126, p. 568]. A higher voltage sensitivity generally improves the performance of a WuRx, as less LF amplification is required to achieve the same sensitivity limit.

We examined all reviewed articles for evidence of voltage sensitivity measurements. If direct values were not provided, we estimated them based on figures or descriptions. Tab. I summarizes the measured voltage sensitivity values found in the literature and the corresponding RF front-end properties.

Del Prete et al. [45] reported the highest voltage sensitivity at 137 mV/µW in the 868 MHz band. Their design included a dual-band microstrip-line matching circuit. The VD configuration, using SMS7630 diodes, was also implemented in several other studies but with lower reported sensitivity values.

In general, voltage sensitivity tends to be lower in the 2.45 GHz band compared to 868 MHz. This can be attributed to increased free-space path loss and reduced efficiency of the RFED at higher frequencies. Additionally, the inclusion of an RF filter results in a decrease in voltage sensitivity due to insertion losses. This effect was confirmed in our direct measurements, comparing WuRxs with and without SAW filters [36], [93].

The SD configuration generally produces lower voltage sensitivity values than the VD configuration. Our measurements in [93] showed an approximately 50% lower voltage sensitivity of SD configurations. This trend is also visible in Tab. I.

Kumberg et al. [136] measured voltage sensitivity in an antenna diversity WuRx node. Their study showed an improvement from 25 mV/µW for a single-antenna configuration to 55 mV/µW when two antennas were combined passively.

In [66], we investigated whether manual tuning of the impedance matching circuit significantly affects voltage sensitivity. A manually tuned RFED achieved 45 mV/µW. However, when we built five additional identical prototypes without individual tuning, variations in component tolerances and diode parasitics caused a spread in voltage sensitivity values, ranging from 20–35 mV/µW.

Unfortunately, no reviewed articles reported voltage sensitivity values for WuRxs using the VM configuration. For later estimations in this article, we assume a typical voltage sensitivity of 40 mV/µW for RFEDs.

6) Other Envelope Detector Technologies: As shown in Fig. 14, most RF WuRx prototypes rely on diode-based RFEDs. However, other technologies have been explored, including transistor-based RFEDs, and power detectors.

RF power detectors are specialized integrated circuits designed to measure received RF power and generate a corresponding voltage output. These devices are capable of detecting RF signals with high sensitivity while maintaining a wide LF bandwidth. Tab. II summarizes the power detectors used in the reviewed literature.

Power detectors are high-precision measurement components and are therefore relatively expensive. Despite this, they can function effectively as RFEDs due to their wide LF bandwidth, which is typically larger than required for WuRx applications.

A trade-off exists between power consumption and sensitivity in power detectors. The LTC5508, for example, has a low power consumption of 1.65 mW at 3 V, but its sensitivity is limited to -32 dBm. In contrast, the LT5538 can detect signals down to -75 dBm but consumes 87 mW at 3 V. When power detectors are used in WuRxs, duty cycling is necessary to reduce average power consumption to the microwatt range.

Petäjäjärvi et al. [44] proposed a super-regenerative receiver operating at 28 MHz for human body communication. The RFED in this design used a BFR92A BJT and achieved a sensitivity of -97 dBm.

Yi et al. [139] presented another BJT-based envelope detector, using the BFU70F transistor in a common-emitter configuration. Simulations predicted an excellent WuRx sensitivity of -70 dBm, but experimental validation was limited to range measurements, which showed a maximum distance of 17 m. Using the Friis equation, this corresponds to an estimated WuRx sensitivity of approximately -45 dBm.

Luo et al. [140] explored the use of the P1110B RF energy harvesting module as an RFED. This module, developed by Powercast, integrates dedicated RF-to-DC conversion circuitry and voltage boosting. Performance measurements showed a voltage sensitivity of approximately 20 mV/µW, comparable to diode-based RFEDs listed in Tab. II.

Rup and Bajic [29] analyzed the EFR32BG22 system-on-chip [9], which integrates a WuRx for the 2.45 GHz band. The authors measured a sensitivity of -30 dBm. Given the maximum transmission power of 6 dBm for the EFR32BG22, this results in an estimated range of less than 1 m.

da Silva et al. [71] implemented a WuRx using the CC1200 MR. Many MRs include an RF power detection feature for carrier sensing. The authors leveraged this capability to detect WuPts on the channel. By duty cycling the MR, they achieved a minimum average power consumption of 93.2 µW.

C. LF Amplifier

LF amplifiers are essential for achieving sensitivity levels below -55 dBm. With a typical voltage sensitivity of 40 mV/µW (as discussed in Subsubsection III-B5), the RFED output at -55 dBm input power is only 126 µV. Such low voltages are challenging to detect, necessitating amplification before signal processing. The following discussion examines the various LF amplifier technologies used in WuRx prototypes.

TABLE I
VOLTAGE SENSITIVITY MEASUREMENTS AND RF FRONT-END

Ref.	RF in MHz	RF filter	Matching	RFED configuration	RFED components	γ in mV/µW
[5]	915	no	—	SD	HSMS-285x	50
[135]	2450	no	LC	VD	HSMS-285x	30
[128]	2450	no	LC	SD	HSMS-286x	7.9
[42]	868	no	mixed	VD	SMS7630	79
[42]	2450	no	mixed	VD	SMS7630	15
[45]	868	no	microstrip	VD	SMS7630	137
[45]	2450	no	microstrip	VD	SMS7630	81
[136]	868	no	LC	VD	HSMS-285x	25 / 55[1]
[137]	915	no	LC	VD	—	72
[32]	868	no	LC	VD	SMS7630	40
[93]	868	no	LC	VD	SMS7630	45
[93]	868	no	LC	VD	HSMS-285x	56
[93]	868	no	LC	SD	SMS7630	28
[93]	868	SAW	LC	VD	SMS7630	22
[105]	2450	no	LC	VD	SMS7630	22.5
[66]	868	no	LC	VD	SMS7630	45, 20–35[2]
[36]	868	no	LC	VD	SMS7630	47
[36]	868	SAW	LC	VD	SMS7630	29

[1] one or two antenna inputs [2] matching circuit verified, range of voltage sensitivities of five unverified prototypes

TABLE II
RF POWER DETECTORS USED IN WAKE-UP RECEIVER PROTOTYPES

Power detector	Frequency range in MHz	Power detector sensitivity in dBm[1]	Supply voltage range in V	Supply current in mA	LF bandwidth in MHz	Costs[2] in $	Reference
LTC5508	300-7000	−32	2.7–6	0.55	2	3	[125]
AD8362	50 Hz–3800	−52	4.5–5.5	20	0.5	13	[107]
LMV221	50–3500	−45	2.7–3.3	7.2	0.45	3	[138]
LT5534	50–3000	−60	2.7–5.25	7	50	9	[124]
MAX2025	100–3000	−65	2.7–5.25	17.3	6[3]	12	[27]
LT5538	40–3800	−75	3–5.25	29	20	8	[69], [70]

Typical performance parameters from the device's datasheet [1] for 900 MHz range [2] per piece for a 100-piece order [3] estimated by slew-rate and $S = \omega A$ [101, p. 328]

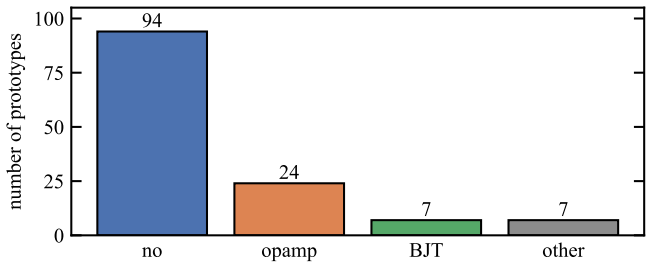

Fig. 19. Reviewed prototypes classified by the utilized LF amplifier

Fig. 19 shows the number of reviewed prototypes classified by LF amplifier type. Most prototypes do not include a dedicated LF amplifier. Among those that do, 27 use opamps, while only seven use amplifiers based on BJTs.

Trinh et al. [75] proposed an LF voltage multiplier (VM) to enhance the detection of an OOK-modulated WuPt at 20 kHz. Their four-stage amplifier achieved a gain of 4.

Bdiri et al. [37], [65] used an instrumentation amplifier, the MAX4461, which requires 700 µA supply current. To maintain low power consumption, they implemented power gating. Although instrumentation amplifiers are typically more precise and robust against interference, they are also costly and consume more power [101, pp. 356f].

Siniscalchi et al. [103] employed the mains-powered SR560 LF amplifier to verify WuRx sensitivity. However, as a mains-powered device, it should not be considered part of a battery-powered WuRx. Additionally, the authors relied on a computer-based data analysis program instead of an integrated low-power circuit for signal processing.

The following subsubsections discuss opamp-based LF amplifiers, their component selection, and schematics utilized. In the last subsubsection, we discuss the different BJT amplifiers used in the reviewed state of research.

1) Operational Amplifier Components: Selecting an appropriate opamp for an LF amplifier is crucial. Key parameters include quiescent current and gain–bandwidth product (GBWP). The GBWP determines the maximum gain achievable per amplifier stage, depending on the LF bandwidth of the WuPt signal. Increasing gain through multiple amplification stages is possible raises the component count and cost. [101, p. 223]

A clear trade-off exists between power consumption and GBWP. Low-power opamps typically have a low GBWP. For

instance, the TLV521 has a quiescent current of only 350 nA but a limited GBWP of 6 kHz. In contrast, the TSV6391A consumes 60 µA while achieving a GBWP of 2.4 MHz. [34], [141]

Decompensated opamps provide higher GBWP for the same power budget but require a minimum gain for stability [101, p. 524]. Since WuRx applications typically require high gain, using decompensated opamps can optimize performance. In [93], we used the decompensated MCP6141 opamp, which is only stable for gains above 10.

The MIC861 and its dual-channel version, the MIC863, are the most frequently used opamps in the reviewed studies [32], [57], [62], [142]. These devices provide a GBWP of 450 kHz while consuming only 4.2 µA per channel. They are among the few commercially available opamps with quiescent currents below 10 µA that provide sufficient gain for kilohertz-range signals.

2) Operational Amplifier Circuits: Various circuit configurations are used as LF amplifiers. Additional capacitors may be included for active filtering or AC coupling, but most circuits fall into three main categories. Fig. 20 illustrates these configurations along with their simplified transfer functions.

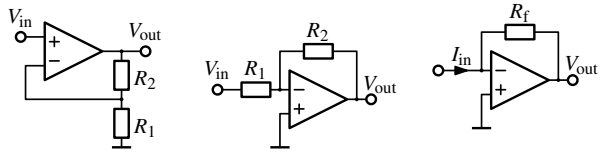

Fig. 20. Three different opamp-based circuits utilized in the reviewed prototypes

The non-inverting amplifier, shown in Fig. 20 (a), is the most common choice in the reviewed prototypes [34], [36], [43], [72], [93], [113]–[115], [141]. This configuration offers high input impedance, which is advantageous for amplifying RFED signals. As discussed in Subsubsection III-B1, the RFED's output impedance, known as video resistance, was measured at approximately 5 kΩ per diode stage in [93]. For a typical VD configuration, the video resistance is in the order of 10 kΩ.

The inverting amplifier, shown in Fig. 20 (b), is used in [68], [92], [143]. Although the signal is inverted, this does not present a major issue since polarity can be corrected either by reversing the RFED polarity or by adding another inverting stage. However, the input impedance of this configuration is approximately equal to resistor R_1, which is the smaller of the two gain-defining resistors [101, pp. 226f]. With high gain, R_1 must be small, typically in the kiloohm range, which loads the RFED output and reduces its efficiency.

A transimpedance amplifier, shown in Fig. 20 (c), is another suitable amplifier circuit. This configuration converts an input current signal into a voltage output [101, p. 537]. While commonly used in optical WuRxs with photodiodes [142]–[144], it is used in the RFED-based WuRxs by Schott et al. [32] and Qaragoez and Schreurs [78]. Designing a stable transimpedance amplifier can be challenging since operating near the GBWP of the opamp may cause instability and frequency response peaking. To mitigate this, a parallel capacitor is often added to R_f, but this significantly limits bandwidth. [145, pp. 283f]

Some WuRxs designed for FSK detection use a difference amplifier to process signals from two RFEDs tuned to different subcarrier frequencies. This approach is seen in [62], [107], [110], where the outputs of two envelope detectors are subtracted to detect the presence of a frequency signature. While the circuit for a difference amplifier is well known [101, p. 227], these articles do not provide details on their implementations.

For the prototypes in [56], [57], [70], there was insufficient information to determine the amplifier configuration used.

3) Operational Amplifier Biasing: Opamps have a limited output voltage swing, even for so-called rail-to-rail devices. This limitation becomes critical in single-supply applications, where the opamp must operate with a single positive voltage supply. Most WuRx prototypes use a single supply, as discussed in Subsubsection II-D1.

For the inverting and transimpedance configurations shown in Fig. 20, biasing is necessary for single-supply applications. If the RFED signal is amplified without biasing, the output voltage becomes negative, which is outside the operational range of a single-supply opamp. A common solution is to bias the non-inverting input and to AC-couple the RFED signal [32].

A simple way to generate a mid-supply bias voltage is by using a resistor divider, as demonstrated by Hakkinen and Vanhala [143]. The resistors should have high values (e.g., 10 MΩ) to minimize current draw. However, resistor dividers should not be heavily loaded, as this alters the output voltage. Adding a capacitor helps stabilize the bias voltage, but large values can lead to long startup times.

An alternative is to use a low-dropout regulator to provide a stable bias voltage. In [32], we used the MCP1811 regulator due to its low quiescent current of 250 nA. However, we observed noise and oscillations on the bias voltage.

For the non-inverting amplifier in Fig. 20 (a), biasing may appear unnecessary when using a rail-to-rail opamp. However, all opamps have an input offset voltage, which varies across devices and with temperature. The offset results from imbalances in the input transistor pair and can be either positive or negative. If the input signal is below this offset, the opamp cannot amplify it correctly. [101, p. 244]

Opamp datasheets specify both typical and maximum input offset voltage values. Designs should account for the worst-case value to ensure consistent performance across all manufactured devices. [101, p. 295] For example, the TLV521 opamp, used in [93], [141], has a typical input offset voltage of 0.1 mV but a maximum of ±3 mV [146]. Fig. 21 replicates the offset voltage distribution from the TLV521 datasheet, showing that only 35% of devices have an offset within ±0.1 mV, while all devices are within ±3 mV.

For most opamps used in WuRxs, the input offset voltage is in the range of 1 mV. Precision opamps with offsets in the microvolt range exist but are either costly or require manual trimming. [101, p. 244] Another option is a chopper-stabilized

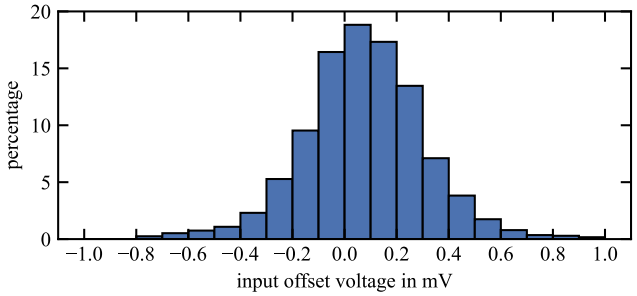

Fig. 21. Input offset voltage distribution of the TLV521 replicated from the datasheet [146]. The datasheet gives a input offset voltage of 0.1 mV typical and ±3 mV maximum.

or zero-drift opamp, such as the TLV333, used by Jong et al. [113]. This device has a maximum input offset voltage of only 15 µV. However, zero-drift opamps with low quiescent current are rare. The TLV333 consumes up to 28 µA, making it unsuitable for most always-on applications.

If the LF amplifier is limited to detecting signals above 1 mV, this significantly impacts WuRx sensitivity. Given the typical RFED voltage sensitivity of 40 mV/µW (Subsubsection III-B5), 1 mV corresponds to an RF power level of −46 dBm. To improve accuracy and sensitivity, biasing is required even for non-inverting configurations.

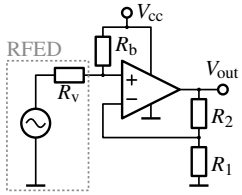

Fig. 22. Biasing circuit proposed in [93]. The RFED is modeled as a Thévenin equivalent.

A simple biasing circuit was proposed in [93] using a single pull-up resistor connected to the supply voltage, as shown in Fig. 22. The RFED is modeled as a Thévenin equivalent. The bias voltage V_{bias}, is determined by the resistor divider equation:

$$V_{\text{bias}} = V_{\text{cc}} \cdot \frac{R_{\text{v}}}{R_{\text{v}} + R_{\text{b}}} \tag{10}$$

For a 3 V supply voltage V_{cc} and a typical 10 kΩ video resistance R_{v}, the bias voltage is approximately 3 mV, sufficient to compensate for most input offsets. However, this resistor also forms a voltage divider with the RFED, reducing signal amplitude. The voltage at the non-inverting opamp input V_{NI} is calculated by

$$V_{\text{NI}} = V_{\text{ED}} \cdot \frac{R_{\text{b}}}{R_{\text{v}} + R_{\text{b}}}. \tag{11}$$

With R_{b} chosen to be 1000 times larger than R_{v}, signal attenuation is minimal (0.1%). However, the impact of back-biasing Schottky diodes in the RFED should be further investigated.

4) Amplifier Transfer Function: Opamp circuits can be equipped with various filters to optimize signal processing. Most opamps inherently act as low-pass filters due to their GBWP limit. Additional capacitors can be integrated into the circuits to create high-pass, band-pass, or sharper filter responses.

Oletic et al. [147] proposed a multi-channel filter system for detecting spectro-temporal features in audio signals. This application required narrow-band LF filters, which were implemented using opamps. The authors employed a generalized impedance converter (GIC) filtering circuit, claiming it has advantages over classical Sallen-Key filters.

Hakkinen and Vanhala [143] designed a band-pass filter centered at 1.2 kHz in their LF amplifier. They used the inverting amplifier design, incorporating additional capacitors in the feedback path to achieve the desired frequency response.

Kang et al. [114] implemented a fifth-order Chebyshev filter in their LF amplifier. Their design used the LM324 opamp in a non-inverting configuration for a two-stage amplifier, while two additional opamps in inverting configurations formed the filter stages. The LM324 typically consumes 240 µA per stage. However, the article reported a total WuRx supply current of only 619 µA.

Kazdaridis et al. [115] emphasized the importance of input bias current in LF receiver design. By amplifying the output of the passive RFED with an LPV811 opamp, they achieved a sensitivity of −70 dBm. The article states that the comparator stage has a trigger level of 27 mV, meaning the amplifier must boost the −70 dBm RFED output to this voltage. Given an estimated peak-to-peak output of 16 µV at −70 dBm, assuming a voltage sensitivity of 80 mV/µW and a peak-envelope power of −67 dBm, the amplifier must provide a gain of approximately 1700. However, the LPV811 has a typical GBWP of 8 kHz, resulting in a limited bandwidth of only 4.7 Hz. Such a low LF bandwidth restricts the data rate, leading to very long WuPt transmissions. The article does not discuss the discrepancy between the LF bandwidth and the estimated data rate, which we derived from an oscilloscope screenshot to be approximately 47.5 sym/s.

5) Amplifier based on Bipolar Junction Transistors: As shown in Fig. 19, only seven reviewed prototypes use amplifiers based on BJTs. Unlike opamp-based amplifiers, BJT circuits can be optimized for WuRx applications by reducing power consumption and increasing voltage gain. Features such as high linearity and output drive capability, which are crucial in general-purpose opamp circuits, are unnecessary for WuRxs. BJT-based amplifiers enable highly sensitive WuRxs, as all reviewed prototypes employing them achieved reception below −60 dBm.

Bdiri et al. [35] implemented a two-stage common-emitter amplifier. Because the WuRx operates with duty cycling, the amplifier was designed for higher current consumption, drawing 14.6 µA. The circuit achieved a voltage gain of 50 dB at 770 kHz.

Woias et al. [46] and Köble et al. [117] designed an LF amplifier consisting of four BJTs. Their circuit includes a current mirror, a common-emitter amplifier, and a push-pull output stage. This design achieved a gain of 20 dB at 32 kHz while consuming only 2 µA.

In [32], we implemented a common-emitter amplifier with a gain of 23 dB while operating at 1.3 µA. However, gain might

be degraded due to the high sensitivity of common-emitter stages to output loading. Later, in [66], we determined that the following LF receiver stage has an input impedance of only 155 kΩ, which can significantly impact amplifier performance.

In [93], we proposed a combined common-emitter and common-collector amplifier. The common-emitter stage provides high voltage gain but has a high output impedance. This impedance, when biased to 300 nA, is highly sensitive to parasitic capacitances, limiting bandwidth. The common-collector stage acts as a buffer, reducing output impedance. The circuit achieved a gain of 33 dB in the 0.5–10 kHz range while consuming only 530 nA.

Liu et al. [105] proposed a four-stage common-emitter amplifier. Their circuit achieved a 37 dB gain at 15 kHz, with a total power consumption of 6.16 µW. Each stage was biased with 770 nA.

D. Analog-to-Digital Conversion

Fig. 23 presents the number of reviewed prototypes categorized by the type of ADC technology used. The two most commonly employed methods are comparators and low-frequency pattern matchers (LFPMs). This subsection focuses on circuit designs using comparators, while LFPMs, which integrate signal reception and address matching, are discussed separately in Subsection III-E.

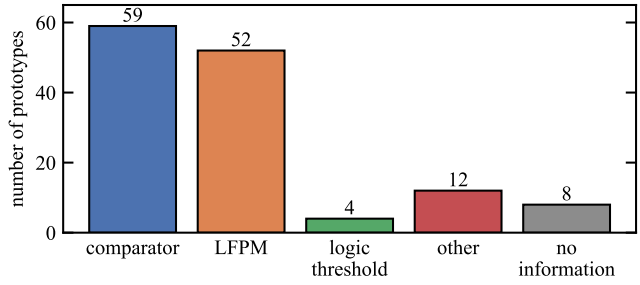

Fig. 23. Number of analyzed prototypes classified by the utilized ADC technology. References [64], [105], [117] occur twice as they utilize comparators together with LFPMs.

1) Alternative Conversion Technologies: Some prototypes utilize conventional ADCs instead of comparators or LFPMs. References [27], [69], [92], [124] implemented ADCs, primarily using microcontroller-integrated ADCs.

Doorn et al. [92] developed a WuRx without address matching, directly sampling the amplified LF signal with an ADC. Kondo et al. [124] compared the ADC readings against a fixed threshold, enabling the WuRx to detect the duration of IEEE 802.11 frames. Ma et al. [69] implemented a duty-cycled WuRx, periodically sampling the power detector output using an ADC. The sampled values were then correlated with a predefined sequence, and the correlation output was compared against a threshold.

Some articles used opamps in open-loop configurations as threshold detectors, effectively functioning as comparators [84], [122], [125]. However, dedicated comparators are generally preferred because they offer faster response times and lower power consumption. When an opamp in open-loop mode rapidly switches its output between supply rails when the input crosses a threshold, the output response is limited by the slew rate. For example, the LPV521 opamp used by Parks [122] has a slew rate of 2.9 V/ms, meaning it takes approximately 1 ms to transition from 0–3 V. The LPV521 typically consumes 346 nA. In contrast, dedicated comparators have propagation delays in the microsecond range. The TLV3691, the lowest-power comparator available, consumes only 75 nA while maintaining a worst-case propagation delay of 45 µs.

Rup and Bajic [29] and da Silva et al. [71] utilite parts of the MR and WuRxs. No dedicated conversion technology was given as the ADC is integrated in the MR.

2) Logic Thresholds: Complementary metal–oxide–semiconductor (CMOS) logic devices are commonly used in low-power applications due to their negligible static power consumption. CMOS gates have specific input voltage thresholds, known as trip points, where their output state transitions. Some articles, including [43], [75], [77], [100], exploited these trip points to generate digital outputs from the RFED's output signal. Trinh et al. [75] and Kaushik et al. [77] used this principle for their passive WuRxs.

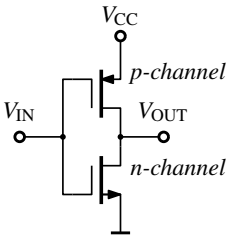

Fig. 24. Typical schematic of a CMOS inverter according to [101]

Fig. 24 illustrates a standard CMOS inverter circuit. As logic signals are either low (near 0 V) or high (near the supply voltage), only one of the complementary metal–oxide–semiconductor field-effect transistors (MOSFETs) conducts. However, at intermediate input voltages, both transistors partially conduct simultaneously, leading to an undesired increase in current supply. This phenomenon, known as the shoot-through effect (STE), can significantly impact power consumption. [101, p. 760]

In [148], we further analyzed this effect by measuring STE currents in various CMOS components, including microcontrollers. Our results showed peak STE currents ranging from 17 µA to 6.0 mA, significantly exceeding typical WuRx power consumption. This unintended current drain can drastically impact the battery life of sensor nodes.

The STE can be completely avoided by using dedicated comparators. For instance, the TLV3691 comparator, which consumes only 75 nA, effectively eliminates STE while maintaining fast switching performance.

Several reviewed studies exhibit potential STE-related issues by directly connecting analog signals to digital inputs. The most prominent example is the preamble detector proposed by Magno et al. [38], whose schematic was previously shown in Fig. 10. Their design employs a low-pass filter formed by resistors and capacitors to smooth the comparator output. However, under continuous noise or interference,

this circuit holds the input voltage at an intermediate level, triggering STE in the connected digital circuit.

We identified potential STE occurrences in the following references: [21], [38], [39], [42], [45], [46], [67], [73], [74], [98], [102], [106], [117], [121], [130], [132], [140], [149]–[153].

3) Comparator Components: Most comparators are designed to operate near the supply voltage rails. Therefore, four key parameters must be considered when selecting a comparator for WuRxs: input offset voltage, internal hysteresis, propagation delay, and quiescent current.

Hysteresis is useful for noise suppression but limits the minimum detectable signal amplitude. The minimum signal required to trigger the comparator is determined by the difference between its upper and lower threshold levels, which depend on hysteresis and input offset voltage. [101, p. 815]

Tab. III summarizes the most commonly used comparators in the reviewed literature. The TLV3691, found in 16 prototypes, has the lowest quiescent current at 75 nA. The LPV7215, also used in 16 prototypes, offers excellent minimum signal detection due to its near-zero internal hysteresis. The TLV3201 is preferred in duty-cycled WuRxs where fast response time is essential.

Magno et al. [38], [151] evaluated three different prototypes using the TLV3691, AS1976, and LPV7215 comparators. Their results showed a direct correlation between power consumption and sensitivity. Magno et al. measured a sensitivity of −32 dBm for the TLV3691, −42 dBm for the AS1976, and −55 dBm for the LPV7215.

In [93], we repeated similar tests with the TLV3691, TS881, and LPV7215, obtaining −31 dBm, −38 dBm, and −47 dBm, respectively. The 8 dB discrepancy for the LPV7215 is likely due to variations in input offset voltage. According to the LPV7215 datasheet, the typical input offset voltage is 0.3 mV, but the maximum can be as high as 6 mV. Such variations can significantly affect the overall WuRx sensitivity.

4) Reference Signal and External Hysteresis: Data slicing refers to the technique of converting an analog signal into a digital output using a comparator. The application note [157] describes several common approaches. Fig. 25 illustrates three typical comparator circuits used in WuRxs.

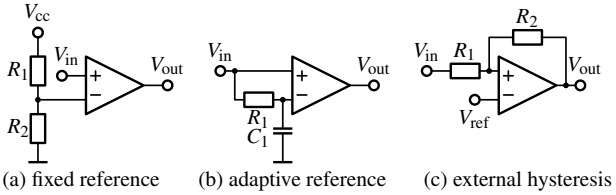

(a) fixed reference (b) adaptive reference (c) external hysteresis

Fig. 25. Comparator circuits used in WuRxs

In Fig. 25 (a), a fixed reference voltage is generated using a resistor divider or an internal voltage reference. For example, the LT1540 comparator includes a 1.18 V reference, which was used by Ma et al. [58] and Perez et al. [144]. Other studies use reference voltages ranging from 0.6 mV to 1 V [107], [122]

The reference voltage determines the sensitivity of the comparator stage. A higher reference voltage requires a larger input signal to trigger the comparator, making the circuit more noise-resistant but less sensitive. A lower reference voltage increases sensitivity but also makes the circuit more susceptible to noise.

For reliable operation, the reference voltage should be significantly larger than the maximum input offset voltage of the comparator. Otherwise, input offset variations may impact detection accuracy. Additionally, any DC offset from preceding WuRx components (such as RFEDs or LF amplifiers) can interfere with signal detection unless high-pass filtering is applied.

The circuit in Fig. 25 (b) eliminates the need for a fixed reference by generating a reference voltage from the input signal itself. A low-pass filter averages the input signal to determine a dynamic threshold. This approach offers two key advantages. The first advantage is offset compensation. Any DC bias in the signal path is automatically corrected. Secondly, unlike a fixed reference, which requires continuous power, the adaptive reference is derived from the signal itself, reducing static power consumption.

The data slicer time constant τ_{DS}, defined by the resistor and capacitor values in the low-pass filter, determines the trade-off between signal responsiveness and robustness. With a high τ_{DS}, a long preamble is needed until the reference voltage reaches the correct level and the comparator is reliably detecting the signals. However, with a low τ_{DS}, the so-called run length limit (RLL) is low. Multiple identical consecutive symbols in the WuPt are able to saturate the data slicer. Therefore, receiving these signals is not reliably possible. If the data slicer is saturated, even small noise amplitudes on the input signals can excite the output. Bit errors will occur more often.

This trade-off is seldom discussed in the reviewed literature. Values like symbol rate and τ_{DS} are often missing. The application note [157] suggests setting τ_{DS} to approximately five times the symbol period.

Frøytlog et al. [150] used a data slicer time constant of 1 ms for a 100 sym/s symbol rate. Here, τ_{DS} is smaller than the symbol period, meaning comparator hysteresis likely plays a role in ensuring stable detection. In their later work [67], they increased the symbol rate to 1.25 ksym/s but kept τ_{DS} constant. To maintain reliability, they used Manchester coding, which enforces a RLL of 2. The implications of coding techniques are discussed further in Subsubsection III-F3.

In Fig. 25 (c), an external hysteresis circuit is added using resistors R_1 and R_2. The hysteresis voltage V_{hys} is defined by:

$$V_{hys} = V_{cc} \cdot \frac{R_1}{R_1 + R_2} \tag{12}$$

This approach increases the robustness of signal detection by preventing small noise fluctuations from causing false transitions. Several studies implemented external hysteresis, including [34]–[36], [113].

Some studies further adapted the circuit to improve reliability. For instance: References [47], [81], [130] introduced a parallel resistor to the capacitor in Fig. 25 (b), reducing sensitivity but improving robustness. Köble et al. [117] replaced the resistor in Fig. 25 (b) with a diode. However, the reasoning for this modification was not discussed in the article.

TABLE III
MOST USED COMPARATORS IN WAKE-UP RECEIVER PROTOTYPES

Comparator	Input offset[1] in mV	Hysteresis in mV	Supply voltage range in V	Supply current in nA	Propagation delay[2] in µs	Costs[3] in $	References
TLV3691	15	17	0.9–6.5	75	45	0.7	[21], [38], [54], [70], [73], [74], [79]–[81], [93], [115], [120], [141], [150]–[152]
AS1976	5	3	1.8–5.5	200	15	obsolete	[38], [121], [151]
TS881	10	2.4	0.85–5.5	300	13	1	[44], [107]
LTC1540	12	50	2.0–11.0	300	60	3	[58], [98], [130], [144], [154]
LPV7215	6	—	1.8–5.5	580	15	1	[38], [42], [45], [67], [93], [106], [113], [116], [140], [143], [149], [151], [153]
TLV3701	5	—	2.7–16	580	67	1	[39], [132]
MAX9119	5	4	1.6–5.5	680	16	1.2	[123], [155], [156]
TLV3201	3	1.2	2.7–5.5	40000	0.055	1	[34]–[36]

Typical performance parameters from the device's datasheet [1] maximum value at room temperature [2] maximum value, approximately 10 mV overdrive [3] per piece for a 100-piece order

E. Low-Frequency Pattern Matcher

Low-frequency pattern matchers (LFPMs) are specialized LF receivers that operate in the range of 15–150 kHz while consuming minimal power. As discussed in Subsubsection II-B1, LFPMs were originally developed for remote keyless entry systems in automobiles. Among the 132 reviewed prototypes, 52 use LFPM technology, highlighting their importance in WuRx research. However, only 50 prototypes support addressing [46], [117].

Most non-RF WuRxs examined in Subsubsection II-B1 rely on LFPMs. Out of 19 non-RF prototypes, 12 utilize LFPMs. However, the majority of LFPM-based WuRxs still operate in the RF domain.

The WuTx design for LFPM-based RF WuRxs must be carefully optimized to match the requirements of the LFPM. Since the LFPM detects OOK signals at LF, and the RFED also detects OOK in the RF domain, the received signal undergoes two stages of envelope detection. The signal processing path of an LFPM-based WuRx is illustrated in Fig. 26.

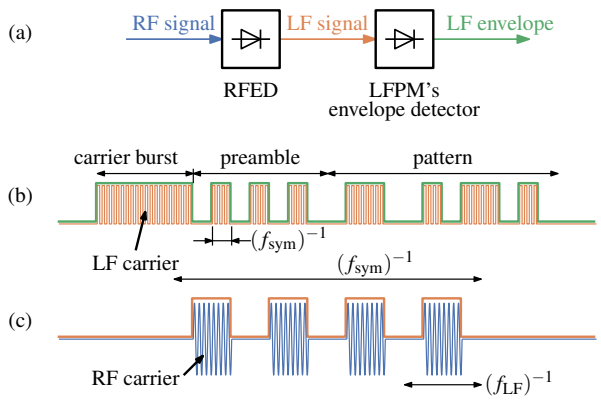

Fig. 26. Requirements for WuPts in LFPM-based WuRxs. (a) Simplified reception path showing two envelope detectors. (b) LF envelope and signal components of the WuPt. (c) LF signal generated by the envelope of the RF signal.

The addressing information for the LFPM is modulated onto an LF carrier at a low symbol rate between 1–8 ksym/s[8]. This LF signal must be extracted from the RFED output, meaning a special RF modulation is required to transmit the LF pattern within the RF envelope. [31]

1) LFPM Components: Tab. IV summarizes the key parameters of the different LFPMs found in the reviewed literature. Most prototypes use LFPMs from the AS393x family, which includes the AS3930, AS3931, AS3932, and AS3933. These devices have similar performance characteristics, with the AS3933 being the most recent version. It supports additional LF bands, an integrated amplifier, and Manchester decoding. The AS3933 also shows the best sensitivity among all analyzed LFPMs. Most LFPMs can store a single fixed pattern of up to 16 symbols. The AS3933 allows for a 32-symbol pattern, but only when using Manchester coding.

Mohammed et al. [22] implemented the RF125 module in their WuRx design, operating at an LF of 32 kHz. The RF125 module includes an LFPM and a microcontroller for interfacing. Based on the module's specifications, it likely integrates the AS3933, though the exact component is not specified in the article or datasheet.

Woias et al. [46] and Köble et al. [117] used the ATA5283, a simplified LFPM. According to its datasheet, this device has a lower power consumption than the AS393x series. However, Atmel discontinued the ATA5283 in August 2008 [118].

Pflaum et al. [68] developed a duty-cycled WuRx using the PMA5110 system-on-chip, which integrates an LFPM, microcontroller, and MR. The LFPM in the PMA5110 can detect a synchronization word for pattern matching, allowing additional data to be sent to the microcontroller. Infineon discontinued the PMA5110 in September 2016 [158].

Boaventura et al. [156] listed the MCP2030. This device does not support internal address matching. It is still commercially available, but no reviewed WuRx prototypes were found using this component.

2) LFPM Frequency Bands: Selecting the LF carrier for an LFPM-based WuRx requires considering two factors. A lower LF value generally improves sensitivity since the WuPt

[8] values based on our analysis, see Section V

TABLE IV
LOW-FREQUENCY PATTERN MATCHERS IN THE STATE OF RESEARCH

LFPM	Sensitivity in μV_{PP} [1]	Supply voltage range in V	Supply current in μA [2]	LF range in kHz	Channels	Pattern size in symbols	Costs [3] in $
AS3930	282	2.4–3.6	2.7	110–150	1	16	3
AS3931	350	2.4–3.5	6.5	19–150	3	16, fixed	no stock
AS3932	282	2.4–3.6	2.7	110–150	3	16	3
AS3933	226	2.4–3.6	3.1	15–150	3	16/32	3
RF125-RA	226	2.5–3.6	9	15–150	3	32	10 [4]
ATA5283	2820	2.0–3.8	1.1	30–180	1	no	obsolete
PMA5110	2500	1.9–3.6	1 [5]	120–130	1	16	obsolete
MCP2030	1000	2.0–3.6	2	typ. 125	3	no	2.5

Typical performance parameters from the device's datasheet [1] RMS to peak-peak conversion with factor 2.82 [2] listening mode, typical [3] per piece for a 100-piece order [4] marketplace product, with breakout board [5] analog front-end of LF receiver only

requires less bandwidth for detection. Additionally, a lower GBWP is sufficient for the LF amplifier. However, reducing the LF limits the symbol rate because each symbol requires a minimum number of LF periods. The ratio between LF and symbol rate is referred to as the LF modulation rate β_{LF}:

$$\beta_{\mathrm{LF}} = f_{\mathrm{LF}} / f_{\mathrm{sym}} \tag{13}$$

In existing research, values for β_{LF} range from 4 to 45 [65], [72], [94], [97].

Köble et al. [117] used the lowest LF of 4.681 kHz but required a crystal oscillator circuit to convert this frequency to 32.768 kHz, which was then fed into the LFPM. The article did not provide details on the WuPt duration or symbol rate.

Gavrikov et al. [110] directly fed an 11.36 kHz signal into the AS3933 LFPM. This frequency was chosen based on the maximum envelope rate achievable with Bluetooth Low Energy transmitters used to generate the WuPt. However, the AS3933 is not optimized for such a low LF [66]. The prototype achieved a sensitivity of only -47.8 dBm.

Twenty-one LFPM-based WuRx prototypes use LF values between 15–25 kHz, which aligns with the lowest frequency band of the AS3933. In [94], we investigated latency optimization, requiring higher LF values (30 and 36 kHz) to achieve response times below 5 ms. This increase in symbol rate led to a 3 dB sensitivity degradation compared to [66].

Sánchez et al. [53], [159] employed an 85 kHz LF, as their WuRxs were acoustic. This frequency matched the center frequency of the acoustic transducers used in their prototypes.

Another set of 20 prototypes operated at 120–125 kHz, enabling lower latency. The fastest response time was achieved by Kumberg et al. [160], reducing latency to 2.2 ms by limiting the pattern size to 4 symbols. However, sensitivity was reduced, with most prototypes not exceeding -55 dBm.

One exception is the duty-cycled WuRx by Pflaum et al. [68], which achieved a sensitivity of -71 dBm. However, LFPMs cannot be duty-cycled effectively, requiring long preambles for packet detection. This reduces the efficiency of duty-cycling, leading to higher power consumption or increased latency.

3) LFPM Features: The AS393x LFPM family includes advanced features commonly found in MRs. However, only a few WuRx prototypes utilize these features. The AS393x chips are capable in measuring an RSSI value. The RSSI is a 5-bit value that estimates the voltage level at the LF input. In [66], we measured the RSSI during an RF power sweep and used to approximate the input impedance of the AS3933 by analyzing voltage drops across additional series resistors. Sánchez et al. [53] applied RSSI for clear channel assessment in underwater network. Mohaghegh et al. [50] used RSSI for distance estimation in localization applications.

The AS393x series can also receive additional data after a successful pattern match. It provides two output signals: one for data and another for clock recovery. However, clock recovery is only supported for Manchester-coded WuPts. Otherwise, only raw data is available. Sánchez et al. [161] used this feature for data transmission in underwater networks. Blobel et al. [91] leveraged it to implement a variable addressing scheme, where WuPts carried address and mask information. By masking specific address bits, multiple WuRxs could be selectively activated. External CMOS logic handled the address decoding.

In [90], we demonstrated a method for simultaneously matching both a fixed cluster address and a variable device address with the AS3933. A fixed 4-bit cluster address was used to wake multiple nodes, a feature required by protocols such as [27], [86]–[88]. Additional address bits were sampled by a microcontroller, allowing for a variable device addressing scheme.

Sutton et al. [108] introduced the Zippy flooding protocol, utilizing an early wake-up output from the AS393x series. This output is triggered as soon as the LF carrier is detected. In Zippy, each sensor node listens for an LF carrier and immediately relays the RF WuPt, creating a network-wide broadcast. A 24-hour evaluation recorded 3166 false wake-ups, highlighting susceptibility to interference and noise, which can erroneously trigger the frequency detector of the AS3933 [66].

To improve flooding reliability, Kumberg et al. [162] proposed using concurrent RF transmission based on beat frequencies. When multiple transmitters send WuPts at the same frequency, constructive and destructive interference reduces reliability. Kumberg et al. suggested transmitting on slightly different carrier frequencies, where the beat frequency naturally forms the required LF modulation for the LFPM. This method improved signal robustness compared to Zippy [108] but at the cost of higher energy consumption and reduced time

efficiency.

The AS393x series supports multiple clock sources. The lowest power consumption is achieved with its internal RC oscillator, which is calibrated via the microcontroller interface to maintain precision. The typical calibration frequency is 32.768 kHz, but values between 25–45 kHz are supported. Increasing the clock frequency enables faster WuPt detection. In [66], [94], we calibrated the LFPM to 45 kHz, achieving WuPt durations below 9 ms and 5 ms, respectively.

4) LFPM and Comparator: In the reviewed research, three prototypes were found that combine LFPMs with comparator circuits. While LFPMs are typically designed to amplify and detect low-level LF signals, these prototypes use a comparator to convert the LF signal into a digital signal, which is then processed by the LFPM. As a result, the LFPM is only responsible for frequency detection and address matching, rather than signal amplification.

Bdiri et al. [64] implemented a fixed-threshold comparator using the AS1976, with its output connected to an AS3932 LFPM. By reducing the AS3932's supply current to 1.3 µA, the entire WuRx achieved an ultra-low power consumption of 4.58 µW.

Köble et al. [117] used a comparator with an adaptive reference voltage to digitize the WuPt at 4.681 kHz. The resulting digital signal was then converted to 32.768 kHz using two crystal oscillators. This specific frequency was chosen because its seventh harmonic is 32.768 kHz, aligning with the ATA5283's expected input frequency. The crystal oscillator-based band-pass filter attenuated the input by 26 dB, reducing the signal to 9 mV, but this was still sufficient for the ATA5283's sensitivity range.

Liu et al. [105] applied an adaptive-threshold comparator to digitize the WuPt before passing it to the AS3933 LFPM. Since the LFPM does not amplify the signal, sensitivity is limited by the comparator. According to Magno et al. [151], the LPV7215 allows for a maximum sensitivity of −55 dBm. However, Liu et al. enhanced sensitivity to −60 dBm by incorporating a four-stage BJT amplifier.

5) LFPM Limitations: In [66], we conducted extensive measurements to improve LFPM-based WuRxs. Several operating conditions were identified where the LFPM exhibited random packet loss. The AS3933 includes a duty-cycling mode to reduce power consumption. However, during testing, packet loss occurred at 25% and 12.5% duty cycles, making the reception unreliable.

We also analyzed the frequency detector of the AS3933. This circuit is responsible for matching the LF carrier and activating the data slicer and pattern detector. It was observed that the frequency detector responds to a broad frequency range. When the LFPM was configured for 18.7 kHz, it incorrectly detected WuPts with frequencies between 9–70 kHz. This creates a risk of false wake-ups, particularly in prototypes that disable the pattern detector [59], [108], as signals across a wide frequency range can mistakenly activate the receiver.

We measured AS3933's input impedance to assess its impact on LF amplifier or filter design. The datasheet specifies an input impedance of 2 MΩ, but experimental results showed significantly lower values. By introducing a series resistor method while observing the RSSI, input impedance was estimated to be 155 kΩ at 18.7 kHz and only 74.3 kΩ for 131 kHz. This suggests that at higher frequencies, input impedance decreases, affecting circuit design considerations.

In [90], we investigated the AS393's pattern detection. We found that the detector is not univocal, meaning it can misinterpret shifted patterns as valid WuPts. This issue was also discussed by Sánchez et al. [161], who found that cross-correlation effects led to unintended wake-ups.

Without Manchester coding, most patterns exhibit RLL greater than two symbols, meaning they contain long sequences of identical symbols. This was identified as a cause of random packet loss. Subsubsection III-F4 and Subsubsection III-F5 provide a detailed analysis of RLL and univocal patterns its impact on wake-up reliability.

To address these issues, in [94], we proposed a special modulation scheme that ensures RLL compliance. This approach modifies the WuPt structure by adding or removing specific pulses to prevent the AS3933 from turning off during long sequences of L symbols and it maintains synchronization during long sequences of H symbols.

F. Address Decoder

In Subsubsection II-B3, all WuRx prototypes were classified by theirs addressing capabilities. Twenty-four of the reviewed prototypes not include an address decoder or lacked information about its implementation. However, in real-world applications, an address decoder is essential to prevent unnecessary power consumption in the sensor node due to false wake-ups. Additionally, an address decoder improves the WuRx's resistance to noise and interference, as it only activates upon detecting a predefined wake-up pattern. However, WuRxs with address decoders experience higher latency because the address information must be transmitted before the system can fully wake up. Additionally, power consumption is higher, as additional components are required to realize the address match.

The previous stage of the WuRx typically outputs a digital signal, which must be processed by the address decoder to identify a pattern. Since WuPts are transmitted asynchronously, the address decoder must synchronize with the incoming data to correctly interpret the transmitted information.

The speed at which the symbols of the WuPt are transmitted is defined by the symbol rate f_{sym}. To avoid confusion, this discussion will refer to wake-up pattern units as "symbols" (represented as L for low and H for high) and decoded address units as "bits" (represented as 0 and 1). Many encoding methods require multiple symbols to represent a single bit. The code efficiency m is defined as the ratio of address bits to pattern symbols, where for digital codes, typically $m \leq 1$. [90]

These definitions are not always consistently used in existing literature. Some articles refer to bits and data rates when discussing pattern size and symbol rate, leading to potential misinterpretations. WuPt duration comparisons between different prototypes are not straightforward, as it depends on

pattern length. Comparing symbol rate alone is insufficient, as the WuPt preamble can significantly affect WuPt duration. In [94], we proposed the concept of net data rate, which is the number of usable address bits divided by the total WuPt duration. However, since the number of usable address bits is seldom stated in the reviewed articles, calculating the net data rate for most prototypes was impossible without deeper knowledge of the prototypes.

1) Address Decoder Device: Fig. 27 shows the distribution of reviewed prototypes based on the device used for address decoding.

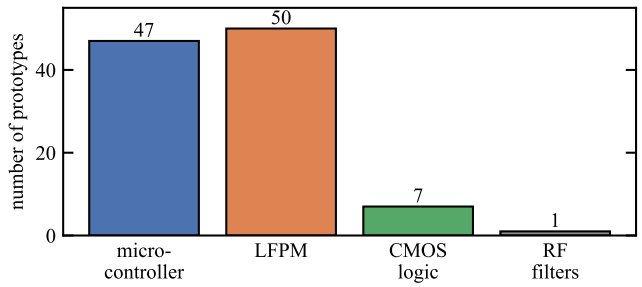

Fig. 27. Reviewed prototypes classified by the device used as address decoder. In total 102 prototypes support addressing. Blobel et al. [91] utilizes LFPM with CMOS logic. In [90], we utilize LFPM with microcontroller decoding. The two LFPM-based prototypes [46], [117] are missing information on addressing capabilities.

The number of prototypes using LFPMs and microcontrollers for address decoding is nearly equal. The LFPM-based approach was discussed previously in detail in Subsection III-E. Address decoding implemented with microcontrollers varies significantly between designs, making comparisons difficult. Additionally, these implementations rarely publish their software, making reproduction challenging.

Seven prototypes incorporated CMOS logic circuits for address decoding. Various approaches were found in the reviewed studies.

Koskela et al. [131] introduced the first CMOS-based address decoder, proposing a 4-bit decoder using a shift register and a magnitude comparator. Magnitude comparators include most of the required logic, reducing component count to only two ICs.

Ammar et al. [100] proposed a standard CMOS address decoder structure, which was previously illustrated in Fig. 11 (a). The circuit consists of XOR gates followed by a tree-like AND gate network. A wake-up signal is generated only if all XOR gate outputs are high, allowing it to pass through the AND gates.

Khodr et al. [98] implemented a different approach, as shown in Fig. 11 (b). Instead of a tree-like AND gate network, a pull-up circuit was used. Open-drain XNOR gates pull the wake-up line low if any output is incorrect. The wake-up signal is only high when all XNOR outputs are high. While this circuit is more cost-effective, it typically has higher quiescent current compared to an AND gate network.

Mafi et al. [163] explored ways to reduce hardware complexity in address decoding. They removed the AND gate network by implementing a stepwise address-matching function between each flip-flop stage. In this approach, the final flip-flop output remains high only if the address match is successful, eliminating the need for XOR and AND gate networks. However, additional logic gates were required to construct the transfer function.

Petäjäjärvi et al. [44] used a complex programmable logic device (CPLD) for address decoding.

Blobel et al. [91] combined an LFPM with CMOS logic. The data output from the LFPM was fed into a CMOS-based address decoder, allowing both single and multicast addressing. The wake-up pattern contained address and mask information, making it possible to target multiple receivers at once.

In [90], we proposed an alternative approach using a microcontroller to sample the LFPM output. The LFPM performed a cluster address match, while the microcontroller processed additional address bits for device-specific or broadcast addressing. This method enables flexible addressing schemes without requiring additional hardware.

Hutu et al. [107] introduced a unique frequency-based address detection method using OFDM-like WuPts. Each WuRx address was identified by a specific frequency signature, dividing the spectrum into four frequency bands. However, only six distinct address patterns were viable within this scheme.

For 29 prototypes, no information about the address decoder was found or no address decoder was implemented. These studies primarily focused on RF and analog circuit design, often neglecting the addressing stage.

2) LF Modulation: In Subsubsection II-D4, different RF modulations used in research were discussed. All LFPM-based WuRxs use OOK for LF modulation, as shown in Subsection III-E and Fig. 26. Outside of LFPM-based WuRxs, LF OOK was used in only three prototypes.

Schulthess et al. [54] and Lattanzi et al. [164] developed acoustic WuRxs with microcontroller-based addressing, utilizing LF OOK with 28 kHz.

In [34], [36], we designed a duty-cycled WuRx using RF amplifiers, achieving a sensitivity of -80 dBm. To improve duty-cycling efficiency, the WuRx remains active for only 50 µs. Within this brief period, the WuRx had to determine whether a WuPt was present on the channel. Continuous modulation was necessary to ensure reliable detection within the 50 µs window. To achieve this, LF FSK was proposed, switching between 50 and 100 kHz to represent H and L symbols.

No other studies proposed similar LF modulation techniques for addressing.

3) Coding Algorithms: Fig. 28 shows the number of reviewed prototypes categorized by coding algorithms. The majority of prototypes did not use coding algorithms and directly convert symbols to address bits. The consequences for address space and reliability will be discussed in the next subsubsections.

With Manchester coding, the sequence HL typically represents 1, while LH represents 0. It was used in 26 prototypes, with 21 of these utilizing LFPMs from the AS393x family,

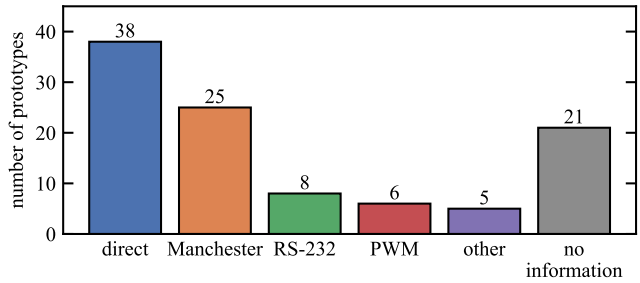

Fig. 28. Reviewed prototypes classified by the utilized coding algorithm. Nine additional prototypes do not support addressing and utilize CW modulation.

which include built-in Manchester decoding. Manchester coding has a coding efficiency of $m = 0.5$. Its key advantage is a RLL of 2, ensuring synchronization and signal integrity.

The RS-232 coding method introduces a start symbol (L) and a stop symbol (H) for every 8-symbol sequence. This ensures clear synchronization when receiving data, but it has a high RLL of 9, which can lead to prolonged sequences of identical symbols. The advantage of RS-232 coding is that it is easily decoded by microcontrollers, as most have built-in RS-232 reception modules that require no additional circuitry or CPU processing.

Perez et al. [144] combined Manchester coding and RS-232. Since start and stop symbols have opposite polarities, both schemes are merged without conflicts. The 8-symbol RS-232 sequence was converted to 4 bits, achieving proper synchronization and an RLL of 2.

In pulse-width modulation (PWM) coding, different prototypes used varied symbol sequences to represent addresses. A distinct difference in duty cycles is required for PWM decoding, which can be recovered using low-pass filtering. Wang et al. [154] proposed uniform-length PWM sequences, where HLLL represents 0 and HHHL represents 1, resulting in low coding efficiency ($m = 0.25$). However, the low RLL makes it robust against synchronization loss.

Other PWM-based designs [28], [74], [102], [155] used variable-length sequences. For instance, Ansari et al. [155] defined HL representing 0 and HLL representing 1. The variable length meant address decoding speed varied, which may be undesirable for time-sensitive applications.

Return-to-zero (RZ) coding was implemented in [58], [77], [131], where LL represents 0 and HL represents 1. While RZ coding provides clear symbol separation, it lowers coding efficiency ($m = 0.5$). However, the RLL is increased, as consecutive 0 bits result in long L sequences.

Kondo et al. [124] introduced a pulse-length-based approach, where pulses ranged from 710–2600 µs, allowing 64 unique symbols to be identified.

A similar pulse-spacing approach was proposed by Oller et al. [165], where the gap between two OOK pulses encoded 4-bit segments. In total a 16-bit address could be decoded.

In [90], we investigated non-Manchester coding for LFPMs. It was observed that patterns with RLL > 2 caused random packet loss. A computer model identified 377 viable 12-symbol patterns that preserved RLL $= 2$, allowing for 8.56 address bits per sequence, achieving higher coding efficiency ($m = 0.71$) than Manchester coding ($m = 0.5$).

To use this scheme, a lookup table was required to convert addresses to patterns. The required memory size depended on the symbol count. While 12-symbol encoding was feasible for small microcontrollers, a 16-symbol encoding would require significantly more storage.

We proposed a new direct symbol-to-bit encoding scheme called 3S2B, where 3 symbols represented 2 bits, achieving a coding efficiency of $m = 0.667$ [90].

In [94], we bypassed the RLL limitation of LFPMs by inserting and removing pulses within WuPt symbols. This allowed direct 8-symbol-to-8-bit conversion, eliminating the need for pattern-to-address lookups.

Additionally, in [94], we tested WuPts with lower modulation ratios β_{LF}. Only RLL $= 2$ patterns were reliable. The remaining 10-symbol sequences were mapped to seven address bits using lookup table encoding.

4) Run-Length Limit and Reliability: LFPMs and comparators with adaptive reference generators rely on a low-pass filter-based data slicer. The input signal is low-pass filtered and used as a reference voltage in the comparator. This approach eliminates the need for an additional reference voltage and makes the circuit immune to offset errors. However, the time constant of the low-pass filter must be carefully designed, as it has a significant impact on both settling time and the RLL.

A long time constant improves the robustness of the data slicer against long sequences of consecutive symbols in the WuPt. However, it also increases the required preamble duration, as the adaptive reference needs more time to reach a stable voltage level before symbols can be decoded reliably. If the WuPt contains too many consecutive identical symbols, the reference voltage may drift away from the optimal level, increasing the likelihood of symbol errors. Even small noise variations or interference can lead to incorrect symbol decoding, making reception unreliable for WuPts with a high RLL.

The maximum tolerable RLL depends on the hardware design and the chosen time constant. In [90], an RLL of 2 was found to be the limit for the tested LFPM. All RLL $= 2$ sequences resulted in zero packet loss, while RLL $= 3$ sequences already showed a significant number of lost packets. No WuPts with RLL $= 4$ were received.

Beyond this study, only Basagni et al. [39] investigated similar constraints. They reported that due to hardware limitations, their WuRx design could not receive sequences containing more than six consecutive H symbols. This restriction reduced the number of viable 8-symbol WuPt sequences to 248.

Several articles claim to support 16-bit addresses without using a coding algorithm [17], [38], [42], [57], [65], [95], [110], [132], [137], [151], [153], [160], [166]–[168]. If these designs truly lack coding, they must be capable of reliably receiving RLL $= 16$ WuPts. However, it is unclear whether the authors thoroughly tested these edge cases, and such claims should be interpreted with caution.

5) Preamble Detector and Univocal Address Patterns: Magno et al. [38] proposed a preamble detector, shown in Fig. 10, which was later used in multiple studies [39], [42], [45], [46], [67], [106], [117], [121], [132], [140], [149]–[153].

The preamble detector consists of a Schottky diode and a passive low-pass filter. When the comparator output is high, the preamble detector's output voltage gradually increases. The preamble detector is directly connected to a CMOS input and triggers at approximately one-half or one-third of the supply voltage. [102] However, this circuit is heavily affected by the STE discussed previously in Subsubsection III-D2. If the analog voltage of the low-pass filter is connected to a CMOS logic device, it can cause additional supply current draw, leading to increased power consumption. [148]

The preamble detector is designed to detect long RF pulses, marking the beginning of a WuPt. However, interference or noise can also trigger the detector, leading to false wake-ups. Since only a certain duration of the high signal is required to activate the detector, spurious signals can wake up the WuRx unnecessarily.

Ziesmann et al. [152] observed that the preamble detector requires at least 37 ms to fully discharge after receiving a WuPt. This delay prevents the WuRx from receiving another WuPt during this interval. This becomes a problem when a WuTx transmits multiple WuPts in rapid succession to wake up multiple nodes. The authors proposed adding a BJT discharge circuit to rapidly reset the capacitor. With this modification, the minimum latency between WuPts was reduced to 1.4 ms.

If a preamble detector is missing or fails, the address decoder may be unable to differentiate the preamble from the pattern. We investigated this issue in [90] for LFPM-based WuRxs, but similar behavior is expected for microcontroller-based and CMOS logic-based address decoders.

If part of the preamble is misinterpreted as address symbols, the addressing pattern is no longer univocal. This means that multiple WuRxs with different addresses may wake up simultaneously, even though the WuPt was intended for a single node. Fig. 29 illustrates this issue. The WuPt is intended for node #68, but nodes #162 and #209 are incorrectly triggered.

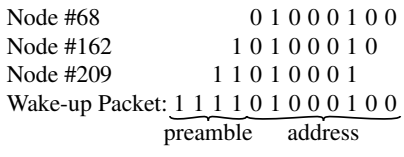

Fig. 29. If bits of the preamble are mistaken for address bits, the address pattern becomes non-univocal. The WuPt is meant for node #68, but nodes #162 and #209 are also triggered.

In [90], we further analyzed this issue using scatter plots, marking all WuRxs that were incorrectly activated by a single WuPt. Scatter plots help to visualize the problem and identify parts of the patterns that are univocal. We suggested a separation sequence to clearly distinguish the preamble from the address pattern. This approach reduces the available address space but is essential to prevent false wake-ups caused by non-univocal patterns.

Other techniques to ensure univocal addressing include adding special symbols at the end of the WuPt, such as parity bits or cyclic redundancy check (CRC) [28], [102]. The start and stop bits used in RS-232 coding also provide separation markers, ensuring that the address pattern remains univocal [35], [40], [80], [81], [120], [144], [156], [164].

The problem of non-univocal addressing is often overlooked in WuRx research. Many studies focus on hardware design, and large-scale tests with multiple WuRx addresses are rarely performed. However, for practical use, ensuring univocal WuR communication is crucial. Only a few prototypes incorporate measures to prevent false wake-ups, and even fewer studies discuss the importance of this issue.

Already in 2002, Ma et al. [58] observed that rotationally equivalent codes could not be uniquely identified by their microcontroller-based decoder. They applied Necklace Theory and concluded that only 36 independent codes were available for 8-symbol patterns. This resulted in a significant address space reduction compared to the LFPM-based approach in [90].

Koskela and Valta [131] stated that the first bit of the address must be 1. Their design uses a CMOS logic-based address decoder, but they do not provide a reason for this requirement. We assume that this measure is intended to ensure univocal communication, preventing false wake-ups caused by non-univocal address patterns.

Petäjäjärvi et al. [169] specified that the last bit of the address must be 1, and the address must contain at least one additional 1. This restriction likely reduces the probability of false wake-ups. However, the authors do not explicitly discuss univocal communication. Based on our analysis [90], we believe that this constraint is sufficient to maintain univocal addressing.

Sánchez et al. [161] conducted a cross-correlation analysis between the programmed and received LFPM patterns, similar to our approach in [90]. Their results indicate the presence of multiple false wake-ups within the address range of the LFPM. However, their cross-correlation patterns differ slightly from ours, which may be due to differences in LFPM configuration. Despite identifying these false wake-ups, the authors do not propose any solutions to eliminate non-univocal patterns.

Frøytlog et al. [150] required that the first symbol of the address be 1, limiting the number of supported devices to 128 for an 8-symbol pattern. They do not explain why this constraint is necessary. However, this approach closely aligns with our measures discussed in [90], which ensure univocal addressing.

6) Error Correction: Most MRs have an internal CRC to ensure that received addresses and data are correct. Additionally, forward error correction (FEC) algorithms can be used to reduce bit errors during transmission. However, most WuRxs do not include error checking or correction mechanisms. Only a few references mention these capabilities.

Ansari et al. [155] proposed a 4-byte WuPt for WuR communication. The structure includes a synchronization sequence, address, command, and a CRC byte. The microcontroller handles the WuPt decoding. Some microcontrollers have dedicated CRC calculation modules, and some MRs offer cryptographic units for external use.

Marinkovic and Popovici [102] described a WuPt consisting of a preamble, synchronization bit, data, and CRC. However, they do not provide details about the CRC field.

Zhang et al. [28] implemented a CRC circuit using CMOS logic. Their design uses linear feedback shift registers and

XOR gates for CRC validation. Additional CMOS ICs handle preamble verification and address matching. The PCB includes approximately 11 CMOS ICs, but despite the high component count, the WuRx power consumption remains low at 9 µW.

Rakovic et al. [109] simulated different error correction methods and concluded that error correction codes in the wake-up address improve WuR communication robustness and sensitivity. However, they emphasize the energy-latency trade-off associated with FEC overhead.

7) Data Transmission Capabilities: Using WuR communication for data transmission involves trade-offs. WuRxs are generally not optimal for data reception due to several limitations. Compared to MRs, they have lower data rates and degraded sensitivity. The lower symbol rate increases air time, raising transmitter power consumption. As discussed in Subsubsection II-D4, most WuRs utilize OOK. OOK modulation is more error-prone than modulations typically used in MR communication. Additionally, as seen in the previous subsection, WuRs rarely implement error checking or correction, which are essential for reliable data transmission in MR communication. [10]

Not all WuRx prototypes in the reviewed literature support data transmission. WuRx prototypes with no or fixed addressing, as classified in Subsubsection II-B3, are unlikely to support data transfer.

One advantage WuR data transmission is that it does not require MR startup. This makes WuRs more efficient for low data sizes and unidirectional communication. Additionally, WuRxs consume less power than MRs when receiving data.

Hierold et al. [170] analyzed the trade-off between MR and WuR data transmission using an LFPM-based WuRx and a low-power MR. The results show that the more efficient method depends on the amount of transmitted data and the number of nodes in range. For single-node communication, WuR is more efficient for fewer than 10 data bits. However, with multiple nodes, MR transmission becomes more effective even for smaller data sizes.

G. Duty Cycling and Power Gating

In Subsubsection II-B2, we classified WuRxs based on their operation modes. We distinguished between always-on, duty-cycled, power-gated, passive WuRxs, and WuRxs with energy harvesting. Always-on, passive, and energy-harvesting WuRxs can receive WuPts at any time and most of their components are continuously active. In contrast, duty-cycled and power-gated WuRxs actively turn off certain circuit components to reduce power consumption.

In duty-cycled WuRxs, additional components are switched on and off based on a predefined schedule, often controlled by a protocol. Power-gated WuRxs, on the other hand, only activate certain components when specific characteristics of the WuPt are detected.

1) Power Gating Mechanism: LFPM-based WuRxs operate with LF values above 10 kHz [110]. One way to improve their sensitivity is by integrating an LF amplifier. However, opamp-based LF amplifiers require a high GBWP for proper signal amplification. Opamps with high GBWP typically consume more than 10 µW, as discussed in Subsubsection III-C1.

Bdiri et al. [37], [65], [72] were the first to implement a power-gated WuRx. Their design includes an opamp-based LF amplifier that is power-gated. The proposed circuit detects the RF carrier using a two-stage opamp-based LF amplifier and a comparator with a fixed threshold. When an RF pulse is detected, the high-power opamp is enabled, allowing the LF signal to be amplified and forwarded to the LFPM.

Benbuk et al. [21], [73] introduced multiple power-gated WuRxs that use a preamble detection circuit to control power gating. The pulse-width detector circuit is only activated when the WuPt preamble is detected. This detector generates the wake signal, as these WuRxs lack addressing capabilities.

In [74], Benbuk et al. proposed a two-stage power gating approach. The preamble detector first enables the pulse-width detector circuit. Only if the RF pulse has the correct duration, the final stage of the WuRx is activated. The pulse-width detector then enables the bit correlator circuit, a CMOS-based address decoder that extracts the WuPt address information and generates the wake signal.

Ziesmann et al. [171] introduced the idea of fully switching off the microcontroller. They proposed using a high-side BJT switch to disconnect the microcontroller's supply voltage completely. This reduces quiescent power consumption compared to keeping the microcontroller in sleep mode. The WuRx turns the microcontroller on when a WuPt is received. An inhibitor signal prevents the microcontroller from being accidentally turned off during data processing. The authors noted that power-gating increases the required WuPt preamble length because of the microcontroller's initialization time. Their analysis suggests that power-gating is only beneficial when the number of wake-ups is below 50 per hour. Microcontrollers with ferroelectric random access memory (FRAM) could benefit from this approach, as their processing state is stored in non-volatile memory.

In general, power-gated WuRxs have a higher false wake-up energy waste (FWuEW) than always-on WuRxs. The FWuEW depends on the power consumption and active time of the duty-cycled circuit. Since the first stage of most power-gated WuRxs can only detect an RF pulse or the WuPt preamble, it is prone to false triggers from interference or noise. Therefore, the power-gating circuit threshold must be carefully calibrated. If the threshold is too low, false signals will activate the power-gated circuit, increasing the average power consumption. If the threshold is too high, the WuRx sensitivity will degrade because only strong signals can activate the power-gating mechanism.

2) Duty-Cycling Mechanism: For duty-cycled WuRxs, the active power consumption is significantly higher, often reaching the milliwatt range. However, by implementing duty cycling, the average power consumption can be reduced to a fraction of this value. Minimizing the active duration t_{active} is critical. Additionally, the duty-cycling period t_{cycle} must be significantly longer than t_{active}. During the passive phase, the WuRx is unable to receive any WuPts. To prevent random packet loss, the WuPt duration must be at least as long as t_{cycle}. This ensures that at least one activation cycle aligns with the WuPt transmission.

Shellhammer et al. [15] and Pflaum et al. [68] described

the concept of synchronized WuR communication. However, as discussed earlier, synchronization has limitations. Clock drift requires frequent resynchronization of devices, leading to additional WuPt transmissions to maintain timing alignment.

No reviewed articles provided direct evidence of synchronized WuR communication implementations. Instead, three different methods were identified to extend the WuPt for asynchronous communication. These methods are illustrated in Fig. 30.

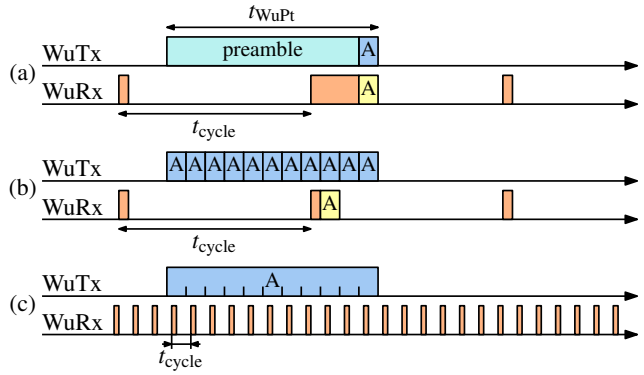

Fig. 30. Timing diagram visualizing the two different methods to trigger duty-cycled WuRxs. $t_{\text{WuPt}} > t_{\text{cycle}}$ ensures reliable triggering of the WuRx. In (a), the WuPt consists of a long preamble. The address information (A) is transmitted once. In (b), the WuPt repeats the address information continuously. In (c), a low symbol rate is used to transmit the address information. t_{cycle} is chosen to ensure each address bit is sampled.

Approach (a) was proposed by Bdiri et al. [40]. A long preamble was proposed that the WuRx can detect. The address information is transmitted only once at the end of the WuPt. When a WuRx detects the preamble, it remains active until the address is received. Frøytlog et al. [67] introduced a similar approach in their DC-MAC protocol.

The second approach was proposed in [35] by Bdiri et al. With this approach, the address information is continuously repeated throughout the WuPt. This approach reduces the WuRx power consumption, as the WuRx can immediately receive the address information without staying active for the entire WuPt duration.

However, synchronization issues may arise. The WuRx must ensure that the WuTx has finished transmission before proceeding with further protocol operations. In [34], we further refined this approach. Our WuRx had to detect a WuPt within 50 µs after activation. To eliminate packet loss, there could be no gaps in the WuPt longer than 50 µs. To achieve this, FSK modulation was introduced in the LF domain of the WuPt, ensuring continuous modulation and preventing packet loss.

Approach (c) was proposed by Ma et al. [69]. An ultra-low symbol rate, as low as 10 sym/s, with the address information transmitted only once per WuPt, was proposed. The WuRx samples a single address symbol whenever it enters active mode and correlates these samples with the expected address pattern. To avoid aliasing issues and packet loss, t_{cycle} must be shorter than the symbol period.

Ma et al. [69] tested symbol rates between 10 sym/s and 10 ksym/s, resulting in different duty-cycling values. The average power consumption varied from 9.3 µW at low symbol rates to 440 µW at high symbol rates.

Zhang et al. [28] analyzed the power consumption of different duty-cycling ratios but did not provide details on how packet loss was prevented.

da Silva et al. [71] and Ma et al. [70] proposed duty-cycled WuRxs without addressing capabilities.

3) Circuit Design Considerations: Designing power-gated or duty-cycled WuRx circuits introduces specific challenges that are less critical in always-on designs.

A key requirement is fast turn-on time. If the circuit takes too long to start up or sensitivity is degraded during activation, leading to degraded performance. Every power-gated circuit must be evaluated to ensure it meets the necessary turn-on time constraints.

One critical factor is the behavior of LF amplifiers. Circuits with high-pass filters or DC blocking capacitors require extra time to stabilize, delaying signal reception. DC blocking capacitors should be carefully selected or avoided to ensure rapid startup.

Another factor is the data slicer in the comparator circuit. The turn-on time of the WuRx is directly related to the data slicer time constant τ_{DS}. A shorter τ_{DS} improves startup time but limits the WuRx's ability to process signals with a high RLL.

Decoupling capacitors are another concern. These are typically required for IC stability, with common values around 100 nF. However, in power-gated or duty-cycled circuits, large decoupling capacitors can increase power consumption. When the supply line is turned on, the capacitors draw a high inrush current. When the supply is turned off, stored charge in the capacitors continues powering the ICs, prolonging active time and increasing average power consumption. For example, in [34], our duty-cycled WuRx consumed 350 nAs during a single reception period of 50 µs. Adding three 100 nF decoupling capacitors would require an additional 900 nAs, tripling the average power consumption. To minimize unnecessary power loss, decoupling capacitors should be carefully sized or alternative stabilization techniques should be explored.

H. Wake-up Transmitter Design

The WuTx is essential for enabling sensor nodes to communicate on the WuR channel. If the WuR and MR channels are identical, it is recommended to use the MR as the WuTx to reduce costs and minimize size. However, for out-of-band WuR communication, an additional WuTx is required.

If the MR supports the required RF modulation for WuPts, typically OOK, implementing the WuTx is straightforward. The MR needs to be reconfigured to the correct modulation type, data rate, and header settings to properly transmit the WuPt. Switching between MR and WuTx modes requires reconfiguration, which can introduce a delay. This reconfiguration time should be considered when designing WuR-based protocols. This delay was previously visualized as t_{setup} in Fig. 9.

If the MR does not support OOK modulation, alternative methods must be used to generate the WuPt. One approach

is to leverage test modes of the MR to output a short CW signal, which can then be switched on and off in software or by using an external antenna switch. Another method is to use standard data packets, since most MRs employ constant-envelope modulations. For example, in FSK transmissions, small frequency variations are usually undetectable by WuRx's RFED. The same applies to phase-shifting keyed signals. However, if a high LF carrier or symbol rate is required, generating a WuPt without native OOK support becomes more difficult due to the limited speed of the MR's communication interface and synthesizer.

Several studies have explored using standard wireless communication protocols to generate WuPts. References [124], [168], [172] investigated the use of IEEE 802.11 transmitters to generate WuPts. By carefully structuring IEEE 802.11 frames, they created RF pulses that served as WuPts. Oller et al. [168] and Lopez-Aguilera et al. [172] demonstrated that this approach could achieve an LF of 16 kHz for an LFPM-based WuRx.

Gavrikov et al. [110] proposed an FSK-based WuRx operating in the 2.45 GHz band. Their approach involved generating the WuPt using two Bluetooth Low Energy transmitters, as the frequency deviation of their FSK was too large for a single transmitter. However, this method required two separate antennas and transmitters, making it impractical for implementation on a wireless sensor node.

For acoustic and optical WuRxs, multiple household devices can serve as WuTxs. Höflinger et al. [56] and Bannoura et al. [57] proposed using a smartphone to generate the WuPt. Additionally, any device equipped with audio or light output, such as speakers or alarms, could function as a WuTx for an acoustic or optical WuRx.

IV. Conclusion

This section summarizes the findings of our study on WuRxs. First, we examine the limitations of key parameters, including sensitivity, power consumption, and WuPt duration, identifying the most optimized designs. Next, we critically evaluate the current state of research, identifying common challenges and areas for improvement. Finally, we explore promising research directions that could enhance WuR communication in future studies.

A. Optimized Wake-up Receivers

This subsection presents the WuRxs that achieve the best performance in sensitivity, power consumption, and WuPt duration.

1) Sensitivity-Optimized Wake-up Receivers: Wu et al. [116] proposed a WuRx operating at 915 MHz with a power consumption of 227 µW. It achieved a sensitivity of −90 dBm at 1 ksym/s, which improved to −98 dBm at a lower symbol rate of 20 sym/s. This design included a reflective RF amplifier, a passive RFED, and a comparator-based data slicer. However, it did not include addressing capabilities or coding schemes. The reflective amplifier contributed significantly to its high sensitivity, but the availability of tunnel diodes, which are essential for this circuit, remains a challenge. The study did not explore duty cycling, which could potentially reduce power consumption. Implementing an LF amplifier might further improve sensitivity with minimal impact on power consumption.

Petäjäjärvi et al. [44] introduced a super-regenerative receiver for human body communication, achieving −97 dBm sensitivity. This was possible due to active mixing, but the design operated at a low 28 MHz carrier frequency. The power consumption of the *LC* oscillator was analyzed, revealing that a minimum supply current of 5 µA was required at 28 MHz, compared to at least 50 µA at 868 MHz. A complex programmable logic device was used for address decoding.

da Silva et al. [71] used the CC1200 MR as a WuRx, achieving −95 dBm sensitivity by reducing the receiver bandwidth. The power consumption varied based on the duty cycle, reaching 93.2 µW with a 30 s latency and 366.7 µW with 8 s latency. Although the WuRx had excellent sensitivity, the high power consumption and latency made it unsuitable for many WuR applications. Since wake-up detection relied on only RSSI values, no addressing capabilities were included. Using a faster MR or shorter carrier sense periods could improve efficiency by reducing active time and power consumption.

Highly sensitive WuRxs are using RF amplifiers and duty cycling to reduce the power consumption. However, they often have high active power consumption and require long WuPts to account for inactive periods. Always-on WuRxs offer a simpler and more reliable circuit design, but every component must be carefully optimized to maintain low power consumption in the micro-watt range. In the following paragraphs, we will present always-on WuRxs with optimized sensitivity values.

Kazdaridis et al. [115] designed an always-on WuRx with −70 dBm sensitivity while consuming only 1.18 µW. The design included a passive RFED, a single-stage opamp LF amplifier, and a comparator-based data slicer. The study did not specify the WuPt timing or symbol rate, but an oscilloscope screenshot suggested a symbol rate of 47 sym/s. However, the GBWP of the opamp appears insufficient for the reported performance, casting doubt on the sensitivity and symbol rate. This highlights the inevitable trade-off between sensitivity, power consumption, and latency in WuRx design.

Woias et al. [46] and Köble et al. [117] used the LFPM ATA5283, achieving −63 dBm sensitivity at 7.4 µW [46] and −63.4 dBm at 8.7 µW [117], respectively. Neither study provided WuPt timing details. Both designs shared the same BJT-based LF amplifier, but it remains unclear whether the sensitivity was achieved due to amplifier performance, superior ATA5283 signal detection, or lower symbol rates.

In [32], we proposed a BJT-based LF amplifier for the LFPM AS3933, reaching −62 dBm sensitivity while consuming 21.9 µW with a 27.7 ms WuPt duration. This design improved sensitivity by incorporating a single-stage common-emitter amplifier, distinguishing it from the approaches used by Woias et al. [46] and Köble et al. [117].

2) Power Consumption-Optimized Wake-up Receivers: Passive and energy-harvesting WuRxs consume no power from the sensor node's battery. Passive WuRxs use only passive components [5], [75], [76]. However, in [148], we showed that a comparator is required to prevent STE currents in CMOS

inputs. Without it, the STE can drain the main battery quickly. Energy-harvesting WuRxs use energy from the WuPt itself [59], [60], [78]–[81] or the environment [61], [84].

The sensitivity of passive and energy-harvesting WuRxs is usually −30 dBm. Some designs achieve better sensitivity, such as Saab et al. with −38 dBm [84] and Qaragoez and Schreurs with −56.5 dBm [78]. However, these designs require large energy-harvesting components.

The lowest power consumption in a battery-powered WuRxs was achieved by Magno et al. [38], [151]. Their design used a passive RFED and a comparator-based data slicer with an adaptive reference generator. The only powered component was the comparator. They tested multiple comparators, each affecting power consumption and sensitivity. The lowest-power comparator, TLV3691, consumed 196 nW and achieved −32 dBm sensitivity.

A comparator is the minimum required component to prevent STE [148]. With an adaptive reference generator, no extra power is needed since the RFED generates the reference voltage. The TLV3691 operates at 0.9 V and has a supply current of 75–150 nA at room temperature. The most power-efficient WuRx would therefore consume between 67.5–135 nW.

Magno et al. [38] also tested the LPV7215 comparator, which improved sensitivity to −55 dBm but increased power consumption to 1.276 µW.

LFPM-based WuRxs consume more power. The supply current is typically 3 µA due to the LFPM. The lowest-power LFPM-based WuRx was by Bdiri et al. [64], but the sensitivity was poor at approximately −29 dBm. Details on reducing the LFPM's power consumption were not provided.

In [66], we optimized the AS3933 LFPM by activating duty cycling and lowering the supply voltage. This reduced power consumption to 5.71 µW, while maintaining −61.6 dBm sensitivity and requiring only 9.02 ms WuPt duration.

3) Latency-Optimized Wake-up Receivers: In Subsubsection II-C2, we explained how latency is defined in our article. We identified the different components contributing to end-to-end latency, including setup time, preamble, symbol rate, and WuPt duration. Comparing WuRx designs by latency alone is not always fair, as the WuPt's address length directly affects the latency. Comparing only the symbol rates is also insufficient because the WuPt preamble cannot be neglected. Many articles did not provide detailed WuPt timing information, making it difficult to determine the actual preamble duration.

WuRxs without addressing capabilities generally achieve the lowest latency. Wang et al. [76] reported a latency of 25 µs. Other articles without addressing capabilities also showed low latency values [27], [47], [93], [102], [139]–[141].

The lowest latency for a WuRx supporting addressing was achieved by Ammar et al. [100]. They reported a latency of 500 µs. This design utilized one of the highest symbol rates among the reviewed prototypes, 200 ksym/s, with 16 symbols per WuPt. However, the article mainly focuses on the working principle of their address decoder. Critical information, such as sensitivity, data slicer behavior, and WuPt preamble duration, is missing. Based on the required 0.8 V amplitude at the RFED output and the voltage sensitivity presented, we estimated the sensitivity to be −23.3 dBm.

Lopez-Aguilera et al. [125] proposed an addressable WuRx with a latency of 148 µs. This article reports the highest symbol rate among the reviewed designs with 250 ksym/s. However, the design uses an RF amplifier that consumes 200 mA at 5 V, resulting in a total power consumption of 1 W. This power consumption is extremely high for typical WuRx applications, and the intended field of use for such a design remains unclear.

Ziesmann et al. [152] improved the design of Magno et al. [38] by modifying the WuPt structure. They added a start symbol to ensure univocal pattern detection. This design uses a symbol rate of 10 ksym/s, achieving a WuPt duration of 1.4 ms. Ziesmann et al. identified a flaw in Magno's preamble detector, which struggled to detect consecutive WuPts. They added a discharge transistor to reset the preamble detector's capacitor, allowing the WuRx to quickly process successive WuPts. This modification reduced the recovery time of the preamble detector from 39 ms to only 37 µs.

WuRxs based on LFPMs generally require longer WuPts due to the minimum preamble duration required for proper detection. Additionally, these designs need double amplitude modulation, as shown in Fig. 26, which further limits the symbol rate. The highest symbol rate for LFPM-based WuRxs is approximately 8 ksym/s [91], [160], [167], [170]. Among these, Kumberg et al. [160] achieved the shortest WuPt duration of 2.2 ms, followed by Hierold et al. [170] with 3.61 ms and Blobel et al. [91] with 3.68 ms.

B. Criticism on the Current State of Research

One of the main issues in this research field is the lack of essential information in many research articles. As shown in Section V, some articles fail to provide critical parameters such as sensitivity, power consumption, or latency. Even in recent studies, these values are missing [22], [70], [84]. It is essential for future articles to report all values listed in Section V, allowing for proper comparison and analysis of improvements.

Each WuRx building block should be evaluated individually. Providing key parameters for every stage ensures that researchers can identify the specific innovation in a given design. Tab. V outlines the key and optional parameters for different WuRx components.

A clear example of missing data is the voltage sensitivity of RFEDs. Without this value, it is difficult to determine how a sensitivity improvement was achieved. RFEDs based on VMs promise better sensitivity but come with drawbacks such as high video resistance, increased noise, and additional cost. However, none of the 11 articles using VM-based RFEDs reported their voltage sensitivity [64], [68], [77], [78], [102], [122], [123], [130], [131], [155], [156]. Even after 15 years of research, it remains unclear whether VM-based RFEDs are truly beneficial for WuRxs. A similar issue arises when evaluating other building blocks. Reporting all key parameters would allow future researchers to trace improvements back to specific design choices.

As discussed in Subsection II-C, there are no universal definitions of sensitivity, power consumption, or latency. Researchers must clearly state how these parameters are mea-

TABLE V
KEY AND OPTIONAL PARAMETERS OF WURX BUILDING BLOCKS

Building block	Key parameter	Optional parameter
RF input	source impedance	—
RF filter	—	insertion loss
RF amplifier	gain, power consumption	*S*-parameters, turn-on time
RFED	voltage sensitivity	*S*-parameter, video resistance
LF amplifier	gain, power consumption	frequency response, input & output impedance
A/D converter	data slicer time constant	minimum detectable voltage signal
address decoder	univocalness, run-length limit, usable address bits, preamble	microcontroller software / LFPM configuration

sured. We recommend using PER-based sensitivity measurements and providing a signal level sweep, as done in [32], [34], [36], [66], [93]. A PER plot improves transparency by revealing issues such as false wake-ups, saturation, and packet loss.

For power consumption, we recommend reporting two values: The quiescent power consumption stating the power consumption without WuPts on the channel. The FWuEW stating the energy consumed when processing a single WuPt or interference. Combining these values allows researchers to estimate real-world power consumption, which depends on the channel traffic. WuRxs can operate in vastly different environments, where interference levels vary significantly.

Duty-cycled WuRxs remain inactive for long periods. During these sleep periods their are unable to receive WuPts. To avoid random packet loss, WuPts must last longer than the sleep interval. This can significantly increase WuPt duration. One solution is synchronized WuR communication, as proposed by Shellhammer et al. [15]. However, synchronization requires continuous readjustment due to clock drift. Future studies should clearly describe how synchronization is maintained over time.

Research using COTS components should ensure that all components are commercially available. Reproducibility is essential for validation and prototype development. Throughout our survey, we found multiple cases where researchers used components that had been discontinued years before publication. If a study relies on discontinued components, it should be clearly stated, along with justifications for their use.

WuRxs must reliably detect WuPts to function properly within MAC-layer protocols [88], [108]. However, many studies claim addressing capabilities but fail to describe their packet detection methods. Many do not implement coding schemes or WuPt preambles, yet claim to support addressing [27], [44], [58], [61], [69], [77], [78], [98], [100], [103], [113], [115], [116], [123], [131], [139], [144].

In [90], we emphasized the importance of including a preamble, separation sequence, and low RLL in the WuPt. Many coding schemes lack these elements, making them non-univocal. Subsubsection III-F5 explains why non-univocal addressing leads to false wake-ups and energy waste. Many WuRxs lack univocal addressing schemes because they fail to clearly define the first address symbol.

Without proper coding schemes, WuPts have high RLLs, meaning addresses contain long sequences of consecutive ones or zeros. In a 16-bit address, sequences of 16 consecutive ones or zeros can appear. Many WuRxs rely on low-pass filtered data slicers, which suffer from saturation after multiple identical symbols [38]. However, RLL limitations are rarely mentioned in research papers. Some studies claim that their entire address space is usable, even when using 16-symbol patterns with an RLL of 16 and more [17], [38], [42], [57], [65], [95], [98], [100], [103], [110], [132], [137], [151], [164], [166]–[168].

C. Future Research Directions

Throughout our survey, we identified several ideas that could enhance future WuR communication. However, these ideas have not been explored in depth, and reliable measurements are often missing. Further investigation and comparison with recent designs could provide valuable insights and serve as a strong foundation for future research.

1) RF Amplifier: Improving the gain and reducing power consumption of the RF amplifier is crucial for enhancing the overall performance of RF amplifier-based WuRxs. The RF amplifier significantly contributes to the power consumption of the WuRx, while its gain directly affects the sensitivity.

RF amplifiers can be designed specifically for WuRx applications, focusing on high gain and low power consumption. Parameters like linearity and output loading can be neglected. Designing RF amplifiers to match the high-impedance characteristics of the RFED, as propose by proposed using a buffer circuit to is a promising approach.

A reflective amplifier based on a tunnel diode, as proposed by Wu et al. [116], demonstrated excellent performance. Unfortunately, tunnel diodes are no longer commercially available, and their future accessibility remains uncertain.

2) Passive Voltage Amplification: Increasing the voltage sensitivity of the RFED reduces the need for active LF amplification. Theoretically, VM-based RFEDs should show enhanced the voltage sensitivity values. However, no article has provided measured data to confirm this advantage. Investigating the performance of VM-based RFEDs and comparing them to VD-based designs would be valuable.

Resonance circuits have also been proposed as a method of passive voltage amplification [17], [117]. Exploring more efficient amplification methods or improving the load-handling of crystal oscillators could enhance the performance of WuRxs.

3) Active Mixing: Most COTS WuRxs use passive RFEDs due to their zero power consumption. However, other methods involving active mixing and local oscillators show promising sensitivity improvements.

Petäjäjärvi et al. [44] proposed a super-regenerative receiver for human-body communication. This design achieved an sensitivity of -97 dBm but operates at a low carrier frequency of 28 MHz. Investigating whether this approach can be adapted

to more common sub-Gigahertz RF bands could be a valuable research direction.

Meller et al. [173] and Zhu et al. [174] proposed RF switching combined with resonators to amplify the RF signal. These designs enable the creation of high-quality band-pass filters, leading to highly sensitive WuRxs. Both studies relied a custom IC or microelectromechanical system (MEMS) for implementation. Further investigations are needed to determine if these methods can deliver comparable performance while maintaining low power consumption.

4) Backscattering: Backscattering RF transceivers are closely related to WuRxs because both rely on low-power receivers. Backscattering transmitters can be designed with minimal energy consumption, as they operate by modulating the antenna's reflective properties. This process scatters the incident RF signal back to the receiver. However, an essential component of backscattering communication is the exciter device, which generates the RF carrier signal. Additionally, backscattering systems typically suffer from limited range because the signal path involves two legs: from the exciter to the transmitter and from the transmitter to the receiver [16], [133], [175].

Jong et al. [113] proposed a backscattering receiver using a design similar to typical WuRxs. Their receiver consists of an RF filter, a passive RFED, an LF amplifier, and a comparator-based data slicer. Implementing an exciter in WuR applications remains challenging because it usually requires mains power.

On the other hand, backscattering transmitters offer a promising solution for reducing power consumption during data transmissions. These transmitters only modify the reflective properties of the antenna rather than actively generating RF signals. Lazaro et al. [135] proposed using PIN diodes to create switchable loads within an antenna array. This approach forms a frequency-selective surface that can be controlled by a bias voltage. Such designs could enable ultra-low-power WuR-based data transmission, especially in energy-constrained environments.

5) Security: WuR-based sensor nodes are particularly vulnerable to channel-blocking and replay attacks. In traditional RF communication, sending and receiving multiple packets simultaneously on the same frequency is generally impossible. An attacker could block the channel by continuously transmitting signals, making the sensor nodes inaccessible. Although most systems resume normal operation after the interference stops, WuR systems are especially vulnerable to energy depletion attacks.

One critical vulnerability of WuRxs is their susceptibility to replay attacks. Most WuRxs use a fixed address in the WuPt. When the WuRx detects a valid WuPt, it activates the MR, leading to a significant increase in power consumption. If an attacker repeatedly transmits the same WuPt, the sensor node's battery can drain rapidly, rendering the device inoperative. [20] To ensure the use of WuRxs in safety-critical applications, effective replay-attack mitigation techniques must be developed.

D. Final Conclusion

In this article, we examined the hardware development of COTS WuRxs in detail. Although this is a narrow and specialized research field, we emphasized its significance by highlighting the advantages of using COTS components. Unlike previous surveys that focused on general aspects of WuR communication [1], [18], [20], we concentrated solely on hardware design. This focus allowed us to analyze 120 articles and 132 WuRx prototypes, a more comprehensive scope than earlier surveys.

We classified the WuRx prototypes based on channel type, operating mode, and addressing capabilities. We provided clear definitions of the three primary performance parameters: sensitivity, latency, and power consumption, and discussed their implications. We also highlighted additional parameters such as supply voltage, robustness, reliability, cost, size, component availability, and modulation, which are critical for real-world implementations. For most categories, we presented visualized data to show the distribution of these parameters across the analyzed prototypes.

We dedicated specific subsections to each WuRx building block, thoroughly discussing their design principles and performance characteristics.

In our performance evaluation, we identified the best-performing WuRxs in terms of sensitivity, power consumption, and latency. While further improvements in sensitivity, power consumption, and latency remain valuable, we argue that the future of WuR development should shift toward reliability and repeatability. In our previous works [34], [36], [90], [148], we demonstrated that many existing prototypes lack consistent and robust performance. Ensuring that WuRxs meet the demands of MAC-layer protocols is crucial for bridging the gap between hardware development and protocol-level implementation.

We also criticized the current state of research, particularly the lack of comprehensive reporting in many articles. Missing essential information about key parameters made it difficult to accurately compare designs and determine which building blocks contributed to specific improvements. We encourage future authors to include all critical performance metrics listed in Section V and Tab. V to improve the transparency and reproducibility of their work.

Finally, we outlined promising directions for future research. Several open questions remain regarding the fundamental operation of WuRx building blocks. Ideas such as passive voltage amplification, active mixing, and backscattering present opportunities for further exploration. Additionally, practical challenges like security vulnerabilities arising from the simplicity of WuRxs must be addressed.

WuR communication is a powerful technique for enabling energy-efficient, battery-powered sensor nodes that are not feasible with traditional duty-cycled MR systems. We are confident that WuR technology will continue to advance and find new applications, eventually leading to the development of commercial products that either rely on or support WuR communication.

V. Literature Review Table

Reference	Channel[1]	Opmode[2]	Addr.[3]	Sens.[4] in dBm	V_{cc}[5] in V	P. cons.[6] in µW	WuPt dur.[7] in ms	LF in kHz	Sym. rate in ksym/s	RF filter	RF amp.	RF match	RFED type	RFED comp.[8]	LF amp.	ADC type	ADC comp.	ADC reference[9]	Addr. type	RF mod.	LF mod.	Coding[10]
Ma [58]	opt.	AON	var.	n/a	3	1.5	22	n/a	2	n/a	n/a	n/a	n/a	n/a	no	comp.	LTC1540	int.	µC	n/a	no	RZ
Perez [144]	opt.	AON	var.	n/a	3	5.4	4	n/a	5	n/a	n/a	n/a	n/a	n/a	OA	comp.	LTC1540	int.	µC	n/a	no	Man.+'232
Kolinko [5]	915M	pass.	—	—	n/a	0	—	455	—	no	no	—	SD	'285x	no	—	—	—	—	—	—	—
Malinowski [43]	300M	AON	no	−46	3	7.8	—	15	n/a	no	no	LC	SD	—	OA	LTh[18]	n/a	n/a	no	CW	no	n/a
Benoît [49]	LF	AON	fix.	n/a	3[12]	84	—	125	—	n/a	n/a	n/a	n/a	n/a	no	LFPM	AS3931	n/a	LFPM	n/a	OOK	—
Hakkinen [143]	opt.	AON	—	n/a	3	12	—	1.2	—	n/a	n/a	n/a	n/a	n/a	OA	comp.	LPV7215	adap., offs.	—	n/a	—	—
Ansari [155]	868M	AON	var.	−40[11]	3	12.5	63.6	n/a	1.88	no	no	LC	VM×10	'285x	no	comp.	MAX9119	fix.	µC	OOK	no	PWM
Doorn [92]	868M	AON	no	−31[11]	—	600	10	0.862	n/a	SAW	no	no	VD	—	OA	ADC	PIC12	n/a	µC	OOK	no	direct
Wang [76]	915M	pass.	no	−27.7	n/a	0	0.025	n/a	n/a	no	no	LC	VD	'285x	no	—	n/a	n/a	no	CW	no	n/a
Gamm [14], [17]	868M	AON	fix.	−52	3	7.76	13	125	2.98	no	no	LC	VD	'285x	no	LFPM	AS3932	n/a	LFPM	OOK	OOK	direct
Koskela [131]	2.4G	AON	fix.	−30	3	4.7	4	n/a	2.04	no	no	no	VM	'286x	no	comp.	LMC7215	adap.	CMOS	OOK	no	RZ
Mathews [142]	opt.	AON	—	n/a	3.3	316	—	n/a	—	n/a	n/a	n/a	n/a	n/a	OA	—	—	—	—	n/a	—	—
Marinkovic [102]	434M	AON	var.	−51	1.5	0.27	2.9[14]	n/a	5.5	SAW	no	LC	VM×4	'285x	no	comp.	NPS1101	adap.	µC	OOK	no	PWM
Marinkovic [130]	434M	AON	var.	—	2	0.47	7.8	n/a	9.6	no	no	no	VM×4	—	no	comp.	LTC1540	adap., offs.	µC	OOK	no	direct
Sanchez [159]	acou.	AON	fix.	n/a	3	8.7	—	85	—	n/a	n/a	n/a	n/a	n/a	no	LFPM	AS3933	n/a	LFPM	n/a	OOK	—
Kondo [124]	2.4G	AON	var.	−82	—	110m	2.6	n/a	n/a	SD[15]	UPC8178	n/a	PD	LTC5534	no	ADC	PIC18	n/a	µC	CW	no	PWM
Sánchez [53]	acou.	AON	fix.	n/a	3.3	8.1	19	85	1.25	n/a	n/a	n/a	n/a	n/a	no	LFPM	AS3933	n/a	LFPM	n/a	OOK	Man.
Sutton [97]	434M	AON	fix.	−43	2.5	8.25	10.8	125	2.73	no	no	LC	VD	'285x	no	LFPM	AS3930	n/a	LFPM	OOK	OOK	Man.
Trinh [75]	434M	pass.	—	−27	n/a	0	—	20	—	no	no	mixed	SD	'285x	VM	LTh[18]	n/a	n/a	—	OOK	—	—
Umbdenstock [176]	868M	AON	fix.	−15	3	6	—	125	—	no	no	—	VD	—	no	LFPM	AS3932	n/a	LFPM	OOK	OOK	—
Wang [154]	915M	AON	var.	−40[11]	3[12]	1.5	—	n/a	—	no	no	LC	VD	'285x	no	comp.	LTC1540	fix.	µC	OOK	no	PWM
Boaventura [156]	868M	AON	var.	−35	3	10.8	7.29	n/a	9.6	no	no	—	VM×8	'285x	no	comp.	MAX9119	fix.	µC	OOK	no	'232
Lattanzi [164]	acou.	AON	var.	n/a	2	1.64	500	40	0.02	n/a	n/a	n/a	n/a	n/a	no	comp.	MCP6541	fix.	µC	n/a	OOK	direct
Lazaro [135]	2.4G	AON	var.	−40	3	—	—	n/a	—	no	no	LC	VD	'285x	no	comp.	—	fix.	µC	OOK	—	—
Oller [123]	868M	AON	var.	−45	3	2.67	42	n/a	1	SAW	no	no	VM×10	'285x	no	comp.	MAX9119	fix.	µC	OOK	no	—
Parks [122]	434M	AON	no	−40	3	1.83	1090	n/a	n/a	LC	no	LC	VM×10	'285x	no	OA	LPV521	fix.	no	CW	no	n/a
Prabhakar [177]	868M	AON	fix.	—	3	6	16	125	—	no	no	—	pED	—	no	LFPM	AS3932	n/a	LFPM	OOK	OOK	—
Pursula [128]	2.4G	AON	fix.	−50	3	20.4	13	—	2.73	no	no	LC	SD	'286x	no	LFPM	AS3930	n/a	LFPM	OOK	OOK	—
Bdiri [64]	868M	AON	fix.	−29[11]	3	4.59	—	—	—	no	no	LC	VM×12	—	no	LFPM+ comp.	AS3932	fix.	LFPM	OOK	OOK	—
Carrascal [59]	opt.	EH	fix.	n/a	—	0	37[14]	21	1.32	n/a	n/a	n/a	n/a	n/a	no	LFPM	AS3933	n/a	LFPM	n/a	OOK	Man.
Catarinucci [138]	2.4G	AON	no	−45	3	21.6m	—	n/a	—	no	no	n/a	PD	LMV221	no	—	—	—	no	CW	no	n/a
Gamm [95]	434M	AON	fix.	−53.2	3	8.4	—	125	—	no	no	LC	VD	'285x	no	LFPM	AS3932	n/a	LFPM	OOK	OOK	direct
Höflinger [56]	acou.	AON	fix.	n/a	3	55.8	—	18	—	n/a	n/a	n/a	n/a	n/a	OA	LFPM	AS3933	n/a	LFPM	n/a	OOK	—
Kumberg [160]	868M	AON	fix.	−50	3	8.1	2.2	125	8.19	no	no	LC	VD	'285x	no	LFPM	AS3932	n/a	LFPM	OOK	OOK	direct
Kumberg [160]	868M	AON	fix.	−50	3	8.1	4.4	125	8.19	no	no	LC	VD	'285x	no	LFPM	AS3932	n/a	LFPM	OOK	OOK	direct
Magno [38]	868M	AON	var.	−55	1.8	1.276	1.6	n/a	10	no	no	LC	VD	'285x	no	comp.	LPV7215	adap.	µC	OOK	no	direct
Magno [38]	868M	AON	var.	−42	1.8	0.426	1.6	n/a	10	no	no	LC	VD	'285x	no	comp.	AS1976	adap.	µC	OOK	no	direct
Magno [38]	868M	AON	var.	−32	1.8	0.196	1.6	n/a	10	no	no	LC	VD	'285x	no	comp.	TLV3691	adap.	µC	OOK	no	direct
Oller [168]	2.4G	AON	fix.	−52	3	10.8	44.7	16.1	0.9	no	no	LC	VD	—	no	LFPM	AS3933	n/a	LFPM	OOK	OOK	direct
Petrioli [27]	2.4G	AON	var.	−83	1.2	—	0.064[14]	n/a	250	LC	yes	n/a	PD	MAX2015	no	—	—	—	µC	FSK	no	—
Ammar [100]	868M	AON	fix.	−23.2[11]	0.9	13.4	0.08	n/a	200	no	no	LC	VD	—	no	LTh[18]	n/a	n/a	CMOS	OOK	no	direct
Bdiri [37]	868M	PG	fix.	−60	—	8.28[13]	10.36	18	—	no	no	LC	VD	'285x	IA	LFPM	AS3933	—	LFPM	OOK	OOK	—
Del Prete [42]	868M, 2.4G	AON	var.	−53.4	1.8	1276	1.6	n/a	10	no	no	mixed	VD	'7630	no	comp.	LPV7215	adap.	µC	OOK	no	direct
Kaushik [77]	915M	pass.	var.	—	n/a	0	—	n/a	50	no	no	—	VM×14	—	no	LTh[18]	MSP430	n/a	µC	OOK	no	RZ
Bannoura [57]	acou.	AON	fix.	n/a	3	420	27	20	1.1	n/a	n/a	n/a	n/a	n/a	OA	LFPM	AS3933	n/a	LFPM	n/a	OOK	direct
Bannoura [167]	868M	AON	fix.	−53	3	7.8	4.76	125	8	no	no	—	pED	—	no	LFPM	AS3933	n/a	LFPM	OOK	OOK	direct
Bdiri [65]	868M	PG	fix.	−60	3	7.5	22[14]	18	4.57	no	no	—	VD	'285x	IA	LFPM	AS3933	n/a	LFPM	OOK	OOK	direct
Blobel [91]	868M	AON	var.	—	—	—	3.675	125	8	no	no	—	pED	—	no	LFPM	AS3933	n/a	LFPM+ CMOS	OOK	OOK	Man.
Prete [45]	868M, 2.4G	AON	var.	−65	—	—	16[14]	n/a	1	no	no	stripl.	VD	'7630	no	comp.	LPV7215	adap.	µC	ICW	no	direct
Hutu [107]	915M	AON	fix.	−47	5	200m[13]	1.2[14]	n/a	n/a	cavity	no	n/a	PD	AD8362	OA	comp.	TS881	fix.	RF fil-ters	OFDM	no	direct
Lebreton [120]	2.4G	AON	var.	—	3[12]	71.4	8.88	n/a	4	no	no	rectenna	pED	—	no	comp.	TLV3691	fix.	µC	OOK	no	'232
Magno [151]	868M	AON	var.	−55	1.8	1.196	1.6[14]	n/a	10	no	no	LC	VD	'285x	no	comp.	LPV7215	adap.	µC	OOK	no	direct
Magno [151]	868M	AON	var.	−42	1.8	0.365	1.6[14]	n/a	10	no	no	LC	VD	'285x	no	comp.	AS1976	adap.	µC	OOK	no	direct
Magno [151]	868M	AON	var.	−32	1.8	0.152	1.6[14]	n/a	10	no	no	LC	VD	'285x	no	comp.	TLV3691	adap.	µC	OOK	no	direct
Petäjäjärvi [44]	28M	AON	fix.	−97	1.5	40	4	n/a	1.25	no	no	n/a	SRO	BFR92A	no	comp.	TS881	—	CPLD	OOK	no	direct
Polonelli [121]	868M	AON	var.	—	1.8	0.4	—	n/a	—	no	no	rectenna	VD	'285x	no	comp.	AS1976	adap.	µC	OOK	no	—
Ramos [60]	opt.	EH	fix.	n/a	3.6	0	—	21	—	n/a	n/a	n/a	n/a	n/a	no	LFPM	AS3933	n/a	LFPM	n/a	OOK	—
Hierold [170]	868M	AON	fix.	—	3.3	8.9	3.61	125	8.19	no	no	—	pED	—	no	LFPM	AS3933	n/a	LFPM	OOK	OOK	Man.
Khodr [98]	2.4G	AON	fix.	−28	3	39	16	n/a	1	no	no	mixed	VD	'7630	no	comp.	LTC1540	fix.	CMOS	OOK	no	direct
Kumberg [136]	868M	AON	fix.	−53.8	—	—	—	125	—	no	no	LC	VD	'285x	no	LFPM	AS3932	n/a	LFPM	OOK	OOK	—
Kumberg [162]	868M	AON	fix.	−51	3	10	6	125	—	no	no	—	pED	—	no	LFPM	AS3932	n/a	LFPM	OOK	OOK	Man.
Ma [69]	880M	DC	var.	−77	3	439.5	3.2	n/a	10	no	no	n/a	PD	LT5538	no	ADC	MSP430	n/a	µC	OOK	no	direct
Ma [69]	880M	DC	var.	−77	3	9.3	3200	n/a	0.01	no	no	n/a	PD	LT5538	no	ADC	MSP430	n/a	µC	OOK	no	direct
Mc Caffrey [129]	2.4G	AON	fix.	−56[11]	—	20.4	—	120	—	no	no	LC	SD	'286x	no	LFPM	AS3930	n/a	LFPM	OOK	OOK	Man.
Saez [62]	opt.	AON	fix.	n/a	±3	70.2	28.7	18	1.16	n/a	n/a	n/a	n/a	n/a	OA	LFPM	AS3933	n/a	LFPM	n/a	OOK	Man.
Saez [62]	836M, 868M	AON	fix.	−61	±3	70.2	28.7	20	1.16	no	no	LC	VD	'285x	OA	LFPM	AS3933	n/a	LFPM	FSK	OOK	Man.
Siniscalchi [103]	2.4G	AON	—	−54.7	1	—	10	n/a	3.27	no	no	LC	SD	'286x	SR560[17]	external	PC	n/a	—	OOK	no	—
Bdiri [40]	—	DC	var.	—	—	—	32	n/a	128	no	no	—	VD	'285x	no	—	—	—	µC	OOK	no	'232
Bdiri [72]	868M	PG	fix.	−61	3	7.2	25	17	4	SAW	no	LC	VD	'285x	OA	LFPM	AS3933	n/a	LFPM	OOK	OOK	Man.
Bdiri [35]	868M	DC	var.	−90	1.8	3	32	n/a	128	SAW	BFG403	—	VD	'285x	BJT	comp.	TLV3201	adap., hyst.	µC	OOK	no	'232
Fabbri [80]	868M	EH	var.	−18.2[11]	—	0	4.55	n/a	2.2	no	no	—	pED	—	no	comp.	TLV3691	adap.	µC	OOK	no	'232
Frøytlog [149]	434M	AON	var.	−49.5	3	1.7	55[14]	n/a	0.1	no	no	LC	VD	'285x	no	comp.	LPV7215	adap.	µC	OOK	no	direct
Gavrikov [110]	2.4G	AON	fix.	−47.8	—	18.5	17.9	11.3	1.43	SAW	no	—	VD	'285x	OA	LFPM	AS3933	n/a	LFPM	FSK	OOK	direct
Pflaum [68]	868M	DC	fix.	−71	3	183	1000	125	4	no	MAX2643	LC	VM×6	'7630	OA	LFPM	PMA5110	n/a	LFPM	OOK	OOK	Man.
Skrimponis [153]	868M	AON	var.	—	3[12]	2.1	20	n/a	1.16	no	no	LC	VD	'285x	no	comp.	LPV7215	adap.	µC	OOK	no	direct
Woias [46]	315M	AON	—	−63	2	7.4	—	32.7	—	no	no	LC	SD	'285x	BJT	LFPM	ATA5283	n/a	—	OOK	OOK	—
Basagni [39]	434M/ 868M	AON	var.	−55	—	1.3	—	n/a	—	no	no	LC	VD	'285x	no	comp.	TLV3701	adap.	µC	OOK	no	direct
Benbuk [73]	2.4G	PG	no	−30	2.6	0.416	800	n/a	—	no	no	—	pED	—	no	comp.	TLV3691	fix.	CMOS	CW	no	direct
Chen [23]	LF	AON	fix.	—	3	18.3	12	125	—	n/a	n/a	n/a	n/a	n/a	no	LFPM	AS3933	n/a	LFPM	n/a	OOK	Man.
Dardari [79]	868M	EH	var.	−16	—	0	200	n/a	2.2	no	no	mixed	pED	—	no	comp.	TLV3691	adap.	µC	OOK	—	—
Frøytlog [67]	434M	DC	var.	−70	6	192	120	n/a	1.25	no	2SC3838	LC	VD	—	no	comp.	LPV7215	adap.	µC	OOK	no	Man.
Frøytlog [106]	434M	AON	var.	−80	6	6m	55[14]	n/a	0.1*	no	2SC3838	buffer	VD	'285x	no	comp.	LPV7215	adap.	µC	OOK	no	direct
Frøytlog [150]	434M	AON	var.	−37.4	3	1.17	95	n/a	0.1	no	no	LC	VD	—	no	comp.	TLV3691	adap.	µC	OOK	no	direct
Köble [117]	434M	AON	—	−63.4	2	8.7	—	4.68	—	no	no	LC	SD	—	BJT	LFPM+ comp.	ATA5283	adap., diode	—	OOK	OOK	—
Lopez-Aguilera [125]	2.4G	AON	var.	−55[11]	3	1000m	0.148	n/a	250	yes	yes	n/a	PD	LTC5508	no	OA	CA3140	fix.	µC	OOK	no	direct
da. Silva [71]	915M	DC	no	−95	—	93.2	30000	n/a	—	no	no	n/a	IC	CC1200	n/a	n/a	n/a	n/a	no	CW	no	n/a
da. Silva [71]	915M	DC	no	−95	—	366.7	8000	n/a	—	no	no	n/a	IC	CC1200	n/a	n/a	n/a	n/a	no	CW	no	n/a

Reference	Channel[1]	Opmode[2]	Addr.[3]	Sens.[4] in dBm	V_{cc}[5] in V	P. cons.[6] in µW	WuPt dur.[7] in ms	LF in kHz	Sym. rate in ksym/s	RF filter	RF amp.	RF match	RFED type	RFED comp.[8]	LF amp.	ADC type	ADC comp.	ADC reference[9]	Addr. type	RF mod.	LF mod.	Coding[10]
Benbuk [21]	2.4G	PG	no	−40	4.5	8.2	4000	n/a	n/a	no	no	—	pED	—	no	comp.	TLV3691	fix.	CMOS	CW	no	direct
Cabarcas [137]	915M	AON	fix.	−50	—	10.5	10	18	4.5	no	no	LC	VD	—	no	LFPM	AS3933	n/a	LFPM	OOK	OOK	direct
Fabbri [81]	868M	EH	var.	−21	2.1	0	4.55	n/a	2.2	no	no	—	VD	—	no	comp.	TLV3691	adap., offs.	µC	OOK	no	’232
Galante-Sempere [112]	868M	AON	fix.	−50	3[12]	9	13.3[14]	125	1.2	no	no	LC	VD	’285x	no	LFPM	AS3933	n/a	LFPM	OOK	OOK	—
de Jong [113]	434M	AON	var.	−54.5	1.8	85	184	n/a	1	SAW	no	LC	VD	’285x	OA	comp.	LPV7215	adap., hyst.	µC	OOK	no	—
Lopez-Aguilera [172]	2.4G	AON	fix.	−52	—	10.8	45.9	16	—	no	no	LC	VD	—	no	LFPM	AS3933	n/a	LFPM	OOK	OOK	—
Ma [70]	868M	DC	—	−70	3	310	—	1	—	no	no	n/a	PD	LT5538	OA	comp.	TLV3691	—	—	—	—	—
Mohaghegh [50]	LF	AON	fix.	—	—	—	70	125	0.457	n/a	n/a	n/a	n/a	n/a	no	LFPM	AS3933	n/a	LFPM	n/a	OOK	—
Saab [84]	2.4G	EH	no	−38	3[12]	2.25m	—	n/a	—	no	no	stripl.	VD	—	no	OA	LMC6001	fix.	µC	CW	—	—
Dudko [61]	opt.	EH	—	n/a	—	—	—	—	40	n/a	n/a	n/a	n/a	n/a	no	MOSFET	—	fix.	—	n/a	—	—
Fromm [141]	868M	AON	no	−47	3	4.2	5	n/a	n/a	SAW	no	LC	VD	’7630	OA	comp.	TLV3691	fix.	no	CW	no	n/a
Kang [114]	900M	AON	fix.	−52	3.3	2.04m	20	18	2.52	no	no	LC	VD	’285x	OA	LFPM	AS3933	n/a	LFPM	OOK	OOK	Man.
Kazdaridis [115]	868M	AON	var.	−70	3.3	1.18	337[14]	n/a	0.047	no	no	LC	VD	’285x	OA	comp.	TLV3691	fix.	µC	OOK	no	direct
Polonelli [47]	3993.6	AON	var.	−48	3.3	100	2.4	n/a	10	yes	no	no	VD	BAT15	no	comp.	LT1017	adap., offs.	µC	OOK	—	—
Benbuk [74]	2.4G	PG	fix.	−40	2.6	0.585	4[14]	n/a	0.5	no	no	—	pED	—	no	comp.	TLV3691	fix.	CMOS	OOK	no	PWM
Fromm [93]	868M	AON	no	−56	3	3.6	2.93	8.19	n/a	SAW	no	LC	VD	’7630	BJT	comp.	LPV7215	adap.	µC	OOK	OOK	direct
Fromm [93]	868M	AON	no	−60	3	3.6	11.7	2.04	n/a	SAW	no	LC	VD	’7630	BJT	comp.	LPV7215	adap.	µC	OOK	OOK	direct
Fromm [93]	868M	AON	no	−51	3	2.58	5	n/a	n/a	SAW	no	LC	VD	’7630	OA	comp.	TLV3691	adap.	no	CW	no	n/a
Fromm [93]	868M	AON	no	−55	3	4.8	11.7	2.04	n/a	SAW	no	LC	VD	’7630	OA	comp.	LPV7215	adap.	µC	OOK	OOK	direct
Fromm [34]	868M	DC	var.	−80	3.3	14.3	103.4	50/100	12.5	SAW	MAX2640	LC	VD	’7630	OA	comp.	TLV3201	adap., hyst.	µC	OOK	FSK	’232
Luo [140]	915M	AON	no	−43.5	2.8	2.1	1	n/a	n/a	no	no	n/a	RF harv.	P1110B	no	comp.	LPV7215	fix.	no	CW	no	n/a
Polonelli [132]	868M	AON	var.	−56	3.3	1.84	24	n/a	—	no	no	—	VD	BAT15	no	comp.	TLV3701	adap.	µC	OOK	no	direct
Schott [32]	868M	AON	fix.	−62	3	21.9	27.7	18.7	2.32	SAW	no	LC	VD	’7630	OA	LFPM	AS3933	n/a	LFPM	OOK	OOK	Man.
Schott [32]	868M	AON	fix.	−54	3	13.2	27.7	18.7	2.32	SAW	no	LC	VD	’7630	BJT	LFPM	AS3933	n/a	LFPM	OOK	OOK	Man.
Wu [116]	915M	AON	—	−90	—	227	16[14]	n/a	1	no	RA[16]	LC	VD	’285x	no	comp.	LPV7215	adap.	—	—	—	—
Wu [116]	915M	AON	—	−98	—	227	800[14]	n/a	0.02	no	RA[16]	LC	VD	’285x	no	comp.	LPV7215	adap.	—	—	—	—
Yi [139]	2.4G	AON	—	−44.6	3	152	0.16[14]	n/a	100	no	no	n/a	BJT	BFU730F	no	comp.	TLV7021	fix.	—	—	—	—
Fromm [66]	868M	AON	fix.	−61.6	2.4	5.71	9.02	25.7	3.21	no	no	LC	VD	’7630	no	LFPM	AS3933	n/a	LFPM	OOK	OOK	Man.
Fromm [66]	868M	AON	fix.	−61.6	2.4	5.71	14	25.7	3.21	no	no	LC	VD	’7630	no	LFPM	AS3933	n/a	LFPM	OOK	OOK	Man.
Liu [105]	2.4G	AON	fix.	−60	2	25.3	7.14[14]	15	2.18	no	no	LC	VD	’7630	BJT	LFPM+ comp.	AS3933	adap.	LFPM	OOK	OOK	Man.
Mohammed [22]	868M	AON	fix.	−46[11]	3	12.1	—	32	—	no	no	LC	VD	—	no	LFPM	RF125	n/a	LFPM	OOK	OOK	—
Schaechtle [55]	acou.	AON	fix.	n/a	2.4	15.8	24.8	18	1	n/a	n/a	n/a	n/a	n/a	no	LFPM	AS3933	n/a	LFPM	n/a	OOK	Man.
Wolling [51]	LF	AON	fix.	n/a	3.3	7.4	4.21	125	4.09	n/a	n/a	n/a	n/a	n/a	no	LFPM	AS3930	n/a	LFPM	n/a	OOK	Man.
Zhang [28]	—	DC	fix.	−54[11]	—	9	6.4	n/a	5	no	no	LC	VD	—	no	—	—	—	CMOS	OOK	no	PWM
Ziesmann [152]	868M	AON	var.	−32[11]	2	0.585	1.4	n/a	10	no	no	LC	VD	—	no	comp.	TLV3691	adap.	µC	OOK	no	direct
Babatunde [166]	434M	AON	fix.	−47[11]	—	6.6	17	125	—	no	no	LC	VD	—	no	LFPM	AS3932	n/a	LFPM	OOK	OOK	direct
Fromm [94]	868M	AON	fix.	−60.1	3	10.2	4.89	36	4.5	no	no	LC	VD	’7630	no	LFPM	AS3933	n/a	LFPM	OOK	OOK	direct
Fromm [94]	868M	AON	fix.	−59.9	3	10.2	4.92	30	7.5	no	no	LC	VD	’7630	no	LFPM	AS3933	n/a	LFPM	OOK	OOK	Look-up
Fromm [90]	868M	AON	var.	−61.6	2.4	5.71	7.15	25.7	3.21	no	no	LC	VD	’7630	no	LFPM	AS3933	n/a	LFPM+ µC	OOK	OOK	Man.
Fromm [90]	868M	AON	fix.	−61.6	2.4	5.71	9.02	25.7	3.21	no	no	LC	VD	’7630	no	LFPM	AS3933	n/a	LFPM	OOK	OOK	3S2B
Hmidi [36]	868M	DC	var.	−78	3.3	14.3	103	50/100	12.5	SAW	MAX2640	LC	VD	’7630	OA	comp.	TLV3201	adap., hyst.	µC	OOK	FSK	’232
Hmidi [36]	868M	AON	fix.	−59.6	2.4	5.71	14	25.7	3.21	SAW	no	LC	VD	’7630	no	LFPM	AS3933	n/a	LFPM	OOK	OOK	Man.
Qaragoez [78]	2.4G	EH	—	−56.5	3[12]	3	1600[14]	n/a	0.01	no	no	rectenna	VM×4	’7630	OA	—	—	—	—	—	—	—
Rup [29]	2.4G	AON	fix.	−30	3	1.326	32	—	1	no	no	n/a	IC	EFR32	n/a	n/a	n/a	n/a	µC	OOK	no	Man.
Schulthess [54]	acou.	AON	var.	n/a	—	63	200	28	0.2	n/a	n/a	n/a	n/a	n/a	no	comp.	TLV3691	adap.	µC	n/a	OOK	direct

n/a: not applicable, —: no information provided in the reference [1] optical, acoustic, LF, or RF carrier frequency in MHz [2] classification by operating mode: always-on (AON), duty-cycled (DC), power-gated (PG), passive, energy harvesting (EH) [3] classification by addressing capabilities: no, fixed, variable [4] sensitivity [5] supply voltage [6] power consumption [7] WuPt duration [8] RFED components: HSMS-285x, HSMS-286x, SMS7630, or others [9] Reference generation of the ADC: internal, adaptive, fixed, hysteresis, and offset [10] WuPt coding: 3 symbols–2 bits (3S2B), direct, look-up table, Manchester, PWM, RF filters, RS-232, return to zero (RZ) [11] estimated sensitivity by Friis equation using range, transmission, and carrier frequency [12] supply voltage not given in the reference. Estimated 3 V to convert supply current to power consumption [13] neither power consumption nor supply current given in the references, calculated by charts, schematics, and component datasheets [14] WuPt duration not given in the reference, calculated by values and figures of the reference, or symbol rate and 16-symbol pattern [15] self-developed RF filter [16] reflective amplifier [17] mains-powered SR560 amplifier utilized [18] logic threshold

ACKNOWLEDGMENTS

This research is funded by the Saxon state government from the state budget approved by Saxon state parliament. We acknowledge support by the Open Access Publication Funds of Leipzig University of Applied Sciences.

REFERENCES

[1] R. Piyare, A. L. Murphy, C. Kiraly, P. Tosato, and D. Brunelli, "Ultra low power wake-up radios: A hardware and networking survey," *IEEE Communications Surveys Tutorials*, vol. 19, no. 4, pp. 2117–2157, 2017.

[2] O. Kanoun, S. Bradai, S. Khriji, G. Bouattour, D. El Houssaini, M. Ben Ammar, S. Naifar, A. Bouhamed, F. Derbel, and C. Viehweger, "Energy-aware system design for autonomous wireless sensor nodes: A comprehensive review," *Sensors*, vol. 21, no. 2, 2021.

[3] "Energizer CR2032," Energizer, datasheet. [Online]. Available: https://data.energizer.com/pdfs/cr2032.pdf

[4] V. Muenzel, A. F. Hollenkamp, A. I. Bhatt, J. de Hoog, M. Brazil, D. A. Thomas, and I. Mareels, "A comparative testing study of commercial 18650-format lithium-ion battery cells," *Journal of The Electrochemical Society*, vol. 162, no. 8, p. A1592, may 2015.

[5] P. Kolinko and L. E. Larson, "Passive RF receiver design for wireless sensor networks," in *2007 IEEE/MTT-S International Microwave Symposium*, 2007, pp. 567–570.

[6] J. Braun and F. Derbel, "Wireless sensor network for fire detection with network coding to improve security and reliability," *Measurement: Sensors*, vol. 37, p. 101404, 2025. [Online]. Available: https://www.sciencedirect.com/science/article/pii/S2665917424003805

[7] J. Pons, J. Brault, and Y. Savaria, "An FPGA compatible asynchronous wake-up receiver for wireless sensor networks," in *10th IEEE International NEWCAS Conference*, 2012, pp. 373–376.

[8] "S2-LP: Ultra-low power, high performance, sub-1 GHz transceiver," STMicroelectronics, 2023, datasheet, revision 11. [Online]. Available: https://www.st.com/en/wireless-connectivity/s2-lp.html

[9] "EFR32BG22 wireless Gecko SoC family data sheet," Silicon Laboratories Inc., Jun. 2021, datasheet, revision 1.1. [Online]. Available: https://www.silabs.com/documents/public/data-sheets/efr32bg22-datasheet.pdf

[10] F. Z. Djiroun and D. Djenouri, "MAC protocols with wake-up radio for wireless sensor networks: A review," *IEEE Communications Surveys & Tutorials*, vol. 19, no. 1, pp. 587–618, 2017.

[11] V. Jelicic, M. Magno, D. Brunelli, V. Bilas, and L. Benini, "Analytic comparison of wake-up receivers for WSNs and benefits over the wake-on radio scheme," in *Proceedings of the 7th ACM Workshop on Performance Monitoring and Measurement of Heterogeneous Wireless and Wired Networks*, ser. PM2HW2N '12. New York, NY, USA: Association for Computing Machinery, 2012, pp. 99–106.

[12] I. Demirkol, C. Ersoy, and E. Onur, "Wake-up receivers for wireless sensor networks: benefits and challenges," *IEEE Wireless Communications*, vol. 16, no. 4, pp. 88–96, 2009.

[13] J. Blanckenstein and H. Karl, "Energy-efficient clock synchronization using wake-up receivers," in *2014 22nd International Conference on Software, Telecommunications and Computer Networks (SoftCOM)*, 2014, pp. 408–413.

[14] G. Gamm, M. Kostic, M. Sippel, and L. Reindl, "Low-power sensor node with addressable wake-up on-demand capability," *IJSNet*, vol. 11, pp. 48–56, Jan. 2012.

[15] S. Shellhammer, A. Asterjadhi, and Y. Sun, *IEEE 802.11ba*. John Wiley & Sons, Ltd, 2023.

[16] U. Gustavsson, P. Frenger, C. Fager, T. Eriksson, H. Zirath, F. Dielacher, C. Studer, A. Pärssinen, R. Correia, J. N. Matos, D. Belo, and N. B. Carvalho, "Implementation challenges and opportunities in beyond-5g and 6g communication," *IEEE Journal of Microwaves*, vol. 1, no. 1, pp. 86–100, 2021.

[17] G. U. Gamm, M. Sippel, M. Kostic, and L. M. Reindl, "Low power wake-up receiver for wireless sensor nodes," in *2010 Sixth International Conference on Intelligent Sensors, Sensor Networks and Information Processing*, 2010, pp. 121–126.

[18] H. Karvonen and J. Petäjäjärvi, "Energy-efficient hierarchical wireless sensor networks based on wake-up receiver usage," in *Wireless Medical Systems and Algorithms: Design and Applications*. CRC Press, 2016, pp. 95–119.

[19] J. Blanckenstein, J. Klaue, and H. Karl, "A survey of low-power transceivers and their applications," *IEEE Circuits and Systems Magazine*, vol. 15, no. 3, pp. 6–17, 2015.

[20] E. Zaraket, N. M. Murad, S. S. Yazdani, L. Rajaoarisoa, and B. Ravelo, "An overview on low energy wake-up radio technology: Active and passive circuits associated with MAC and routing protocols," *Journal of Network and Computer Applications*, vol. 190, p. 103140, 2021.

[21] A. A. Benbuk, N. Kouzayha, A. Eid, J. Costantine, Z. Dawy, F. Paonessa, and G. Virone, "Leveraging UAVs for passive RF charging and ultralowpower wake-up of ground sensors," *IEEE Sensors Letters*, vol. 4, no. 5, pp. 1–4, 2020.

[22] A. S. Mohammed, O. Khalifa, A. Alhejab, A. S. Abdelrahman, A. Al-Radhwan, H. ElSawy, N. Kouzayha, N. Al-Harthi, J. Elmirghani, M. Hanif, and T. Y. Al-Naffouri, "Demo abstract: Energy-efficient aerial data aggregation in IoT networks with WuR," in *2023 IEEE International Black Sea Conference on Communications and Networking (BlackSeaCom)*, 2023, pp. 147–149.

[23] J. Chen, Z. Dai, and Z. Chen, "Development of radio-frequency sensor wake-up with unmanned aerial vehicles as an aerial gateway," *Sensors*, vol. 19, no. 5, 2019.

[24] A. Guidara, F. Derbel, G. Fersi, S. Bdiri, and M. B. Jemaa, "Energy-efficient on-demand indoor localization platform based on wireless sensor networks using low power wake up receiver," *Ad Hoc Networks*, vol. 93, p. 101902, 2019.

[25] R. Souissi, S. Sahnoun, M. K. Baazaoui, R. Fromm, A. Fakhfakh, and F. Derbel, "A self-localization algorithm for mobile targets in indoor wireless sensor networks using wake-up media access control protocol," *Sensors*, vol. 24, no. 3, 2024.

[26] M. Magno, S. Marinkovic, B. Srbinovski, and E. Popovici, "Wake-up radio receiver based power minimization techniques for wireless sensor networks: A review," *Microelectronics Journal*, vol. 45, no. 12, pp. 1627–1633, 2014.

[27] C. Petrioli, D. Spenza, P. Tommasino, and A. Trifiletti, "A novel wake-up receiver with addressing capability for wireless sensor nodes," in *2014 IEEE International Conference on Distributed Computing in Sensor Systems*, 2014, pp. 18–25.

[28] Y. Zhang, G. Zhang, and X. Shao, "A low power wake-up receiver design based on commercial off-the-shelf components," in *2023 3rd International Conference on Electronic Information Engineering and Computer Communication (EIECC)*, 2023, pp. 1–5.

[29] C. Rup and E. Bajic, "Green and sustainable industrial internet of things systems leveraging wake-up radio to enable on-demand IoT communication," *Sustainability*, vol. 16, no. 3, 2024.

[30] H. Bello, Z. Xiaoping, R. Nordin, and J. Xin, "Advances and opportunities in passive wake-up radios with wireless energy harvesting for the internet of things applications," *Sensors*, vol. 19, no. 14, 2019.

[31] J. Oller, I. Demirkol, J. Casademont, J. Paradells, G. U. Gamm, and L. Reindl, "Performance evaluation and comparative analysis of SubCarrier modulation wake-up radio systems for energy-efficient wireless sensor networks," *Sensors*, vol. 14, no. 1, pp. 22–51, 2014.

[32] L. Schott, R. Fromm, G. Bouattour, O. Kanoun, and F. Derbel, "Analytical and experimental performance analysis of enhanced wake-up receivers based on low-power base-band amplifiers," *Sensors*, vol. 22, no. 6, 2022.

[33] M. Bouraoui, I. Barraj, and M. Masmoudi, "Study on wake-up receiver design for IoT applications," in *2019 IEEE International Conference on Design Test of Integrated Micro Nano-Systems (DTS)*, 2019, pp. 1–4.

[34] R. Fromm, O. Kanoun, and F. Derbel, "Reliable wake-up receiver with increased sensitivity using low-noise amplifiers," in *2022 19th International Multi-Conference on Systems, Signals & Devices (SSD)*, 2022, pp. 1523–1528.

[35] S. Bdiri, F. Derbel, and O. Kanoun, "A tuned-RF duty-cycled wake-up receiver with -90 dBm sensitivity," *Sensors*, vol. 18, no. 1, 2018.

[36] S. Hmidi, R. Fromm, R. Barrak, and F. Derbel, "Experimental investigations on RF filters in wake-up receiver circuits," in *2024 21st International Multi-Conference on Systems, Signals & Devices (SSD)*, 2024, pp. 286–291.

[37] S. Bdiri and F. Derbel, "An ultra-low power wake-up receiver for real-time constrained wireless sensor networks," May 2015.

[38] M. Magno and L. Benini, "An ultra low power high sensitivity wake-up radio receiver with addressing capability," *International Conference on Wireless and Mobile Computing, Networking and Communications*, pp. 92–99, Nov. 2014.

[39] S. Basagni, F. Ceccarelli, C. Petrioli, N. Raman, and A. V. Sheshashayee, "Wake-up radio ranges: A performance study," in *2019*

IEEE Wireless Communications and Networking Conference (WCNC), 2019, pp. 1–6.

[40] S. Bdiri, F. Derbel, and O. Brini, "Digital back-end based on a low-power listening protocol for wake-up receivers," *Sensors and Transducers*, vol. 224, pp. 22–27, Sep. 2018.

[41] H. T. Friis, "A note on a simple transmission formula," *Proceedings of the IRE*, vol. 34, no. 5, pp. 254–256, 1946.

[42] M. Del Prete, D. Masotti, A. Costanzo, M. Magno, and L. Benini, "A 2.4 GHz-868 MHz dual-band wake-up radio for wireless sensor network and IoT," in *2015 IEEE 11th International Conference on Wireless and Mobile Computing, Networking and Communications (WiMob)*, 2015, pp. 322–328.

[43] M. Malinowski, M. Moskwa, M. Feldmeier, M. Laibowitz, and J. Paradiso, "CargoNet: A low-cost micropower sensor node exploiting quasi-passive wakeup for adaptive asychronous monitoring of exceptional events," in *Proceedings of the 5th international conference on Embedded networked sensor systems (SenSys '07)*, Jan. 2007, pp. 145–159.

[44] J. Petäjäjärvi, K. Mikhaylov, R. Vuohtoniemi, H. Karvonen, and J. Iinatti, "On the human body communications: wake-up receiver design and channel characterization," *EURASIP Journal on Wireless Communications and Networking*, vol. 2016, p. 179, Aug. 2016.

[45] M. Del Prete, A. Costanzo, M. Magno, D. Masotti, and L. Benini, "Optimum excitations for a dual-band microwatt wake-up radio," *IEEE Transactions on Microwave Theory and Techniques*, vol. 64, no. 12, pp. 4731–4739, 2016.

[46] P. Woias, S. Heller, and U. Pelz, "A highly sensitive and ultra-low-power wake-up receiver for energy-autonomous embedded systems," *Journal of Physics: Conference Series*, vol. 1052, p. 012024, Jul. 2018.

[47] T. Polonelli, F. Villani, and M. Magno, "Ultra-low power wake-up receiver for location aware objects operating with UWB," in *2021 17th International Conference on Wireless and Mobile Computing, Networking and Communications (WiMob)*, 2021, pp. 369–376.

[48] A. Richardson, "Security of vehicle key fobs and immobilizers," 2015, online. [Online]. Available: http://www.cs.tufts.edu/comp/116/archive/fall2015/arichardson.pdf

[49] D. Benoît, D. Almer, M. Würms, M. Meli, and H. Käser, "Asynchronous wake-up scheme for wireless light curtains." WEKA Fachmedien, 2008, 5. Wireless Congress: Systems & Applications, Munich, 12-13 November 2008.

[50] P. Mohaghegh, D. Pravica, A. Boegli, and Y. Perriard, "Investigating optimal settings for distance calculation with a low frequency low-power RF system," in *2020 23rd International Conference on Electrical Machines and Systems (ICEMS)*, 2020, pp. 401–405.

[51] F. Wolling, F. Hauck, G. Schröder, and K. Van Laerhoven, "OpenIBC: Open-source wake-up receiver for capacitive intra-body communication," in *Proceedings of the 2022 International Conference on Embedded Wireless Systems and Networks*, ser. EWSN '22. New York, NY, USA: Association for Computing Machinery, 2023, pp. 186–191.

[52] A. Sanchez, S. Blanc, P. Yuste, and J. Serrano, "RFID based acoustic wake-up system for underwater sensor networks," in *2011 IEEE Eighth International Conference on Mobile Ad-Hoc and Sensor Systems*, 2011, pp. 873–878.

[53] A. Sánchez, S. Blanc, P. Yuste, A. Perles, and J. J. Serrano, "An ultra-low power and flexible acoustic modem design to develop energy-efficient underwater sensor networks," *Sensors*, vol. 12, no. 6, pp. 6837–6856, 2012.

[54] L. Schulthess, P. Mayer, L. Benini, and M. Magno, "A passive and asynchronous wake-up receiver for acoustic underwater communication," 2024.

[55] T. Schaechtle, F. Höflinger, G. K. J. Fischer, J. Helmerich, I. Häring, and S. J. Rupitsch, "Low-power ultrasonic wake-up through metal," in *2023 IEEE 13th International Conference on RFID Technology and Applications (RFID-TA)*, 2023, pp. 41–44.

[56] F. Höflinger, G. U. Gamm, J. Albesa, and L. M. Reindl, "Smartphone remote control for home automation applications based on acoustic wake-up receivers," in *2014 IEEE International Instrumentation and Measurement Technology Conference (I2MTC) Proceedings*, 2014, pp. 1580–1583.

[57] A. Bannoura, F. Höflinger, O. Gorgies, G. U. Gamm, J. Albesa, and L. M. Reindl, "Acoustic wake-up receivers for home automation control applications," *Electronics*, vol. 5, no. 1, 2016.

[58] H. Ma and J. A. Paradiso, "The FindIT flashlight: Responsive tagging based on optically triggered microprocessor wakeup," in *UbiComp 2002: Ubiquitous Computing*, G. Borriello and L. E. Holmquist, Eds. Berlin, Heidelberg: Springer Berlin Heidelberg, 2002, pp. 160–167.

[59] C. Carrascal, I. Demirkol, and J. Paradells, "A novel wake-up communication system using solar panel and visible light communication," in *2014 IEEE Global Communications Conference*, 2014, pp. 461–467.

[60] J. S. Ramos, I. Demirkol, J. Paradells, D. Vössing, K. M. Gad, and M. Kasemann, "Towards energy-autonomous wake-up receiver using visible light communication," in *2016 13th IEEE Annual Consumer Communications Networking Conference (CCNC)*, 2016, pp. 544–549.

[61] U. Dudko and L. Overmeyer, "Optical wake-up from power-off state for autonomous sensor nodes," *IEEE Sensors Journal*, vol. 21, no. 3, pp. 3225–3232, 2021.

[62] J. Saez, T. Ungan, L. M. Reindl, and T. Kumberg, "Development and characterization of a robust differential wake-up receiver for wireless sensor networks," in *2017 13th International Wireless Communications and Mobile Computing Conference (IWCMC)*, 2017, pp. 1209–1214.

[63] "AS3933 - 3D Low Frequency Wake-Up Receiver," ams AG, Sep. 2015, datasheet.

[64] S. Bdiri and F. Derbel, "A nanowatt wake-up receiver for industrial production line," in *2014 IEEE 11th International Multi-Conference on Systems, Signals Devices (SSD14)*, 2014, pp. 1–6.

[65] S. Bdiri, F. Derbel, and O. Kanoun, "An 868 MHz 7.5 µW wake-up receiver with -60 dBm sensitivity," *Journal of Sensors and Sensor Systems*, vol. 5, pp. 433–446, Dec. 2016.

[66] R. Fromm, O. Kanoun, and F. Derbel, "An improved wake-up receiver based on the optimization of low-frequency pattern matchers," *Sensors*, vol. 23, no. 19, 2023.

[67] A. Frøytlog, M. A. Haglund, L. R. Cenkeramaddi, and B. Beferull-Lozano, "Design and implementation of a long-range low-power wake-up radio and customized dc-mac protocol for lorawan," in *2019 IEEE International Conference on Advanced Networks and Telecommunications Systems (ANTS)*, 2019, pp. 1–5.

[68] F. Pflaum, R. Weigel, and A. Koelpin, "Ultra-low-power sensor node with wake-up-functionality for smart-sensor-applications," in *2018 IEEE Topical Conference on Wireless Sensors and Sensor Networks (WiSNet)*, 2018, pp. 107–110.

[69] T. Ma, "A bit sampled wake-up receiver with logarithmic detector architecture," in *2017 International Conference on Cyber-Enabled Distributed Computing and Knowledge Discovery (CyberC)*, 2017, pp. 445–449.

[70] T. Ma, Z. Tao, and J. Zhang, "A new OOK wake-up receiver with sampling technique," 2020.

[71] A. R. da. Silva, R. Akbar, R. Chen, K. B. Dogaheh, N. Golestani, M. Moghaddam, and D. Entekhabi, "Duty-cycled, sub-GHz wake-up radio with -95 dBm sensitivity and addressing capability for environmental monitoring applications," in *2019 IEEE 10th Annual Ubiquitous Computing, Electronics & Mobile Communication Conference (UEMCON)*, 2019, pp. 0183–0191.

[72] S. Bdiri, F. Derbel, and O. Kanoun, *A wake-up receiver for online energy harvesting enabled wireless sensor networks: Technology, Components and System Design*. De Gruyter Oldenbourg, Nov. 2018, pp. 305–320.

[73] A. A. Benbuk, N. Kouzayha, J. Costantine, H. Jaafar, and Z. Dawy, "A nano-watt dual-mode address detector for a Wi-Fi enabled RF wake-up receiver," in *2019 IEEE SENSORS*, 2019, pp. 1–4.

[74] A. A. Benbuk, N. Kouzayha, J. Costantine, and Z. Dawy, "Tunable, asynchronous, and nanopower baseband receiver for charging and wakeup of IoT devices," *IEEE Internet of Things Journal*, vol. 9, no. 4, pp. 3023–3036, 2022.

[75] L. Trinh, T. Hoang, F. Perret, and F. Ferrero, "Improving wake-up receiver's sensitivity by using novel architecture," *Electronics Letters*, vol. 48, pp. 659–660(1), May 2012.

[76] J. Wang, Q. Gao, H. Wang, and W. Sun, "A method to prolong the lifetime of wireless sensor network," in *2009 5th International Conference on Wireless Communications, Networking and Mobile Computing*, 2009, pp. 1–4.

[77] K. Kaushik, D. Mishra, S. De, J.-B. Seo, S. Jana, K. Chowdhury, S. Basagni, and W. Heinzelman, "RF energy harvester-based wake-up receiver," in *2015 IEEE SENSORS*, 2015, pp. 1–4.

[78] Y. Qaragoez and D. Schreurs, "Listening to the whispers: Enhanced SWIPT wake-up receiver for IoT sensors," in *2024 IEEE Wireless Power Technology Conference and Expo (WPTCE)*, 2024, pp. 235–239.

[79] D. Dardari, N. Decarli, D. Fabbri, A. Guerra, M. Fantuzzi, D. Masotti, A. Costanzo, A. Romani, M. Drouguet, T. Feuillen, C. Raucy, L. Vandendorpe, and C. Craeye, "An ultra-wideband battery-less positioning system for space applications," in *2019 IEEE International Conference on RFID Technology and Applications (RFID-TA)*, 2019, pp. 104–109.

[80] D. Fabbri, M. Pizzotti, and A. Romani, "Micropower design of an energy autonomous RF tag for UWB localization applications," in *2018 IEEE International Symposium on Circuits and Systems (ISCAS)*, 2018, pp. 1–5.

[81] D. Fabbri, A. Romani, A. Costanzo, and D. Masotti, "An orientation-independent UHF battery-less tag for extended-range applications," in *2020 XXXIIIrd General Assembly and Scientific Symposium of the International Union of Radio Science*, 2020, pp. 1–4.

[82] Z. Yue, X. Xu, S. H. Wu, and X. Q. Lin, "High-efficiency and wide-dynamic-range rectifier based on power reflection for wireless power transfer in sensor networks," *IEEE Journal of Microwaves*, vol. 5, no. 3, pp. 666–676, 2025.

[83] H. Rahmani, D. Shetty, M. Wagih, Y. Ghasempour, V. Palazzi, N. B. Carvalho, R. Correia, A. Costanzo, D. Vital, F. Alimenti, J. Kettle, D. Masotti, P. Mezzanotte, L. Roselli, and J. Grosinger, "Next-generation iot devices: Sustainable eco-friendly manufacturing, energy harvesting, and wireless connectivity," *IEEE Journal of Microwaves*, vol. 3, no. 1, pp. 237–255, 2023.

[84] S. Saab, N. Kouzayha, A. Eid, A. A. Benbuk, J. Costantine, and Z. Dawy, "Recycling ambient Wi-Fi signals for low energy wake-up of wireless sensors," *IEEE Sensors Letters*, vol. 4, no. 10, pp. 1–4, 2020.

[85] H. Ba, I. Demirkol, and W. Heinzelman, "Passive wake-up radios: From devices to applications," *Ad Hoc Networks*, vol. 11, no. 8, pp. 2605–2621, 2013.

[86] L. Guntupalli, D. Ghose, F. Y. Li, and M. Gidlund, "Energy efficient consecutive packet transmissions in receiver-initiated wake-up radio enabled WSNs," *IEEE Sensors Journal*, vol. 18, no. 11, pp. 4733–4745, 2018.

[87] A. V. Sheshashayee and S. Basagni, "Multi-hop wake-up radio relaying for the collection tree protocol," in *2019 IEEE 90th Vehicular Technology Conference (VTC2019-Fall)*, 2019, pp. 1–6.

[88] M. Weber, G. Fersi, R. Fromm, and F. Derbel, "Wake-up receiver-based routing for clustered multihop wireless sensor networks," *Sensors*, vol. 22, no. 9, 2022.

[89] H. Yetgin, K. T. K. Cheung, M. El-Hajjar, and L. H. Hanzo, "A survey of network lifetime maximization techniques in wireless sensor networks," *IEEE Communications Surveys & Tutorials*, vol. 19, no. 2, pp. 828–854, 2017.

[90] R. Fromm, O. Kanoun, and F. Derbel, "Univocal and reliable addressing patterns for wake-up receivers based on low-frequency pattern matchers," *IEEE Sensors Journal*, vol. 24, no. 8, pp. 13 431–13 438, 2024.

[91] J. Blobel, J. Krasemann, and F. Dressler, "An architecture for sender-based addressing for selective sensor network wake-up receivers," in *2016 IEEE 17th International Symposium on A World of Wireless, Mobile and Multimedia Networks (WoWMoM)*, 2016, pp. 1–7.

[92] B. Doorn, W. Kavelaars, and K. Langendoen, "A prototype low-cost wakeup radio for the 868 MHz band," *IJSNet*, vol. 5, pp. 22–32, Jan. 2009.

[93] R. Fromm, L. Schott, and F. Derbel, "Improved wake-up receiver architectures with carrier sense capabilities for low-power wireless communication," in *Sensor Networks*, A. Ahrens, R. V. Prasad, C. Benavente-Peces, and N. Ansari, Eds. Cham: Springer International Publishing, 2022, pp. 60–84.

[94] R. Fromm, O. Kanoun, and F. Derbel, "Quasi-real-time wireless communication based on wake-up receivers with a latency below 5 ms," in *2024 IEEE International Instrumentation and Measurement Technology Conference (I2MTC)*, 2024, pp. 1–6.

[95] G. U. Gamm, S. Stoecklin, and L. M. Reindl, "Wake-up receiver operating at 433 MHz," in *2014 IEEE 11th International Multi-Conference on Systems, Signals Devices (SSD14)*, 2014, pp. 1–4.

[96] "Short range devices (SRD) operating in the frequency range 25 MHz to 1000 MHz; part 1: Technical characteristics and methods of measurement," ETSI, EN 300 220-1, 02 2017.

[97] F. Sutton, "Ultra-low power wireless hierarchical sensing," Master's thesis, ETH Zurich, 2012.

[98] H. Khodr, N. Kouzayha, M. Abdallah, J. Costantine, and Z. Dawy, "Energy efficient IoT sensor with RF wake-up and addressing capability," *IEEE Sensors Letters*, vol. 1, no. 6, pp. 1–4, 2017.

[99] L. Berghella, A. Depari, P. Ferrari, A. Flammini, S. Rinaldi, E. Sisinni, and A. Vezzoli, "Low-power wireless interface for handheld smart metering devices," in *2014 IEEE Sensors Applications Symposium (SAS)*, 2014, pp. 317–322.

[100] Y. Ammar, S. Bdiri, and F. Derbel, "An ultra-low power wake up receiver with flip flops based address decoder," in *2015 IEEE 12th International Multi-Conference on Systems, Signals Devices (SSD15)*, 2015, pp. 1–5.

[101] P. Horowitz and W. Hill, *The Art of Electronics*, 3rd ed. USA: Cambridge University Press, 2015.

[102] S. Marinkovic and E. Popovici, "Nano-power wireless wake-up receiver with serial peripheral interface," *Selected Areas in Communications, IEEE Journal on*, vol. 29, pp. 1641–1647, Oct. 2011.

[103] M. Siniscalchi, A. Pieruccioni, F. Vanzini, L. Reyes, and L. Barboni, "Schottky diode assessment for implementing a rectenna for radio-triggered wireless sensor networks," *IEEE Microwave and Wireless Components Letters*, vol. 27, no. 8, pp. 763–765, 2017.

[104] U. Kulau, F. Büsching, and L. Wolf, "Undervolting in WSNs: Theory and practice," *IEEE Internet of Things Journal*, vol. 2, no. 3, pp. 190–198, 2015.

[105] G. Liu, T. Ma, W. Yin, J. Zhang, H. Gao, and B. Wu, "A 2.4GHz band highly sensitive low power wake-up receiver," in *2023 International Conference on Ubiquitous Communication (Ucom)*, 2023, pp. 116–120.

[106] A. Frøytlog, M. A. Haglund, L. R. Cenkeramaddi, T. Jordbru, R. A. Kjellby, and B. Beferull-Lozano, "Design and implementation of a long-range low-power wake-up radio for IoT devices," in *2019 IEEE 5th World Forum on Internet of Things (WF-IoT)*, 2019, pp. 247–250.

[107] F. Hutu, D. Kibloff, G. Villemaud, and J. Gorce, "Experimental validation of a wake-up radio architecture," in *2016 IEEE Radio and Wireless Symposium (RWS)*, 2016, pp. 155–158.

[108] F. Sutton, B. Buchli, J. Beutel, and L. Thiele, "Zippy: On-demand network flooding," in *Proceedings of the 13th ACM Conference on Embedded Networked Sensor Systems*, ser. SenSys '15. New York, NY, USA: Association for Computing Machinery, 2015, pp. 45–58.

[109] V. Rakovic, R. Adamovski, A. Risteski, and L. Gavrilovska, "Improving energy efficiency and reliability in WuR-based IoT systems: An error correction approach," *Wireless Personal Communications*, vol. 126, no. 1, pp. 123–134, Sep. 2022.

[110] P. Gavrikov, P. E. Verboket, T. Ungan, M. Müller, M. Lai, C. Schindelhauer, L. M. Reindl, and T. Wendt, "Using Bluetooth Low Energy to trigger an ultra-low power FSK wake-up receiver," in *2018 25th IEEE International Conference on Electronics, Circuits and Systems (ICECS)*, 2018, pp. 781–784.

[111] "Product obsolescence notification," Broadcom Limited, Dec. 2017, OBS120117WSD3. [Online]. Available: https://docs.broadcom.com/doc/OBS120117WSD3

[112] D. Galante-Sempere, D. Ramos-Valido, S. Lalchand Khemchandani, and J. del Pino, "Low-power RFED wake-up receiver design for low-cost wireless sensor network applications," *Sensors*, vol. 20, no. 22, 2020.

[113] R. J. de Jong, R. A. R. van der Zee, and A. B. J. Kokkeler, "Analysis of a 1kbps backscatter receiver with up to -80dBm tag-to-tag receive sensitivity," in *2020 IEEE International Conference on RFID (RFID)*, 2020, pp. 1–8.

[114] M.-G. Kang, J.-W. Park, and Y.-S. Kim, "Design of a 900 MHz band wake-up receiver with -52 dbm sensitivity," *The Journal of Korean Institute of Electromagnetic Engineering and Science*, vol. 32, no. 3, pp. 243–249, 2021.

[115] G. Kazdaridis, N. Sidiropoulos, I. Zografopoulos, and T. Korakis, "eWake: A novel architecture for semi-active wake-up radios attaining ultra-high sensitivity at extremely-low consumption," *CoRR*, vol. abs/2103.15969, 2021.

[116] B. Wu, D. Zhang, T. Ma, R. Jiang, H. Gao, and G. Liu, "A high-sensitivity wake-up receiver using tunnel diode for ISM band," in *2022 IEEE 22nd International Conference on Communication Technology (ICCT)*, 2022, pp. 1493–1496.

[117] S. Köble, S. Heller, and P. Woias, "A narrow-band and ultra-low-power 433 MHz wake-up receiver," *Journal of Physics: Conference Series*, vol. 1407, p. 012093, Nov. 2019.

[118] "Product end-of-life notification," ATMEL Germany GmBH, Aug. 2008, EOL Number: HE083201. [Online]. Available: https://www.ineltek.com/wp-content/uploads/eolpcnpdf/HE083201.pdf

[119] P. Li, Z. Long, and Z. Yang, "RF energy harvesting for batteryless and maintenance-free condition monitoring of railway tracks," *IEEE Internet of Things Journal*, vol. 8, no. 5, pp. 3512–3523, 2021.

[120] J. Lebreton, N. Murad, S. Kandukuri, and R. Lorion, "An energy-efficient addressing mechanism for wake-up radio systems," in *2016 Wireless Telecommunications Symposium (WTS)*, 2016, pp. 1–6.

[121] T. Polonelli, T. Le Huy, L. Lizzi, F. Ferrero, and M. Magno, "A wake-up receiver with ad-hoc antenna co-design for wearable applications," in *2016 IEEE Sensors Applications Symposium (SAS)*, 2016, pp. 1–6.

[122] B. D. Parks, "Analysis of the feasibility of utilizing wakeup radios to optimize energy and latency performance of wireless sensor networks," Ph.D. dissertation, University of Nebraska-Lincoln, 2013.

[123] J. Oller, I. Demirkol, J. Casademont, and J. Paradells, "Design, development, and performance evaluation of a low-cost, low-power wake-up radio system for wireless sensor networks," *ACM Trans. Sen. Netw.*, vol. 10, no. 1, Dec. 2013.

[124] Y. Kondo, H. Yomo, S. Tang, M. Iwai, T. Tanaka, H. Tsutsui, and S. Obana, "Energy-efficient WLAN with on-demand AP wake-up using IEEE 802.11 frame length modulation," *Computer Communications*, vol. 35, no. 14, pp. 1725–1735, 2012, special issue: Wireless Green Communications and Networking.

[125] E. Lopez-Aguilera, M. Hussein, M. Cervia, J. Paradells, and A. Calveras, "Design and implementation of a wake-up radio receiver for fast 250 kb/s bit rate," *IEEE Wireless Communications Letters*, vol. 8, no. 6, pp. 1537–1540, 2019.

[126] I. Bahl and P. Bhartia, *Microwave Solid State Circuit Design*. New York: Wiley, 2003.

[127] Y. Chen and C. Chiu, "Maximum achievable power conversion efficiency obtained through an optimized rectenna structure for RF energy harvesting," *IEEE Transactions on Antennas and Propagation*, vol. 65, no. 5, pp. 2305–2317, 2017.

[128] P. Pursula, V. Viikari, and J. Saari, "Wake-up radio architecture utilizing passive down conversion mixing," *Microwave and Optical Technology Letters*, vol. 55, May 2013.

[129] C. Mc Caffrey, T. Sillanpää, H. Huovila, J. Nikunen, S. Hakulinen, and P. Pursula, "Energy autonomous wireless valve leakage monitoring system with acoustic emission sensor," *IEEE Transactions on Circuits and Systems I: Regular Papers*, vol. 64, no. 11, pp. 2884–2893, 2017.

[130] S. Marinkovic and E. Popovici, "Nano-power wake-up radio circuit for wireless body area networks," in *2011 IEEE Radio and Wireless Symposium*, 2011, pp. 398–401.

[131] P. Koskela and M. Valta, "Simple wake-up radio prototype," in *Proceedings of the 6th Workshop on Hot Topics in Embedded Networked Sensors*, ser. HotEmNets '10. New York, NY, USA: Association for Computing Machinery, 2010.

[132] T. Polonelli, M. Magno, V. Niculescu, L. Benini, and D. Boyle, "An open platform for efficient drone-to-sensor wireless ranging and data harvesting," *Sustainable Computing: Informatics and Systems*, vol. 35, p. 100734, 2022.

[133] R. Torres, R. Correia, N. B. Carvalho, S. Daskalakis, G. Goussetis, Y. Ding, A. Georgiadis, A. Eid, J. Hester, and M. M. Tentzeris, "Backscatter communications," *IEEE Journal of Microwaves*, vol. 1, no. 4, pp. 864–878, 2021.

[134] G. Michetti, L. Colombo, G. Giribaldi, A. Mittal, H. Elkotby, R. Pragada, A. Shrivastava, and M. Rinaldi, "A micro-acoustic enhanced low-impedance antenna system for IoT wake-up receivers," *IEEE Internet of Things Journal*, vol. 10, no. 10, pp. 8696–8705, 2023.

[135] A. Lazaro, A. Ramos, D. Girbau, and R. Villarino, "A novel UWB RFID tag using active frequency selective surface," *IEEE Transactions on Antennas and Propagation*, vol. 61, no. 3, pp. 1155–1165, 2013.

[136] T. Kumberg, R. Tannhaeuser, and L. M. Reindl, "Wake-up receiver with equal-gain antenna diversity," *Sensors*, vol. 17, no. 9, 2017.

[137] F. Cabarcas, J. Aranda, and D. Mendez, "OpenWuR - an open WSN platform for WuR-based application prototyping," in *Proceedings of the 2020 International Conference on Embedded Wireless Systems and Networks on Proceedings of the 2020 International Conference on Embedded Wireless Systems and Networks*, ser. EWSN '20. USA: Junction Publishing, 2020, pp. 212–217.

[138] L. Catarinucci, R. Colella, G. D. Fiore, L. Mainetti, V. Mighali, L. Patrono, and M. L. Stefanizzi, "A cross-layer approach to minimize the energy consumption in wireless sensor networks," *International Journal of Distributed Sensor Networks*, vol. 10, no. 1, p. 268284, 2014.

[139] B. Yi, F. Wang, C. Huang, X. Cao, and K. Li, "A low-cost and low-power 2.4 GHz wake-up receiver," in *2022 IEEE 10th Asia-Pacific Conference on Antennas and Propagation (APCAP)*, 2022, pp. 1–2.

[140] Y. Luo and L. Pu, "WUR-TS: Semi-passive wake-up radio receiver based time synchronization method for energy harvesting wireless networks," *IEEE Transactions on Mobile Computing*, vol. 21, no. 11, pp. 4172–4186, 2022.

[141] R. Fromm, L. Schott, and F. Derbel, "An efficient low-power wake-up receiver architecture for power saving for transmitter and receiver communications," in *Proceedings of the 10th International Conference on Sensor Networks - SENSORNETS,*, INSTICC. SciTePress, 2021, pp. 61–68.

[142] J. Mathews, M. Barnes, A. Young, and D. K. Arvind, "Low power wake-up in wireless sensor networks using free space optical communications," in *2010 Fourth International Conference on Sensor Technologies and Applications*, 2010, pp. 256–261.

[143] T. Hakkinen and J. Vanhala, "Ultra-low power wake-up circuit for short-range wireless communication," *IET Conference Proceedings*, pp. 24–24(1), Jan. 2008.

[144] G. B. Perez, M. Malinowski, and J. A. Paradiso, "An ultra-low power, optically-interrogated smart tagging and identification system," in *Fourth IEEE Workshop on Automatic Identification Advanced Technologies (AutoID'05)*, 2005, pp. 187–192.

[145] P. Horowitz and W. Hill, *The Art of Electronics: The x Chapters*. Cambridge University Press, 2020.

[146] "TLV521 NanoPower, 350nA, RRIO, CMOS input, operational amplifier," Texas Instruments, May 2016, datasheet.

[147] D. Oletic, V. Bilas, M. Magno, N. Felber, and L. Benini, "Low-power multichannel spectro-temporal feature extraction circuit for audio pattern wake-up," in *2016 Design, Automation & Test in Europe Conference & Exhibition (DATE)*, 2016, pp. 355–360.

[148] R. Fromm, O. Kanoun, and F. Derbel, "The necessity of comparators in wake-up receiver circuits," in *2024 21st International Multi-Conference on Systems, Signals & Devices (SSD)*, 2024, pp. 480–485.

[149] A. Frøytlog and L. R. Cenkeramaddi, "Design and implementation of an ultra-low power wake-up radio for wireless IoT devices," in *2018 IEEE International Conference on Advanced Networks and Telecommunications Systems (ANTS)*, 2018, pp. 1–4.

[150] A. Frøytlog, T. Foss, O. Bakker, G. Jevne, M. A. Haglund, F. Y. Li, J. Oller, and G. Y. Li, "Ultra-low power wake-up radio for 5G IoT," *IEEE Communications Magazine*, vol. 57, no. 3, pp. 111–117, 2019.

[151] M. Magno, V. Jelicic, B. Srbinovski, V. Bilas, E. Popovici, and L. Benini, "Design, implementation, and performance evaluation of a flexible low-latency nanowatt wake-up radio receiver," *IEEE Transactions on Industrial Informatics*, vol. 12, no. 2, pp. 633–644, 2016.

[152] M.-C. Ziesmann, C. Fühner, and F. Büsching, "HotWire – decreasing latency between wake-up calls in semi-active WUR-scenarios," in *2023 IEEE 12th International Conference on Intelligent Data Acquisition and Advanced Computing Systems: Technology and Applications (IDAACS)*, vol. 1, 2023, pp. 655–660.

[153] P. Skrimponis, "Design and implementation of a wake-up radio architecture for wireless sensor networks," Ph.D. dissertation, University of Thessaly, 2018.

[154] J. Wang, Q. Gao, Y. Yu, H. Wang, and M. Jin, "Radio-triggered power management in wireless sensor networks," in *Wireless Sensor Networks*, M. Matin, Ed. Rijeka: IntechOpen, 2012, ch. 3.

[155] J. Ansari, D. Pankin, and P. Mähönen, "Radio-triggered wake-ups with addressing capabilities for extremely low power sensor network applications," *International Journal of Wireless Information Networks*, vol. 16, no. 3, pp. 118–130, Sep. 2009.

[156] A. S. Boaventura and N. B. Carvalho, "A low-power wakeup radio for application in WSN-based indoor location systems," *International Journal of Wireless Information Networks*, vol. 20, no. 1, pp. 67–73, Mar. 2013.

[157] "Data slicing techniques for UHF ASK receivers," Maxim Integrated, Dec. 2005, application Note 3671. [Online]. Available: https://pdfserv.maximintegrated.com/en/an/AN3671.pdf

[158] "Product discontinuation," Infineon Technologies AG, Sep. 2016, PD_089_16. [Online]. Available: https://www.mouser.com/PCN/Infineon_cPD_089_16.pdf

[159] A. Sanchez, J. Aguilar, S. Blanc, and J. J. Serrano, "RFID-based wake-up system for wireless sensor networks," in *VLSI Circuits and Systems V*, T. Riesgo and E. de la Torre-Arnanz, Eds., vol. 8067, International Society for Optics and Photonics. SPIE, 2011, p. 806708.

[160] T. Kumberg, R. Tannhaeuser, G. U. Gamm, and L. M. Reindl, "Energy improved wake-up strategy for wireless sensor networks," in *Sensors and Measuring Systems 2014; 17. ITG/GMA Symposium*, 2014, pp. 1–6.

[161] A. Sánchez, S. B. Clavero, P. Y. Pérez, I. R. P. Gozalbes, and J. J. S. Martín, "Advanced acoustic wake-up system for underwater sensor networks," 2012.

[162] T. Kumberg, C. Schindelhauer, and L. Reindl, "Exploiting concurrent wake-up transmissions using beat frequencies," *Sensors*, vol. 17, no. 8, 2017.

[163] Y. Mafi, F. Amirhosseini, S. A. Hosseini, A. Azari, M. Masoudi, and M. Vaezi, "Ultra-low-power IoT communications: A novel address decoding approach for wake-up receivers," *IEEE Transactions on Green Communications and Networking*, vol. 6, no. 2, pp. 1107–1121, 2022.

[164] E. Lattanzi, M. Dromedari, V. Freschi, and A. Bogliolo, "A sub-μA ultrasonic wake-up trigger with addressing capability for wireless sensor nodes," *International Scholarly Research Notices*, vol. 2013, 2013.

[165] J. Oller, I. Demirkol, J. Paradells, J. Casademont, and W. Heinzelman, "Time-knocking: A novel addressing mechanism for wake-up receivers," in *2012 IEEE 8th International Conference on Wireless and Mobile Computing, Networking and Communications (WiMob)*, 2012, pp. 268–275.
[166] S. Babatunde, A. Alsubhi, J. Hester, and J. Sorber, "Greentooth: Robust and energy efficient wireless networking for batteryless devices," *ACM Trans. Sen. Netw.*, vol. 20, no. 3, Apr. 2024.
[167] A. Bannoura, "Algorithms and applications for low power wireless sensor networks using wake-up receivers," 2016.
[168] J. Oller, E. Garcia, E. Lopez, I. Demirkol, J. Casademont, J. Paradells, U. Gamm, and L. Reindl, "IEEE 802.11-enabled wake-up radio system: design and performance evaluation," *Electronics Letters*, vol. 50, no. 20, pp. 1484–1486, 2014.
[169] J. Petäjäjärvi, K. Mikhaylov, H. Karvonen, R. Vuohtoniemi, and M. Hämäläinen, "Loose synchronization method for low-power super-regenerative wake-up receiver," in *2015 9th International Symposium on Medical Information and Communication Technology (ISMICT)*, 2015, pp. 209–212.
[170] M. Hierold, R. Weigel, and A. Koelpin, "Assessment of transmitter initiated wake-up radio versus pure wake-up receiver decoding," *IEEE Microwave and Wireless Components Letters*, vol. 27, no. 4, pp. 413–415, 2017.
[171] M.-C. Ziesmann, C. Fühner, and F. Büsching, "STFO – power-saving deep-sleep states are overrated," in *2023 IEEE 12th International Conference on Intelligent Data Acquisition and Advanced Computing Systems: Technology and Applications (IDAACS)*, vol. 1, 2023, pp. 747–751.
[172] E. Lopez-Aguilera, I. Demirkol, E. Garcia-Villegas, and J. Paradells, "IEEE 802.11-enabled wake-up radio: Use cases and applications," *Sensors*, vol. 20, no. 1, 2020.
[173] G. Meller, M. Methfessel, B. Lindner, J. Wagner, R. Kraemer, and F. Ellinger, "Wakeup receiver using passive amplification by means of a switched SAW resonator," in *2022 19th Annual IEEE International Conference on Sensing, Communication, and Networking (SECON)*, 2022, pp. 136–144.
[174] W. Z. Zhu, T. Wu, G. Chen, C. Cassella, M. Assylbekova, M. Rinaldi, and N. McGruer, "Design and fabrication of an electrostatic AlN RF MEMS switch for near-zero power RF wake-up receivers," *IEEE Sensors Journal*, vol. 18, no. 24, pp. 9902–9909, 2018.
[175] F. Pereira, R. Correia, P. Pinho, S. I. Lopes, and N. B. Carvalho, "Challenges in resource-constrained IoT devices: Energy and communication as critical success factors for future IoT deployment," *Sensors*, vol. 20, no. 22, 2020.
[176] E. Umbdenstock, F. Schaefer, M. Kleinsteuber, and H. Meyer, "Wake-up-receiver in energy efficient wireless sensor networks for security applications," 2012.
[177] T. V. Prabhakar, N. S. Soumya, P. Muralidharan, and H. S. Jamadagni, "A novel wake-up radio WSN mote," in *2013 Texas Instruments India Educators' Conference*, 2013, pp. 362–368.

Author Contributions

R.F. contributed by way of conceptualization, methodology, original draft, writing, visualization, and editing. F.D. and O.K. contributed by way of supervision, reviewing, editing, and funding acquisition. All authors have read and agreed to the published version of the manuscript.

ROBERT FROMM (Student Member, IEEE) received the M. Sc. degree in Electrical Engineering and Information Technology from the Leipzig University of Applied Sciences (HTWK) in the field of Electronic Circuit Design and Signal Procession. In 2019 he joined the research group "Smart Diagnostic and Online Monitoring" of Professor Derbel at HTWK. Since 2020 he is a doctoral candidate and holder of the HTWK scholarship. His current research topics are always-on wake-up receivers for wireless sensor nodes with ultra-low power consumption. He was awarded the Best Paper Award (2nd Place) at IEEE I²MTC 2025.

OLFA KANOUN (Senior Member, IEEE) graduated in electrical engineering and information technology from the Technical University of Munich, in 1996. She got her Ph.D. in 2001 from the University of the Bundeswehr Munich, Germany. Since 2007, she has been a full professor in measurement and sensor technology with the Chemnitz University of Technology, Germany. Her research interests include impedance spectroscopy, sensors based on carbonaceous nanomaterials, and energy aware wireless sensors. She received seven best paper awards of international conferences and published more than 800 publications in peer-reviewed scientific journals and international conferences.

FAOUZI DERBEL is Professor of Smart Diagnostics and Online Monitoring at the Leipzig University of Applied Sciences since 2013 and serves as Vice-Rector for Research and Sustainability since 2023. His research focuses on condition monitoring, particularly in the areas of power-aware design for wireless sensor networks and smart signal processing systems. Following his Ph.D., he held various leadership positions in industry, including Head of Product Innovation at Siemens Building Technologies and Head of R&D at QUNDIS, Germany. He is an active member of national and international technical committees, including ETSI ERM TG28 and the Smart Cities technical group within DKE.